Assessing Urban Overheating Under Climate Change through Representative Methods on Large Spatial and Temporal Scales

Jiwei Zou

A Thesis

In the Department

of

Department of Building, Civil and Environmental Engineering

Presented in Partial Fulfillment of the Requirements

For the Degree of

Doctor of Philosophy (Building Engineering) at

Concordia University

Montreal, Quebec, Canada

September 2024

© Jiwei Zou, 2024

CONCORDIA UNIVERSITY
SCHOOL OF GRADUATE STUDIES

This is to certify that the thesis prepared

By: Jiwei Zou

Entitled: Assessing Urban Overheating Under Climate Change through Representative Methods on Large Spatial and Temporal Scales

and submitted in partial fulfillment of the requirements for the degree of

DOCTOR OF PHILOSOPHY (Department of Building, Civil and Environmental Engineering)

complies with the regulations of the University and meets the accepted standards with respect to originality and quality.

Signed by the final examining committee:

____ Chair
Dr. Fariborz Haghighat

____ External examiner
Dr. Bing Dong

____ Examiner
Dr. Carly Ziter

____ Examiner
Dr. Alireza Nazemi

____ Thesis Supervisor
Dr. Liangzhu Leon Wang

____ Thesis Supervisor
Dr. Gaur Abhishek

____ Thesis Supervisor
Dr. Jianlei Niu

Approved by ____
Dr. Mohamed Ouf

Month/Day/Year ____
Dr. Mourad Debbabi
Gina Cody School of Engineering and Computer Science

Abstract

Assessing Urban Overheating Under Climate Change through Representative Methods on Large Spatial and Temporal Scales

Jiwei Zou, Ph.D.

Concordia University, 2024

Climate change has led to prolonged, more frequent, intense, and severe extreme weather events, such as summertime heatwaves, creating many challenges on the economy and society and human health and energy resources. For example, the 2010 and 2018 heatwave in Quebec, Canada, resulted in about 280 and 93 heat-related deaths, and there were around 500 fatalities due to overheated indoor environments in 2021 around entire Canada. Therefore, it is imperative to evaluate historical urban overheating conditions as well as predict the future scenarios. Considering a large temporal scale when assessing future climates (up to hundred years) and a large spatial scale when assessing the microclimate of an entire urban area, this thesis developed a representative method which could serve for both large temporal and spatial scale to select typical and extreme scenarios for overheating assessment.

Firstly, future indoor and outdoor overheating conditions are evaluated in Canadian cities by assessing the effectiveness of a reference year selection method. Onsite long-term climate data sourced from the Coordinated Regional Climate Downscaling Experiment (CORDEX) is bias-corrected and analyzed to evaluate overheating conditions in Montreal, Toronto, and Vancouver under various future climate scenarios. Secondly, the typical and extreme days are selected from

reference year as the input of CityFFD-CityBEM co-simulation for assessing climate change impacts on urban overheating in downtown Montreal. The analysis points out a shift from mild thermal stress to extreme heat stress under future climate conditions, highlighting the critical need for interventions in urban design and infrastructure to maintain outdoor comfort. Last but not least, this thesis expands the scope by developing a spatial and temporal representative method combined with Weather Research and Forecasting (WRF) and CityFFD simulations to evaluate overheating across Montreal. The results emphasize the importance of selecting representative locations for simulations to accurately capture the varying microclimate conditions across the city. Findings suggest significant increases in urban heat, necessitating targeted mitigation strategies.

The contributions of this thesis are significant in advancing the understanding of urban overheating dynamics and mitigation strategies. It provides municipalities and urban planners with validated tools and methods to forecast and counteract the adverse effects of urban overheating. This research underscores the critical role of detailed, localized climate simulations in urban planning and highlights innovative strategies to enhance urban resilience against climate change-induced overheating.

Acknowledgements

I extend my profound gratitude to my supervisor, Dr. Liangzhu (Leon) Wang, for his steadfast support, patience, motivation, and extensive knowledge throughout my Ph.D. journey. Equally, I am immensely grateful to my co-supervisors, Dr. Gaur Abhishek and Dr. Jianlei Niu, for their detailed advice and inspiring mentorship, without which this dissertation could not have been realized. My thanks also go to the examining committee members, Dr. Fariborz Haghighat, Dr. Carly Ziter, Dr. Alireza Nazemi, and Dr. Bing Dong, for their perceptive and beneficial critiques of my research.

Additionally, I appreciate the support and guidance provided by Dr. Lin Wang, Dr. Michael Lacasse, Mr. Henry Lu, and Dr. Zahra Jandaghian during my internship at the National Research Council Canada. I owe a special thanks to my colleagues Dr. Senwen Yang, Dr. Mohammad Mortezazadeh, Dr. Ali Katal, Dr. Yichen Yu, Dr. Danlin Hou, Miss Dongxue Zhan, Dr. Lili Ji, Dr. Chang Shu, Mr. Saeed Rayegan, and Mr. Dingyang Geng, for their substantial support in both professional and personal capacities.

Profound appreciation is due to my family—my mother Hui Shen, my father Hui Zou, and my parents-in-law Dongling Guo and Yue Yan—for their constant spiritual and financial backing. A warm acknowledgment to my cat Cola and my dog Coffee Bean, for being a comforting companion.

Finally, my deepest love and gratitude to my wife, Shujie Yan, whose unwavering support and encouragement have been the cornerstone of my resilience. Her companionship has been crucial throughout this challenging and fulfilling journey.

Table of contents

List of figures

List of Tables

Preface and contribution of authors

This is a manuscript-based thesis, a collection of three published journal papers:

Section 1.2 is prepared based on published paper: Zou, J., Lu, H., Shu, C., Ji, L., Gaur, A., & Wang, L. L. (2023). Multiscale numerical assessment of urban overheating under climate projections: a review. Urban Climate, 49, 101551. Jiwei Zou conceived and designed the analysis, collected the data, performed the analysis and wrote the paper. Henry Lu, Chang Shu, and Lili Ji contributed to the methodology, review and editing. Liangzhu (Leon) Wang and Abhishek Gaur contributed to review and editing.

Chapter 2 is prepared based on the published paper: Zou, J., Gaur, A., Wang, L. L., Laouadi, A., & Lacasse, M. (2022). Assessment of future overheating conditions in Canadian cities using a reference year selection method. Building and Environment, 218, 109102. Jiwei Zou conceived and designed the analysis, collected the data, performed the analysis and wrote the paper. Abhishek Gaur contributed to the conceptualization, methodology, review and editing. Liangzhu (Leon) Wang, Michael Lacasse, and Laouadi Abdelaziz contributed to review and editing.

Chapter 3 is prepared based on the published paper: Zou, J., Yu, Y., Mortezazadeh, M., Lu, H., Gaur, A., & Wang, L. L. Evaluating Climate Change Impacts on Building Level Steady-State and Dynamic Outdoor Thermal Comfort. Available at SSRN 4782099. Jiwei Zou proposed the concept and method, conceived and designed the analysis, collected the data, performed the analysis and wrote the paper. Yichen Yu contributed to the conceptualization, methodology, data collection, review and editing. Mohammad Mortezazadeh and Henry Lu contributed to the methodology and review. Liangzhu (Leon) Wang and Abhishek Gaur contributed to review and editing.

For easy reading, these three manuscripts are modified from the original ones. The numbering of equations, tables, and figures includes the numbers of the chapters, and the references of different chapters are combined at the end of the thesis.

Nomenclature

AIJ	Architectural Institute of Japan
AMY	Actual meteorological year
ANNs	Artificial neural networks
AT	Ambient Temperature
Ave	Average value of monthly 20-years overheating hours
AWD	Ambient Warmness Degree
BES	Building energy model
BPG	Best practice guidelines
CDD	cooling degree-day
CDF	Cumulative distribution function
CFD	Computational fluid dynamics
CFL	Courant–Friedrichs–Lewy
CIBSE	Chartered Institution of Building Services Engineers criteria
CMIP5	Coupled Model Intercomparison Project Phase 5
CMIP6	Coupled Model Intercomparison Projects 6
CORDEX	Coordinated Regional Downscaling Experiment

CRI	contribution ratio of indoor climate
CWEC	Canadian weather year for energy calculations
DSY	Design Summer Year
ECD	Extreme Cold Day
ECY	Extreme Cold Year
EWD	Extreme Warm Day
EWY	Extreme Warm Year
FFD	Fast Fluid Dynamics
GCMs	Global Climate Models
GHG	Greenhouse Gas
GIS	Geographic information system
GPU	High-end video card
HAMT	heat, air, and moisture transfer
hurs	Relative Humidity
IOD	Indoor Overheating Degree
IPCC	The Intergovernmental Panel on Climate Change
IWEC	International weather Year for Energy Calculations
LCZ	Local climate zones
Max	Maximum value of monthly 20-years overheating hours

MBCn	Multivariate quantile mapping bias correction method
Min	Minimum value of monthly 20-years overheating hours
MOHC	MOHC-HadGEM2-ES
MOS	Model output statistics
MPI	MPI-ESM-LR
NARCCAP	North American Regional Climate Change Assessment Program
NCC	NCC-NorESM1-M
PET	Physiological Equivalent Temperature
PMV	Predicted mean vote
PPD	Predicted Percentage of Dissatisfied
PT	Perceived Temperature
RANS	Reynolds-averaged Navier–Stokes model
RCM	Regional Climate Model
RCP	Representative Concentration Pathway
rsds	Solar Radiation
RSWY	Reference summer weather years
SDD	Statistical-dynamical downscaling methods
sfcWind	Wind Velocity at ground surface

SLUCM	Single Layer Urban Canopy Model
SRY	Summer reference year
SSP	Shared Socioeconomic Pathway
PDISC	Practical thermal discomfort scale
tas	Air Temperature
TDD	Typical Downscaled Day
TDY	Typical Downscaled Year
TMM	Typical meteorological months
TMY	Typical Meteorological Year
TRY	Test reference year
t-SET	Modified Standard Effective Temperature
UBL	Urban Boundary Layer
UCL	Urban Canopy Layer
UTCI	Universal Thermal Comfort Index
WRF	Weather Research and Forecasting model
WUDAPT	World Urban Database and Access Portal Tools
WYEC	Weather Year for Energy Calculations
α_{IOD}	Overheating Escalation Factor

Chapter 1

Introduction and Literature Review

1.1 Introduction

Climate change, defined as a long-term alteration in average weather patterns, particularly changes in temperature, precipitation, and wind, largely due to increased concentrations of greenhouse gases in the atmosphere. Due to the climate change, recent decades have witnessed significant climate shifts globally, which have triggered more frequent, severe, and prolonged extreme weather events, including devastating heatwaves that pose a direct threat to human health and safety. For instance, the European summer of 2003, one of the hottest on record, resulted in over 30,000 deaths, illustrating the acute impact of extreme temperatures [1]. Similarly, in Canada, the 2021 heatwave led to approximately 500 fatalities, underscoring the ongoing risk associated with such events [2]. The increasing frequency and intensity of these heat events are projected to escalate further, with deadly heatwaves expected to occur around 60 days annually by 2100, affecting up to 74% of the global population [3]. This rising trend highlights the urgent need for a deeper understanding of multiscale urban overheating under climate change impacts to develop effective mitigation and adaptation strategies.

Urban overheating, defined as "the exceedance of locally-defined thermal thresholds that lead to negative impacts on people and urban systems," occurs predominantly in urban areas, which are vulnerable hotspots due to their dense infrastructures and heat-absorbing materials [4]. This phenomenon significantly influences the urban microclimate, thereby affecting air quality, energy demand, and public health [5, 6]. Although various mitigation strategies have been proposed to reduce urban overheating in recent years, the intensity and frequency of such events have increased due to climate change, rendering current strategies less effective. This escalating trend underscores the importance of not only understanding historical overheating events but also predicting future conditions. Therefore, focusing on urban overheating necessitates robust methodologies for evaluating and predicting thermal conditions under future climate scenarios, which is crucial for ensuring sustainable urban development and protecting urban populations from the adverse effects of heat extremes.

Projected climate data or future climate data, derived from Global Climate Models (GCMs) and Regional Climate Models (RCMs), serve as foundational elements in this research. GCMs are complex computer models that simulate the Earth's climate system, including the atmosphere, oceans, land surface, and ice, to project changes in climate at a global scale [7]. RCMs, on the other hand, provide more detailed climate projections within specific regions by refining the coarse data obtained from GCMs, allowing for better resolution and accuracy at a regional level [8]. These models, although effective at a broader spatial and temporal scale, present challenges such as high computational demands and the need for downscaling to capture local urban microclimates accurately [9, 10].

Computational Fluid Dynamics (CFD) simulations, on the other hand, emerges as a pivotal approach for detailed microclimate analysis [11, 12]. CFD, a method that employs numerical analysis to model fluid flows and heat transfer, enables the nuanced assessment of local thermal conditions and airflow patterns, crucial for the detailed assessment of outdoor thermal comfort [13, 14], which refers to the degree to which external environmental conditions contribute to a person's subjective satisfaction with the surrounding thermal environment. By integrating broader-scale and low-resolution climate projections with CFD, this study aims to provide a comprehensive understanding of future urban overheating risks, focusing on both steady-state and dynamic thermal comfort across multiple urban scales.

1.2 Literature review

This section is prepared based on published paper: Multiscale numerical assessment of urban overheating under climate projections: a review.

Abstract

The interactions between climate change and urbanization have generated mounting concerns regarding outdoor and indoor overheating within urban populations, impacting thermal comfort, heat-related mortality, and energy consumption, particularly during heat waves that are becoming more frequent, intense, and prolonged. Various strategies have been proposed to mitigate overheating in urban environments among the past few years. To effectively examine the impacts of overheating and evaluate mitigation strategies in both current and future climates, it is first necessary to produce reliable climate projections that can accurately describe the state of the urban climate; which is a complex system comprising of unique microclimate phenomena connected to regional and global. This chapter presents a systematic review of the application of climate model projections for future indoor and outdoor overheating impact assessments, divided into four primary stages: (1) Mesoscale raw future climate data generation using GCM-RCMs; (2) Local-scale future climate input preparation through bias-correction and reference year data generation; (3) Microscale indoor and outdoor simulations with building performance models or computational fluid dynamics (CFD) software; (4) Overheating evaluation based on various overheating criteria. These stages are essential for advancing our understanding of overheating and informing future studies in this area. With the target keywords of above four stages, the methodology applied to identify and select articles from search results as suitable candidates was shown in Section 1.2.2. Key research gaps illustrated by this review include challenges in generating climate data, improving projected data reliability, and addressing indoor/outdoor

climate simulation complexities. Additionally, incorporating social-economic factors into overheating evaluation methods is crucial for a comprehensive assessment. Although the focus is future urban overheating assessment, the general methodologies and procedure of future climate projections may also apply to other building performance simulations considering the climate change impacts. Notable research gaps were then identified as avenues for future research.

Keywords: Climate change; future projection; bias correction; reference year data; multiscale simulation; overheating

1.2.1 Introduction

Anthropogenic-induced climate change is one of the greatest challenges that society faces. Around the world, the impacts of climate change are already being felt [15] in the form of increased intensity, frequency, and duration of extreme weather events such as warm spells and heat events, drought, heavy rainfall, storm surges, and sea-level rise. Even if international efforts to limit global warming to 1.5 °C are met according to the 2015 Paris Agreement, there will still be significant ramifications to the climate requiring considerable adaptations [16]. In 2003, Europe experienced one of the hottest summers in the past 500 years, with more than 30000 deaths [17, 18] and record-high temperatures of 5 to 10 °C above the average of June to mid-August [19]. In the Netherlands, around 2000 heat-related deaths occurred during summer with a maximum temperature of 35 °C [20]. The 2010 heatwave in Quebec, Canada, resulted in a significant increase of 33% in the crude death rate (about 280 extra deaths) [21] and the 2018 heatwave in Quebec caused 93 deaths. Although outdoor and indoor overheating have garnered much attention in recent years around the world, the heatwave in 2021 still caused about 500 deaths across Canada [22]. More recently, from June to August 2022, temperatures of 40–43 °C were recorded in parts of Europe, with the highest temperature recorded as 47.0 °C in Pinhão, Portugal [23]. During the 2022 heatwave in Germany, 1636 probable heat-related deaths were attributed to temperatures reaching 39.2 °C during the June heatwave, and around 6500 excess deaths were caused by the July heatwave [24]. As a consequence of global warming, the frequencies, magnitudes, and intensities of heat events around the globe are expected to keep increasing in the future [25, 26]. The deadly heatwaves are expected to occur about 60 days annually in the mid-latitudes and affect from 48% to74% of the world's population by 2100 [3]. Thus, substantial changes to the urban environment are required to support a growing urbanized population under an increasingly hot climate, and a better understanding of the urban overheating conditions for evaluating the hazards is needed.

There have been some existing reviews on the overheating hazards but focusing on different aspects such as the overheating criteria, mitigation strategies, chronic year-round overheating [27-29], and the impacts of overheating on energy consumption [30, 31], indoor and outdoor air quality [31], and human health [4, 31, 32]. Overheating criteria are a standardized set of thresholds used to evaluate indoor overheating in buildings based on human comfort, health, and safety [28, 33]. They are crucial for conducting overheating assessments and enable the comparison of severity levels across different buildings, locations, and climates, making it the most important and one of the first steps when conducting the overheating assessment. Rahif, et al. [27] reviewed the overheating evaluation methods in eleven international standards and five national building codes, and compared three promising overheating indices. They also provided suggestions and recommendations for overheating criteria under different scenarios. Evaluating overheating hazards makes it possible to test the effectiveness of various mitigation strategies, such as the urban green infrastructure, including cool materials, green roofs, vertical gardens, urban greenery, and water-based technologies [12, 30]. According to Pisello, et al. [12], it has been shown that the ambient outdoor air temperature could be reduced by 1 °C with trees and hedges, by 0.2 °C with green roofs and green walls, by 0.3 °C by reflective roofs and pavements, and by 1.5 °C when applying two or more techniques at the same time. Besides, the increase in the ambient temperature during summer overheating will impact the supply and demand of electricity used for cooling purposes [31]. Santamouris [31] critically reviewed the actual and future impact of urban overheating on the energy demand of buildings and cities. The increase in the cooling load was found to vary between 0.5 to 8 kWh/(m^2·°C·year).

An essential part of future overheating assessments is to prepare future climate projections which will be treated as the inputs for indoor and outdoor climate simulations. Projected climate data are usually from global climate models (GCMs), which is a combination of an atmospheric model, ocean model, land surface scheme, and a sea ice model [34]. However, there are many uncertainties inherent in using GCMs. For instance, there are many different climate models, each with many different physics options, and the preceding simulations may follow multiple greenhouses gas emission scenarios creating many options and complexities. For the Coupled Model Intercomparison Project Phase 5 (CMIP5), forty GCMs from 20 research groups were proposed and publicly available [35]. The Intergovernmental Panel on Climate Change (IPCC) has four Representative Concentration Pathways (RCPs) representing different future greenhouse gas emission scenarios, including RCP 2.6, RCP 4.5, RCP 6.0, and RCP 8.5. More recently, led by the IPCC, the energy modeling community developed a new set of emission scenarios driven by different socioeconomic assumptions, the so-called 'Shared Socioeconomic Pathways (SSPs). A number of these SSP scenarios have been selected to drive climate models as part of the Coupled Model Intercomparison Projects 6 (CMIP6). The previous RCP scenarios have been updated in CMIP6 in the form of SSP1-2.6, SSP2-4.5, SSP4-6.0, and SSP5-8.5, each of which results in similar 2100 radiative forcing levels as their predecessors in RCPs. Additionally, several new scenarios were applied in CMIP6, such as SSP1-1.9, SSP4-3.4, SSP5-3.4OS, and SSP3-7.0, to account for more socioeconomic drivers.

However, while GCMs can take into account the effects of urban areas on a large scale, these results should not be considered as reliable on a local scale. The coarse spatial resolution of GCMs is one of the reasons why downscaling methods are necessary. Moreover, due to the bias in the climate model, which is defined as 'the systematic difference between a simulated climate statistic and the corresponding real-world climate statistics' [36], it is necessary to perform bias correction for calibration purposes when using climate model projections for smaller scale impact assessments. Last but not least, such a large number of climate models and RCP scenarios may complicate the process of applying their different combinations to one specific assessment with potentially high computational costs. Therefore, a representative or reference future-year method is often needed. Different and inconsistent methods of choosing reference years were found based on the literature. In summary, from the generation of future climate data, processing climate inputs to conducting the actual overheating assessment, there is a lack of a collective and comparative review study specifically for the future overheating assessments of indoor and outdoor conditions. Recently. Du, et al. [37] conducted a comprehensive review on the modeling, assessment, and improvement methods of the urban thermal and wind environment (UTWE) across various scales, providing valuable insights into the current state of the field. To expand former work, our review offers a novel and complementary perspective by specifically focusing on the application of climate model projections for future indoor and outdoor overheating impact assessments in the context of climate change and urbanization. This targeted approach allows for a more in-depth understanding of urban overheating in a changing climate.

This chapter presents a systematic review of the application of climate model projections for future indoor and outdoor overheating impact assessments, divided into four primary stages as depicted in Fig. 1.1. Section 1.2.2 presents the scope of the review as well as the methodology of collecting paper. Section 1.2.3 focuses on generating raw future climate data at the mesoscale using GCM-RCMs. In Section 1.2.4, the review discusses two main preparation steps of future climate input files for simulation which are bias-correction and reference year data generation, utilizing data from GCM-RCMs to generate local climate data input. Section 1.2.5 examines microscale indoor and outdoor simulations conducted using building performance models or other tools, such as computational fluid dynamics (CFD) software, drawing upon the input data obtained in Section 1.2.3. Furthermore, Section 1.2.6 examines overheating evaluation based on various overheating criteria, including the emulation technique that relies on the numerical outcomes derived from the indoor and outdoor simulations. This review aims to provide a clear structure and detailed procedure assessing urban overheating conditions under the impacts of future climate projections. Although the focus is future urban overheating assessment, the general methodologies and procedure of future climate projections may also apply to other building performance simulations considering the climate change impacts.

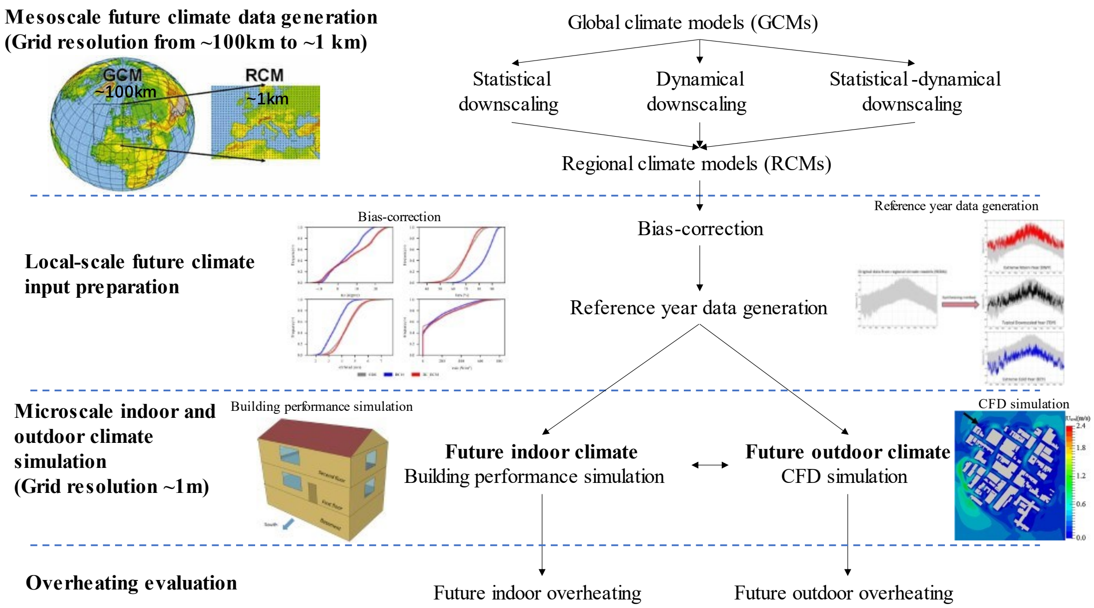

Fig. 1.1 Structure of the current review [34, 38-40].

1.2.2 Scope of the review and methodology of collecting paper

The main focus of the present work is to a systematic review of the application of climate model projections for future indoor and outdoor overheating impact assessments which aims to provide a clear structure and detailed procedure assessing urban overheating conditions under the impacts of future climate projections. There are following four main topics to be reviewed in this chapter:

1. Future climate data generation: GCM-RCMs and their corresponding downscaling methods;
2. Future climate data input preparation: Bias-correction and Reference year data selection;
3. Indoor and Outdoor simulation: Building performance simulation and CFD simulation
4. Overheating evaluation: Overheating standards and criteria

Fig. 1.2 showcases the methodology we applied to identify and select articles from search results as suitable candidates. The search results, generated based on the target scope's keywords, produced a considerable number of papers. Nevertheless, not every paper was pertinent to the focus of our review. By adhering to the illustrated guidelines in the figure, we successfully compiled the final papers for our analysis. Furthermore, while the primary emphasis of this chapter is on future urban overheating, we have included papers in this systematic review that may not specifically address overheating but contribute significantly to the targeted method.

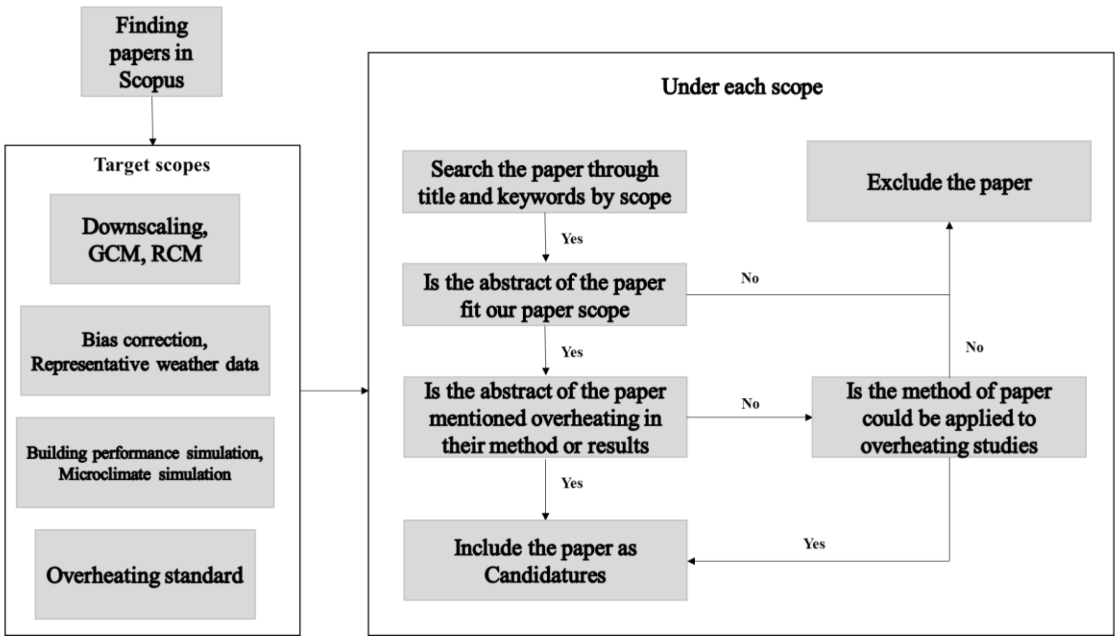

Fig. 1.2 The methodology of collecting papers.

Although plenty of reviews have covered different aspects of overheating studies, our literature search found that the prediction and assessment of future overheating still seems inadequate, considering its importance when studying climate change. This can be shown by a temporal and spatial comparison of the studies using “overheating” and “future overheating” as keywords, as reported in Fig. 1.3. The search is performed by inputting “overheating” and “future overheating” in the search field of the Scopus scientific database, including the article title, abstract, and keywords, and all the results were updated by September 2022. Although the Scopus database may not be considered completely exhaustive of the whole literature in the field, it has been selected for assessing the qualitative trends in a similar field based on the former literature [12]. Fig. 1.3 (a) shows that since 2015 there has been a dramatic increase in the number of publications on "overheating", and most overheating studies were conducted in China, Europe, and the US, as shown in Fig. 1.3 (b). However, despite its importance, only 9% of these studies focused on "future overheating" for all regions summing all time period from 2010 to 2021. Therefore, it could be concluded that there is a significant remaining area to be investigated regarding "future overheating", and more research are estimated [41] to focus on the "future overheating" in the following decades.

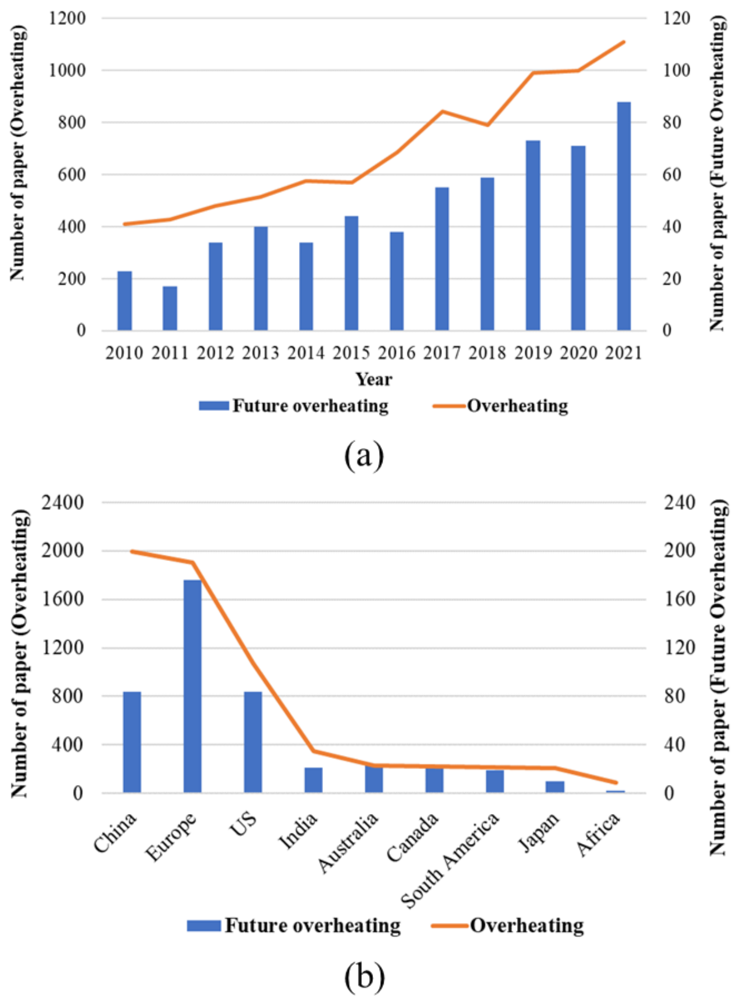

Fig. 1.3 Statistic information of overheating and future overheating publications in the Scopus database for (a) publication year and (b) country and region.

1.2.3 Future climate data generation

There are many methods to modeling the climate in an urban environment. The way in which the built environment is depicted in an urban climate model depends heavily on the spatial scales used in the model. Therefore, selecting appropriate spatial scales is crucial for accurately representing the urban environment and its impact on climate. The availability of climate models allows researchers to study the current and future climate of a city. On the largest scale, GCMs are commonly used to provide projections of climate change over the long term [42, 43]. These numerical models are employed to simulate the major processes and interactions that govern the climate across a spatial resolution of a few hundred kilometers, allowing the study of various degrees of climate change induced by different representative concentration pathways on a global scale [44]. The grid resolution of GCMs can be considered absolutely adequate at higher level of the atmosphere boundary layer, where it is not necessary to catch small scale phenomena. However, the spatial resolution of GCMs is often insufficient for resolving city-scale mechanisms, and their large time-step is usually unsuitable for studying overheating evaluations at hourly resolutions. Besides, these models are too coarse in spatial resolution to simulate the microclimate inside the urban boundary layer and urban canopy layer adequately, where most of the human activities take place. Additionally, most climate models do not include parameterizations of the urban land cover in their surface schemes [45, 46].

Therefore, studying the urban climate, especially under the evolution of climate change, requires high-resolution climate data in both time and space [47]. To enhance the applicability of climate projections to the scale of buildings, communities, and urban areas, a method called "downscaling" is applied to refine global climate data to a higher resolution by translating large-scale climate model output into finer spatial and temporal scales. Researchers have proposed statistical (section 1.2.3.1), dynamic (section 1.2.3.2), and statistical-dynamical downscaling (SDD) methods (section 1.2.3.3). These methodologies are quite versatile as they can be applied to a large set of climate projections, including different greenhouse gas emission scenarios and long-term periods. This allows various model and scenario uncertainties to be considered.

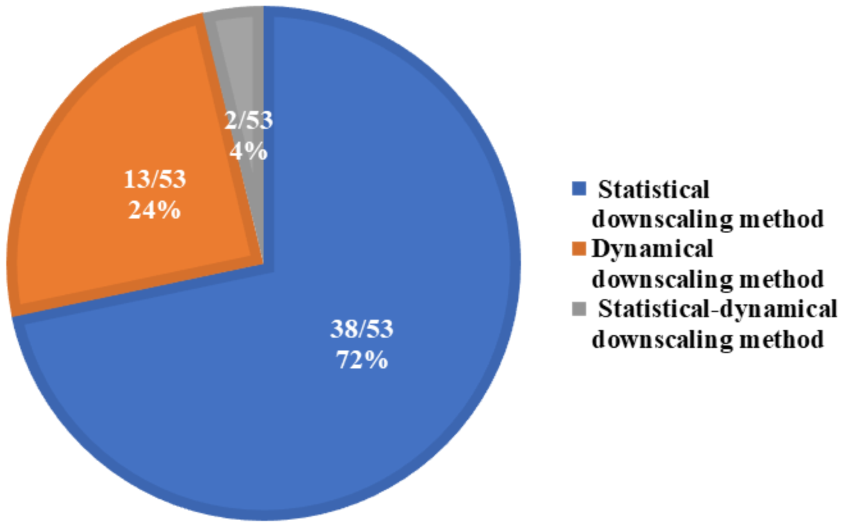

Fig. 1.4 Portion of paper using different downscaling method

Based on our review of the various downscaling methodologies with a total number of 53 paper, we found that a large portion of the existing literature is based on statistical downscaling methodologies (72%) while dynamical and SDD methods make up the remaining 24% and 4%, respectively, as shown in Fig. 1.4. The main reason for this large count of statistical downscaling methods in the literature is due to the fact that this field has begun much earlier than the other methods and is still an active area of research. On the other hand, accurate and reliable dynamical methods that are appropriate in the urban context have only relatively recently been introduced. Consequently, the portion of literature discussing dynamical downscaling methods are increasing rapidly due to advances in methodology and improvements in computing. As a result, the hybrid approach that combines the strengths of both statistical and dynamical downscaling methods makes up the smallest portion of research so far. In recent years, while the body of literature on statistical downscaling is still growing, there is increasingly more focus towards dynamical and statistical-dynamical downscaling methodologies as a means to generate high-resolution long-term climate data for urban environments in the context of climate change.

1.2.3.1 Statistical downscaling method

Statistical downscaling can be divided into three broad categories: regression models, weather classification, and weather generators [48-51]. Statistical downscaling assumes that the regional climate is governed by the large-scale state of the climate and regional/local geographic features such as proximity to water, topography, and land use [52]. By linking large-scale climate variables (predictors) to regional/local variables (predictands) through a statistical model, outputs from GCMs can be used as inputs to the statistical model to estimate regional climate characteristics. Since the statistical downscaling method is relatively easy to implement and computationally inexpensive, it can be easily applied to different climate models. Fig. 1.5 shows an application of a simple statistical downscaling which captures the difference between the fine-resolution 2-km data from the Weather Research and Forecasting (WRF) model and coarse-resolution 50-km data from the NARCCAP (North American Regional Climate Change Assessment Program). The statistical downscaling method was then applied to a series of regional climate models to directly predict high-resolution precipitation [53]. However, statistical downscaling assumes that statistical relationships derived for the present climate must also hold under different future forcing scenarios, which is not a verifiable assumption [54]. Consequently, when used to conduct impact assessments, downscaled climate data needs to be combined with results from multiple climate model outputs to account for the uncertainties in the models' projections. Even with these caveats, the accuracy of statistically downscaled data remains questionable, which challenges their usefulness in evaluating adaption scenarios [55]. Therefore, statistical downscaling methods may not be as reliable as other methods in generating urban climate data projections.

Regression models represent a relatively simple quantitative relationship between the predictors and predictands. The most straightforward method is to produce a model where one variable is regressed upon others. Multiple regression introduces more complexity by relating multiple predictors to a single predictand based on large-scale atmospheric forcing [56]. Canonical correlation analysis extends the idea further by locating the optimal linear combination of predictors that results in the most variance in the predictand [57, 58]. This allows the model to use a wider field of information and determine the most related patterns between predictors and predictands. Alternatively, artificial neural networks can be used to model systems with complex non-linear relationships between predictors and predictands [58, 59]. Subsequently, this approach can be used to study the regional urban climate by downscaling temperature and precipitation data [60]. For instance, Hoffmann, et al. [61] used a linear statistical model to downscale climate data for Hamburg, Germany, to investigate the regional urban climate under two climate change scenarios.

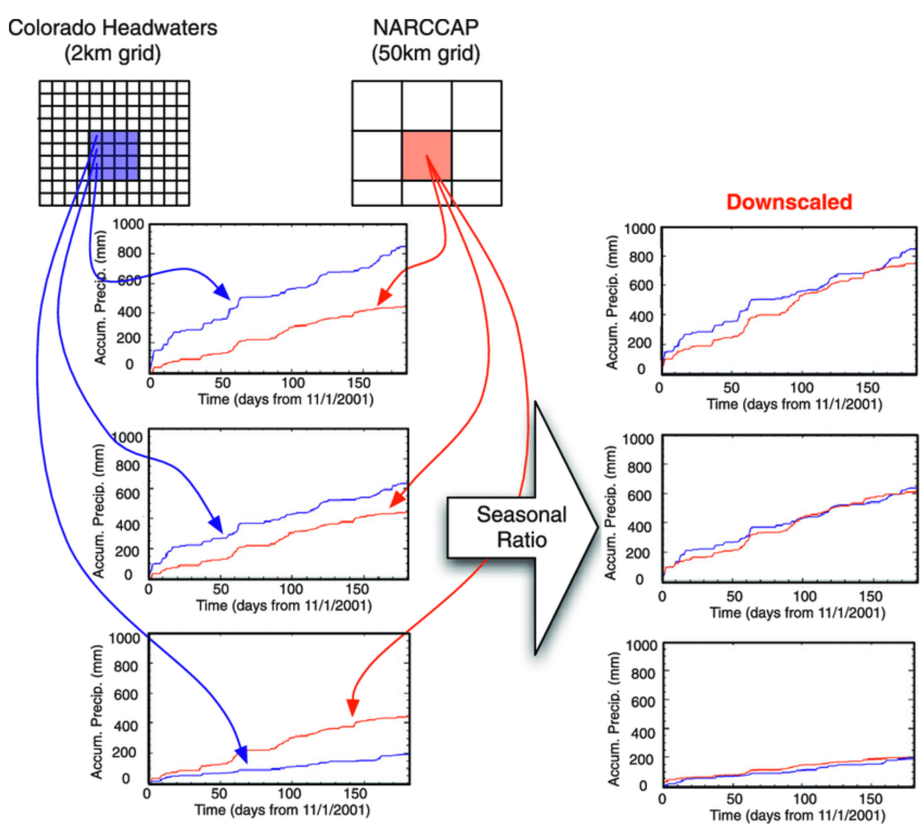

Fig. 1.5 Statistical downscaling of a time series of accumulated precipitation at three WRF 2-km grid cells (blue), with 50-km NARCCAP (North American Regional Climate Change Assessment Program) data (red) [53].

Weather generators are a stochastic model where the statistical attributes of the local climate variable, such as the mean and variance, are replicated but not the specific sequence of events [62]. Most of these methods focus on precipitation frequency and intensity, but time series for other variables such as temperature, relative humidity, and solar radiation can be produced as well [63]. Alternatively, the parameters of the weather generator can be conditioned based on the large-scale climatic state or the relationship between large-scale predictors and local predictands [62]. Future climate projections can then be obtained by perturbing the weather generator parameters by delta change factors, which can be calculated by comparing trends between historical and future climate projections [64]. Lindberg, et al. [65] used a similar method to study the heat stress present in Gothenburg, Sweden, by calculating the variation in temperature and solar radiation and subsequently applying the trends to future projections to examine the changes in heat stress in the context of climate change.

Weather classification methods group local weather patterns with large-scale predictands into a limited number of weather types [66-68]. Projections for the local climate are obtained by reconstructing the time series day by day, according to the weather types defined by the climate projections, and by matching an analogous day from the reference data of local weather events [69]. Changes in the climate due to global warming can then be estimated by calculating the change in frequency of different weather types. Hoffmann, et al. [70] adapted this approach to improve climate data used to study the local urban climate by introducing high-resolution dynamical simulations as the basis to reconstruct a long time series.

Several issues with statistical downscaling affect its ability to estimate the climate accurately. Regression has difficulty replicating the temporal variability of variables [71], such as daily precipitation, where the distribution is not normal. Therefore, statistically, downscaling precipitation often requires large amounts of observational data to fit a more complex non-linear model. Additionally, the choice of predictors is extremely important in determining the accuracy of the downscaled data. For instance, Hewitson and Crane [72] found that downscaled precipitation projections can vary significantly if humidity is included as a predictor. Similarly, Huth [73] compared a relatively large number of predictors' ability to estimate local daily mean temperature and concluded that temperature fields result in a more accurate representation than circulation variables among the predictors. Lastly, evaluating statistical downscaling models is problematic as validation techniques rely on comparing available observational data with the performance of statistically modeled predictions [74]. However, the accuracy of the statistical downscaling model in representing the present day does not signify that it will be as competent under climate change conditions [54, 75].

1.2.3.2 Dynamical downscaling method

Due to the limitations of statistical downscaling methods, many researchers have used the fully dynamic downscaling method. It is known as a limited-area, high-resolution model (a regional climate model, or RCM) driven by boundary conditions from a GCM to reproduce the local climate at a higher resolution [76]. Dynamical downscaling adopts similar physical equations and parameterizations as GCMs but employs them at a much higher spatial resolution. In addition to the higher resolution, RCMs need to explicitly include representations of urban areas and processes to accurately simulate the urban climate, as shown in Fig. 1.6.

Recent advances in climate science and climate models, such as the WRF model, allow researchers to downscale data to a resolution of 1 km, accounting for urban parameterizations and land use. For instance, Gaur, et al. [77] examined the sensitivity of the WRF model in Ottawa, Canada, with different urban parameterization schemes and land cover data. Climate data from similar experiments can be used to study local urban impacts on urban climate and its population [78-80]. For example, Kusaka, et al. [81] used the WRF model coupled with an urban canopy model to examine the future heat stress in several Japanese cities due to climate change.

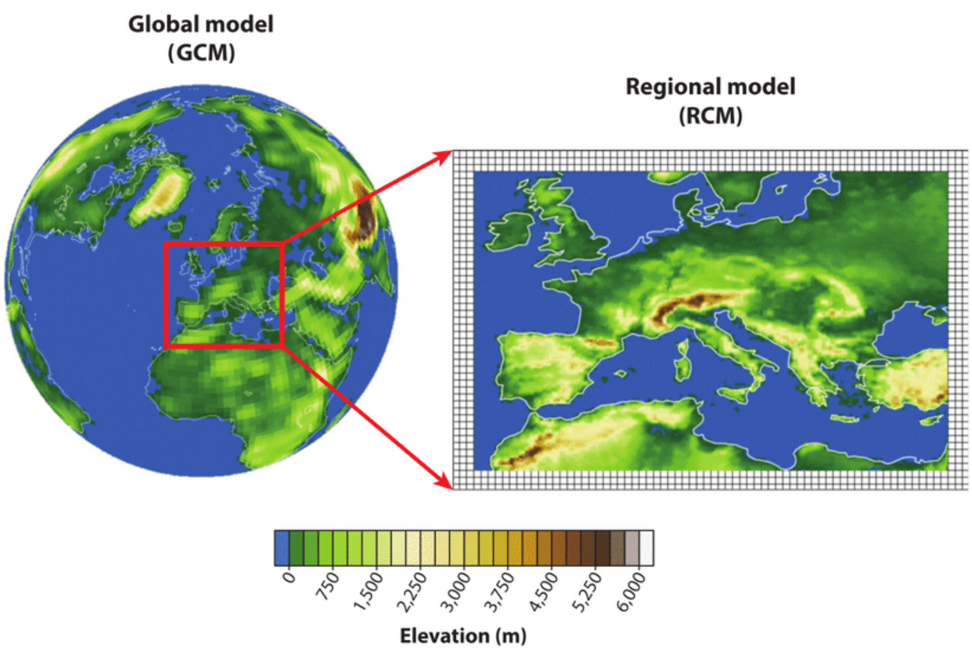

Fig. 1.6 Schematic description of the dynamical downscaling technique. A refinement of the topography and coastlines is obtained by using the RCM [76].

More recent experiments couple a Single Layer Urban Canopy Model (SLUCM) with WRF model [82], which has resulted in numerous studies validating the accuracy of such a model when compared to observational data in various climates [83-85]. Although SLUCMs add much-needed complexity to the climate model, they only represent general aspects of the urban environment and do not consider microscale characteristics such as individual buildings [86]. Multi-level UCMs provide more details about the urban environment and divide the building facades into several patches, each with its parameters and energy exchanges modeled [87]. Multi-level UCMs are useful in studying the interactions in cities, but the complexity comes with a high computational cost. Fortunately, later studies have found that simpler models perform as well as these more complex schemes [88]. Consequently, using SLUCMs has become prevalent in studying the urban climate with RCMs.

1.2.3.3 Statistical-dynamical downscaling method

Downscaling methods used for urban climate predictions need to satisfy several criteria in order to be practical and useful. First, the downscaling method needs to be physically realistic and accurately represent the complex interactions between the urban environment and the atmosphere. This requires an understanding of the underlying physics and dynamics of the urban climate system, as well as accurate representations of the urban geometry, land cover, and surface characteristics. Secondly, it needs to have a high spatial and temporal resolution to adequately capture the fine-scale features and short-term variability of urban climate conditions. Lastly, it needs to be computationally efficient to allow for the simulation of large areas and long time periods to be of any practical use. Ideally, dynamical downscaling would be the best approach as these models physically simulate interactions between large-scale and local phenomena and do indeed produce physically consistent data. However, to estimate the uncertainty of long-term climate projections, it is necessary to build a database consisting of an ensemble of climate simulations spanning a few decades. Consequently, dynamical downscaling is not often used in this context as it is computationally too expensive, limiting subsequent analyses' scope.

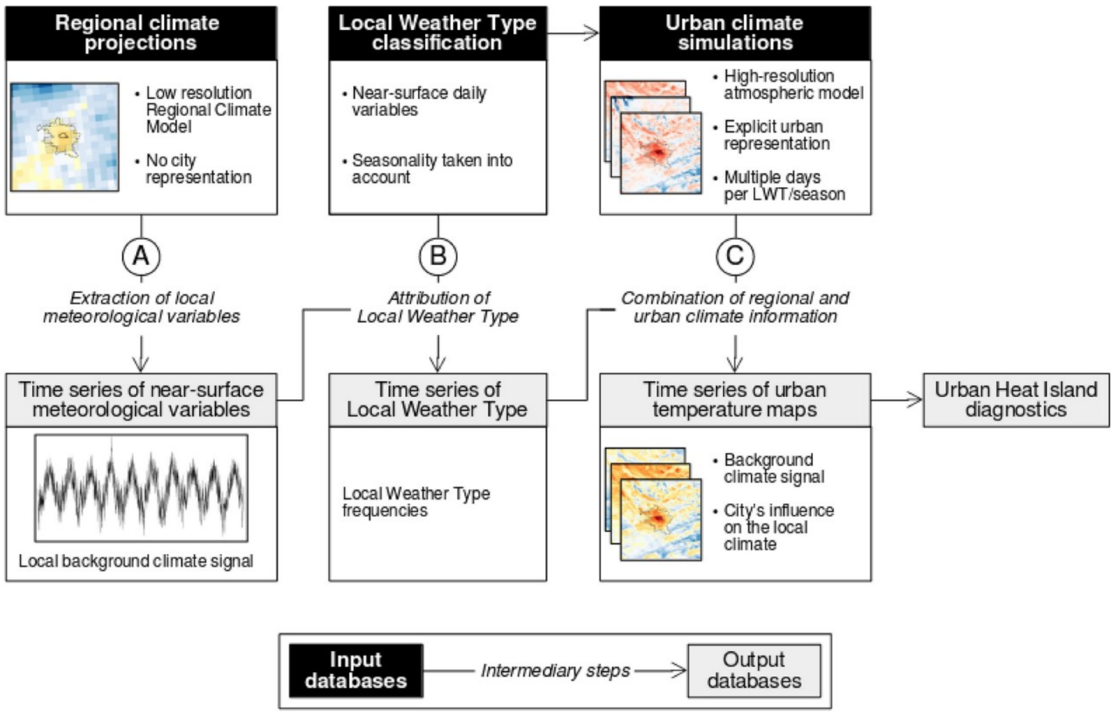

Fig. 1.7 Simplified flow chart of the statistical-dynamical downscaling (SDD) methodology used to study excess urban heat [89].

Statistical dynamical downscaling (SDD) techniques provide an approach that combines the benefits of relatively low computational costs of statistical downscaling and the efficacy of dynamical models. To reproduce the effects of the urban environment, SDD techniques statistically combine the relationship between large-scale and local-scale interactions with dynamical simulations that resolve urban characteristics. For example, Le Roy, et al. [89] developed an SDD method incorporating local weather types and short-term high-resolution urban climate simulations, as shown in Fig. 1.7. Subsequently, to calculate the impacts of the urban morphology, two high-resolution simulations of the local climate were performed, where one includes urban parameterizations while the other replaced it with natural land covers. By doing so, the differences can be superimposed on coarse climate projections while correcting them for urban effects. Gaur, et al. [90] validated a physical scaling downscaling model to downscale future surface temperature projections from three GCMs and two extreme Representative Concentration Pathways in the urban and rural areas of the cities. In the physical scaling downscaling model, the local climate is modeled considering both global scale climate dynamics and local scale geophysical characteristics of a location. Large-scale climatic interactions are incorporated into the model formulation by including a large-scale climate model as one of the predictors. Local-scale geophysical characteristics are incorporated by considering the elevation and land-cover properties of the location of interest as additional predictors. According to their validation results, the performance of the physical scaling downscaling model is found most superior during the summer months in the nighttime and worst during the summer months in the daytime.

This section mainly describes the progress of future climate data generation, from the raw climate data of GCM to three main downscaling methods. It could be concluded that conducting multi-decadal urban climate simulations at high resolutions with multiple global climate models under multiple greenhouse emission scenarios for different cities remains a daunting task. At the same time, long-term urban climate projections incorporating the effects of urban form at climatological timeframes are necessary for accurately evaluating the long-term risk of overheating in cities. Therefore, the statistical-dynamical method is suggested for urban climate applications since it takes advantage of developing long-term urban climate projections incorporating the effects of urban form by combining short-term high-resolution urban climate simulations with advanced statistical and data-driven modeling techniques.

1.2.4 Future climate input preparation

1.2.4.1 Bias correction

According to Maraun [36], climate model bias is defined as 'the systematic difference between a simulated climate statistic and the corresponding real-world climate statistics'. There are various reasons for the bias in climate model simulations, and the primary among them is the coarse resolution of climate models at which several local scale climate processes cannot be resolved [91-94]. As such, it is crucial to correct for bias in climate model simulations to ensure accurate assessments of overheating in cities both presently and under future projections. Bias correction is a method used to adjust climate model outputs by reducing systematic discrepancies between modeled and observed climate data, enhancing the accuracy of simulations at local and regional scales. Although it may not be possible to completely eliminate bias, using bias correction techniques can significantly reduce its impact on the results, thereby improving the accuracy of the assessment.

A fundamental assumption of bias correction is that the climate model under consideration produces inputs for a bias correction, including a plausible representation of climate change [36]. The origin of bias correction is the model output statistics (MOS) [95] in numerical weather prediction, which applied the prognosis statistical downscaling approach [96]. Due to its simplicity and limited computational cost under a rapidly growing database of multiple global and regional climate model simulations, bias correction has become one of the most important steps in climate impact research [36]. Over the last decade, various methods have been developed for different purposes [80, 85, 86] which were widely applied to post-process climate projections [40, 97-99].

From the literature [36, 92, 100-102], a bias correction is often performed when using climate model projections for local scale impact assessments, and the bias-correction step significantly reduces the bias associated with climate models. Many bias-correction methods, such as simple scaling and additive corrections [103-105], advanced histogram equalization [101, 106, 107], multivariate methods [108, 109], and multivariate quantile mapping bias correction method (MBCn) [108] exist in the literature. Fig. 1.8 [40, 99] shows that by applying MBCn, the average errors between observational data and RCM data for Montreal reduced from 2.78 ℃ to 0.05 ℃ for outdoor air temperature, from 68.3 W/m^2 to 0.1 W/m^2 for global solar radiation, from 0.9 m/s to 0.001 m/s for wind speed, and from 14.5% to 0.01% for relative humidity. Thus, the bias-correction method is one of the most important steps to conduct impact assessments of climate changes by significantly improving the reliability of future projected data.

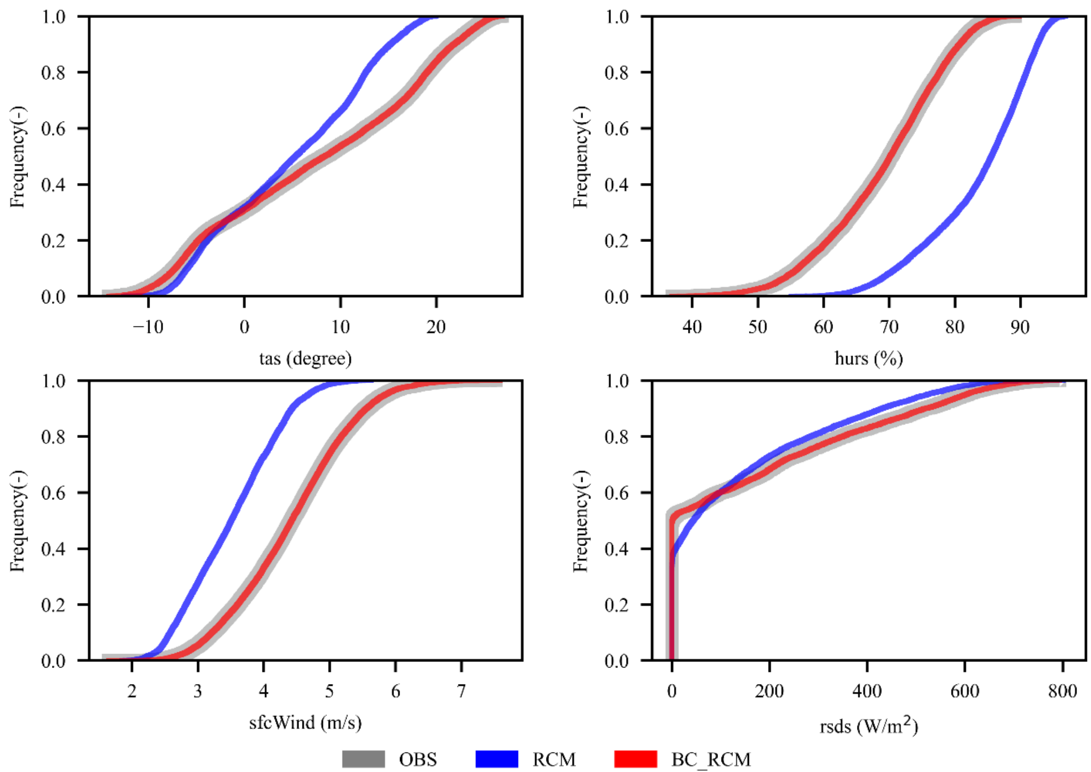

Fig. 1.8 Cumulative distribution function comparison of observational, raw RCM, and bias-corrected RCM data of dry-bulb outdoor air temperature (tas), relative humidity (hurs), wind speed (sfcWind), and global solar radiation (rsds) (City: Montreal; GCM: MPI-M-MPI-ESM-LR; Time periods: 1998-2017) [40, 99].

1.2.4.2 Reference year selection

Due to multiple GCMs and RCMs, considerable uncertainties exist in future climate projections [94]. To account for the uncertainties, ideally, the ensemble of climate projections needs to be considered when performing future overheating assessments. However, this is time-consuming and computationally expensive. Furthermore, climate change assessments are performed over multidecadal timescales, which makes climate projections from multiple GCMs and RCMs even more challenging [110, 111].

The reference year method, also known as, representative year selection method, synthesizing weather datasets, or typical weather year, usually generate one or a few years as the reference to capture aspects of interest from the long-term datasets (decades to few decades) [40]. By applying the reference year data method, studies on assessing future climate impacts could focus on the climate data of the reference year instead of every single year inside the time period of interest, significantly reducing the computational cost as well as repetitive labor work. Table 1.1 is created to show the widely applied reference year selection methods.

Table 1.1 Summary of widely applied reference year selection methods

Name of reference year	**Abbreviation**	**Method**	**Target variable**	**Reference**
Typical Meteorological Year	TMY	This method is developed by selecting 12 months of weather data from a long-term dataset that best represent the typical weather conditions for a location, based on statistical criteria including temperature, humidity, wind speed, and solar radiation.	Temperature, Humidity, Solar Radiation, Wind Speed	[112-118]

Weather Year for Energy Calculations	WYEC	This method is developed by determining the individual month with the average dry-bulb temperature, closest to the long-term monthly average.	Dry-bulb Temperature	[119-122]
International Weather Year for Energy Calculations	IWEC	This method applied a selection process similar to TMY but with different weighting factors.	Temperature, Humidity, Solar Radiation, Wind Speed	[119, 120, 123, 124]
Canadian Weather year for Energy Calculations	CWEC	This method applied a selection process similar to TMY but with different weighting factors.	Temperature, Humidity, Solar Radiation, Wind Speed	[119, 120, 125, 126]
Test Reference Year	TRY	This method is developed by eliminating those years that contain months with extremely high or low monthly mean dry-bulb air temperature until only one year	Dry-bulb Temperature	[125, 127-129]
Design Summer Year	DSY	This method ranks the average dry bulb temperature from April to September of each year and then selects the year that falls in the top 12.5% quartile of the rank (i.e., the 3rd warmest year in a set of 20 years)	Dry-bulb Temperature	[129-132]
Actual Meteorological Year	AMY	This method was created from actual hourly data for a particular calendar year.	Field Measurement Data	[133]

Summer Reference Year	SRY	This method adjusts the TRY of a given site with meteorological data in order to represent near-extreme conditions.	Dry-bulb Temperature	[134]
Reference Summer Weather Year	REWY	This method includes generating historical climate data, developing a heat stress metric for the definition, and characterizing heat events. A modified Standard Effective Temperature (t-SET) considering both environmental and psychological factors was used to generate RSWY for selected Canadian cities.	Temperature, Humidity, Solar Radiation, Wind Speed	[135-137]
Typical Downscaled Year Extreme Cold Yea r Extreme Warm Year	TDY ECY EWY	Typical/extreme year data are selected by identifying twelve typical/extreme meteorological months and combining them as one year of continuous data. For each month, the cumulative distribution function (CDF) of the outdoor air temperatures for each year is compared with the CDF of the outdoor air temperatures from all years. The month of the year with the least absolute difference is identified as the typical month. Extreme cold and warm year data are prepared in a similar way while selecting the month with the least absolute difference. The month with the maximum and minimum difference between CDFs is selected as the extremely warm and cold months, respectively.	Dry-bulb Temperature	[34, 40, 99, 138-141]

The typical meteorological year (TMY) [118] is often used for building energy applications, which is a combination of multiple typical meteorological months (TMM). TMY was widely applied to evaluating building energy performance [112-117] and the overheating assessment [112-117, 142-144]. In comparison, Weather Year for Energy Calculations (WYEC), International weather for energy calculations (IWEC) and Canadian weather year for energy calculations (CWEC) were developed by the American Society of Heating, Refrigerating, and Air-conditioning Engineers (ASHRAE) [119, 120]. The test reference year (TRY) from were intended to capture typical or average aspects of climatic variables of the long-term datasets [125, 127, 128].

There are also reference year methods for assessing overheating aiming to capture extreme summer conditions from long-term data as the reference datasets, like the design summer year (DSY) from Levermore and Parkinson [130], actual meteorological year (AMY) from Hong, et al. [133], summer reference year (SRY) from Jentsch, et al. [134]. For a cold climate, such as Canada, several studies have focused on overheating assessment in different cities [135, 136, 145-147]. Baba and Ge [146] evaluated the performance of existing buildings under a current extreme year and projected future climates. Studies from Laouadi [135-137] developed a new reference year method called reference summer weather years (RSWY) to evaluate indoor overheating. This method includes generating historical climate data, developing a heat stress metric for the definition, and characterizing heat events. A modified Standard Effective Temperature (t-SET) considering both environmental and psychological factors was used to generate RSWY for selected Canadian cities. This method was also applied to evaluate future climate change impacts on indoor overheating [148].

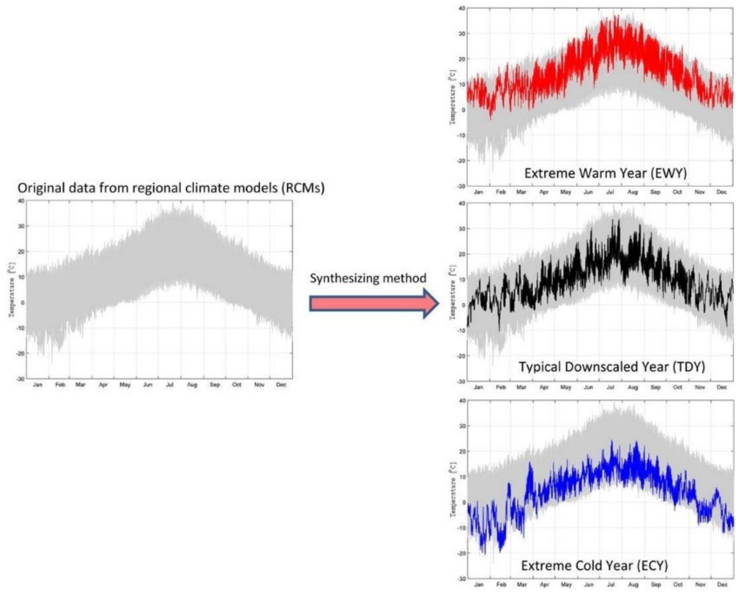

Fig. 1.9 Reference year method by Nik [34] generating extreme warm year, typical downscaled year, and extreme cold year

Recently, Nik [34] developed an approach for selecting reference years for climate change impact assessment on buildings where three reference years, as shown in Fig. 1.9: typical downscaled year (TDY), extreme cold year (ECY), and extreme warm year (EWY), were selected to capture the typical, coldest and warmest conditions within a climate time-series. Typical/extreme year data are selected by identifying twelve typical/extreme meteorological months and combining them as one year of continuous data. For each month, the cumulative distribution function (CDF) of the outdoor air temperatures for each year is compared with the CDF of the outdoor air temperatures from all years. The month of the year with the least absolute difference is identified as the typical month. Extreme cold and warm year data are prepared in a similar way while selecting the month with the least absolute difference. The month with the maximum and minimum difference between CDFs is selected as the extremely warm and cold months, respectively. They are combined to prepare the extremely cold and warm year data.

This method selects the limited number of hourly weather datasets from RCMs considering the climate uncertainties, extremes, and variations in different time scales without weighting weather parameters in time series. The selected three reference years are found to efficiently capture the range of climatic projections and building energy response from an ensemble of regional climate projections. The approach has since been applied in many studies to prepare reference datasets for building energy and building hygrothermal applications [138, 139, 141, 149]. More recently, Nik [34] method was also applied to the future projected changes in indoor thermal comfort and degree-days evaluation of a European city [71]. It is found that cooling degree days increase by 45% for typical weather conditions and even up to 500% for an extremely warm July from one 30-year period to another. Zou, et al. [40] evaluated the reference year selection method based on future climate datasets to assess both outdoor and indoor overheating in the future in three Canadian cities. Their studies [40, 99] found that the reference year selection method could efficiently capture maximum and minimum monthly outdoor and indoor overheating conditions as the upper and lower boundaries of future overheating conditions.

1.2.5 Indoor and outdoor climate simulations

After future climate projection mentioned in the above sections are obtained as the boundary conditions, it was then be applied to the indoor environment simulations (Section 1.2.5.1) and outdoor climate simulations (Section 1.2.5.2) for evaluating the urban overheating problem.

1.2.5.1 Indoor climate simulation

Building thermal models can be developed based on building energy simulation models that include the heat transfer processes or based on heat, air, and moisture transfer (HAMT) analysis of the building envelope and indoor environment. With the boundary conditions from building thermal models, the detailed indoor airflow and temperature distribution can be simulated with

CFD analysis or other alternatives. By calibrating and validating the models based on monitored indoor climate data or thermal comfort surveys, building energy models such as EnergyPlus [150], ESP-r [151], TRNSYS [152], and Pleiades-Comfie [153] can be used to study the indoor thermal condition [154-156]. Because ventilation and infiltration produce heat transfer related to airflows, airflow network models are often integrated with the building energy models to develop combined thermal and airflow calculations [157-164]. In such models, the thermal condition in a zone is considered uniform. Thus, a thermal zone should be divided into smaller cells to capture the spatial variations of indoor temperature in a room [165]. IDA Indoor Climate and Energy (ICE) is another tool widely used to simulate indoor climate, which can model indoor air flows, thermal conditions, and energy performance [166-169]. In addition, it can model buildings with multiple zones and variable time steps [170].

The hygrothermal analysis takes into account the HAMT of building envelope and indoor spaces and, therefore, can specifically model the indoor thermal conditions under the effect of the outdoor climate. Whole building hygrothermal models such as WUFI+ [171] and DETECt [172] were developed by integrating HAMT through the building envelope with indoor heat and moisture balances [173]. Simplified indoor climate models were also developed to predict the dynamic indoor situation in response of outdoor climate and building operation. Building an indoor model can be developed based on the analytic solution of Fourier’s equation to consider the heat transfer, but the moisture was ignored [174, 175]. The benefit of the simplified building physics models is that they could be continuously recalibrated with the operation of buildings to capture the time-dependent change of building characteristics for more efficient indoor climate control [176].

The surface temperatures outputted from building thermal models can be used as boundary conditions for the CFD to simulate air movements and temperature distribution [166, 177], and the results can then be validated with measured indoor thermal data. This way, indoor climate distribution can be predicted and evaluated in different usage conditions such as seasons, occupancy densities, and air diffusers [178]. Considering the computationally time-consuming CFD, an alternative simplified way to simulate indoor air temperature distribution is based on the contribution ratio of indoor climate (CRI), which indicates the individual impact of all factors and can achieve similar accuracy with CFD, making the simulation more time efficient [179, 180]. Modelica-based room thermal modeling is another way to simulate the detailed indoor climate, which can consider the view factors for arbitrary polygon for radiation calculation, vertical temperature gradient, and airflow under the effect of other room features [181, 182].

Data-driven methods like Artificial neural networks (ANNs) were also used to simulate the indoor climate [183-186]. Because of unclear connections to physical parameters, this method had limited usage, which did not apply to renovated buildings with modified thermal characteristics or different building types. The parameters of Linear Time Invariant (LTI) models can be determined with physical data, which was suitable for predicting the indoor climate of building insensitive to short-term disturbances [187].

The indoor climate and overheating problems under the impact of climate change were evaluated in previous research, and consistent conclusions about the increased indoor heat stress were made. Zou et al. [40, 99] proposed and evaluated a new reference year selection method in terms of typical and extreme reference years based on future climate datasets to assess indoor overheating in the future, considering three Canadian cities. It is found that the reference year selection method could reasonably capture typical and extreme indoor overheating conditions. In their study, overheating hour is used to evaluate indoor and outdoor overheating, which is defined as the number of hours when the air temperature difference between the baseline and simulated temperature is greater than or equal to one degree following the concept of hours of exceedance from the guideline of CIBESE TM52. Through the simulation of an archetype building model of a typical single-detached Canadian home, they found that due to climate change, average monthly indoor overheating hours typically increase by around one time until the mid-term future (2041-2060) and by around two to three times (even up to nine times for some scenarios) during the long-term future (2081-2100).

Dodoo [188] studied the overheating risk and indoor thermal comfort of a modern multi-story residential building in Sweden and found that without cooling intervention, the overheating hours and Predicted Percentage of Dissatisfied (PPD) in the living area of the building increased significantly under the future climate scenarios. Hosseini et al. [140] simulated the indoor climate of residential buildings in Sweden under climate change and microclimate effects. The buildings were built before 1930s and partially renovated. For the building with a cooling system, 17% rise in cooling degree-day (CDD) and 25% increase in daily peak cooling load on an extremely warm day were found when considering microclimate. For the building without cooling system, the overheating hours would increase by 140% in the future climate. Lei et al. [189] studied the current and future indoor overheating situation in bedrooms of heritage apartments in China. Without cooling intervention of the buildings, at least 41% increase in overheating hours was found in 2050 than the current climate. Fiorito et al. [190] evaluated the thermal comfort in naturally ventilated historic buildings in Italy under current and future climates. They found that the discomfort levels would not be acceptable in the 2050 and 2080 scenarios because of the rising temperature caused by climate change. Escandón et al. [191] studied the overheating situation of social housing stock in Spain. It was found that by 2050, without upgrading the buildings, according to the Chartered Institution of Building Services Engineers (CIBSE) criteria, 100% of social housing would be overheated due to global warming. Rahif et al. [192] assessed the discomfort in a nearly zero-energy dwelling in Brussels and found that overheating risk would increase to 528% by the end of this century without new cooling intervention.

1.2.5.2 Outdoor microclimate simulation

In addition to the climate data downscaled at a regional to city scale, the future urban climate could be directly simulated under a microclimate scale through some detailed models such as CFD based models. These models provide the capacity to reproduce the microclimate in a city district, neighborhood, or street canyon.

CFD models can be coupled with solar radiation models, heat conduction and moisture transfer models so that the physical environment in the city can be resolved in detail, scaled from the buildings to the neighborhood, even to the entire city. Therefore, the computational domain should be carefully defined to avoid oversimplification. The environmental fluid flow simulation [193, 194] requires professional expertise. The best practice guidelines (BPG) and related studies have been extensively reviewed [13, 195]. The most well-known BPGs come from the Architectural Institute of Japan (AIJ) [196] and the European Cooperation in Science and Technology (COST) [197], which specify the requirements of how the computational domain, boundary conditions, wind profiles, and turbulence models should be defined to ensure the quality of the simulation. Blocken, et al. [194] also raised a framework to use CFD to design and optimize pedestrian wind comfort. To consider the thermal effects in urban areas, the grid size of the microclimate models can be simulated down to a sub-meter scale, which allows researchers to resolve physical phenomena in detail. To that end, Tsoka, et al. [198] summarized the publication trend and global distribution of the studies using ENVI-met, which reported 280 papers before March 2018, most of which came from Europe and Asia. The studies also cover a wide range of Koppen climate zone types.

One of the challenges of microclimate modeling is that urban climate models are normally oversimplified [199]. CFD enhances predictions within the lower segment of the Atmospheric Boundary Layer (ABL), specifically in the Urban Boundary Layer (UBL) and Urban Canopy Layer (UCL), where the majority of human activities occur [5, 6, 200]. Mesoscale models, such as the WRF model, despite incorporating parametrization schemes for UCL effects, struggle to accurately predict small-scale and localized effects caused by buildings and other structures. To address this issue, CFD, with its high-resolution grid, is frequently integrated with mesoscale models or field measurements to precisely simulate microscale (i.e., local scale) phenomena. Martilli [201] conducted a comprehensive review on statistical and dynamical downscaling including CFD. The paper [201] focuses on the positive feedback that occurs among experimental investigations and numerical modeling in mesoscale urban studies, exploring the current state-of-the-art techniques to parameterize urban-induced dynamical and thermal effects in mesoscale models and their future developments. More recently, Ricci, et al. [202] presented a novel method for downscaling from mesoscale using onsite measurements to microscale by employing CFD models. The static downscaling approach, as outlined in this chapter, incorporates onsite measurements into the UCL by determining transfer coefficients, which are calculated using 3D steady RANS simulations for two distinct spatial extents of the urban texture. This innovative technique facilitates accurate wind flow prediction within the UCL and has been thoroughly verified against field measurements in a realistic UCL environment.

Besides, it is necessary to consider the various environmental elements in the study area, such as anthropogenic heat emission [203], vegetation [204], and water bodies (blue infrastructure) [205].

Despite these challenges, case studies in existing publications further demonstrate the capability of CFD models. For example, Antoniou, et al. [206] performed an unsteady-state RANS (Reynolds-averaged Navier–Stokes model) simulation for a highly heterogeneous district in Nicosia, Cyprus, over four days in July 2020. The simulation was validated by a high-resolution experimental dataset with measured outdoor air temperature, wind speed, and surface temperature in the same area. Mortezazadeh, et al. [39] evaluated the 2017 heatwave in Montreal by coupling WRF and CityFFD and investigated the impacts of three canyon aspect ratios and three anthropogenic heat regimes, i.e., surface temperature differences, on the boundary conditions setups. Their study shows the importance of microclimate simulations for regional climate models when studying urban heatwaves.

The use of CFD models to simulate the whole city is limited because the number of mesh grids required would be enormous to capture the city's geometry with all the buildings. Some other challenges are known as preserving the mesoscale meteorological effects during the CFD simulation and upscaling the CFD model for a much larger area under the mesoscale meteorological impacts [207]. Also, the availability of multiple years of future climate data raises a new challenge regarding how to simulate the “climatological” time periods of 30 years and longer with limited computing resources which raises the need of the reference year method. In recent days, some new research adopted Fast Fluid Dynamics (FFD) to run the CFD simulation on a high-end video card (GPU) to accelerate the simulation [208] and a new software focusing on the urban-scale CFD simulation is developed named CityFFD [39, 208-212]. They adopted a semi-Lagrangian approach with high-order temporal and spatial schemes [210], which is feasible for coarse grid meshes and large timesteps while ensuring accuracy.

The geographic information system (GIS) allows users to create, manage, analyze, and map different data types, as shown in Fig. 1.10. GIS has become a critical tool in modeling detailed characteristics of a city. Vuckovic, et al. [213], [214] first adopted the GIS tool to collect the urban environment's salient geometric and physical features in Vienna, Austria. Two representative locations were selected in the city, including the most developed part of the city and an abandoned industrial site on the periphery of the urban center, to perform microclimate simulations in ENVI-met. Demuzere, et al. [215] used the World Urban Database and Access Portal Tools (WUDAPT) platform to combine the building and district morphology from GIS and remote sensing information to classify the local climate zones (LCZ) for Al Ain City in the United Arab Emirates. Six districts of different types were selected for microclimate evaluation in ENVI-met, and the simulation was validated with site measurements. The results exhibited a similar temperature pattern shown by the LCZ map (Fig. 1.11).

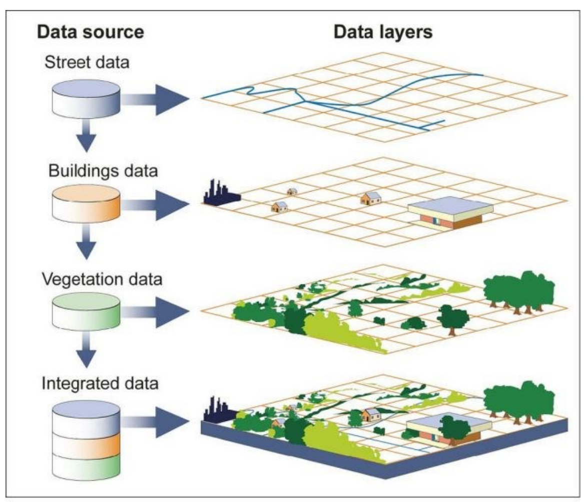

Source: GAO.

Fig. 1.10 Example of geographical information system (GIS) mapping in environmental studies [216].

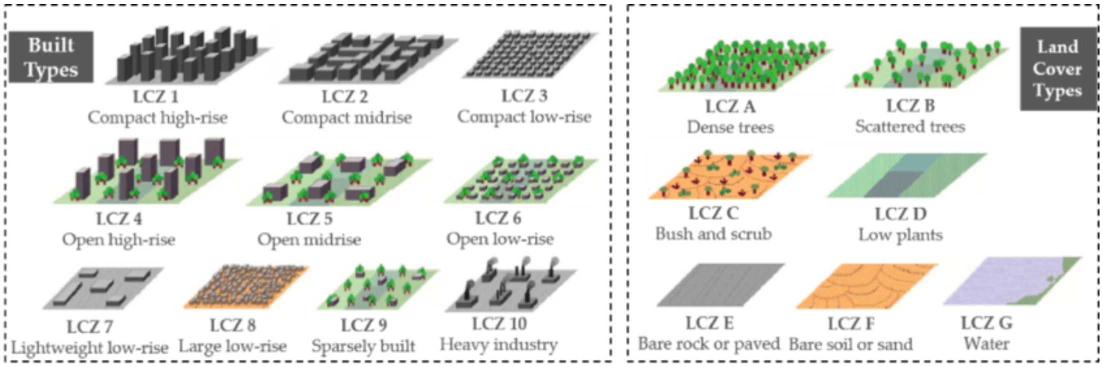

Fig. 1.11 The scheme of the local climate zone [217].

The geometry of the urban canopy can significantly affect urban microclimate conditions, as illustrated in a review conducted by Shafaghat, et al. [218]. To solve this problem, Pađen, et al. [219] developed a tool to automatically reconstruct 3D city models for use in computational fluid dynamics simulations and ultimately generate geometric models without errors to enhance the accuracy and efficiency of fluid dynamics simulations. This research introduces innovation through the significant reduction in preparation time for error-free geometry models, while also ensuring a high degree of automation and controllability within the workflow process.

Allegrini, et al. [220] assessed the performance of six different urban morphologies on the climate in Zurich, Switzerland. The thermal boundary conditions of the buildings are determined by coupling with a building energy model (BES), and the short and longwave radiation convective/conductive heat transfer of the surfaces is also considered. They found a more complex geometry may lead to a lower facade temperature because of the shading effect, which affects the local microclimate and the cooling and heating demand of buildings. This CFD and BES coupled simulation method is also used to evaluate the heat flux from the building in the microclimate that is affected by the building morphology and the urban wind conditions [221, 222]. Where they found that the heat flux from the upstream building blocks may affect the downstream environment.

This effect is less important when low wind speed and the buoyancy effect mainly drive the flow. To evaluate the impact of the variation of building heights and [222] designed generic urban geometry configurations, they found the building height topologies may not change the mean temperature in the whole area, but the distribution can vary a lot which may cause a local overheating effect. To further verify their study in a real urban configuration, Allegrini and Carmeliet [221] selected a specific district in Zurich with relatively dense buildings to evaluate the building geometry, material, and the wind and buoyancy effect on urban microclimate.

CFD models can also take the boundary conditions from the Regional Climate Modelling data and simulate the sub-grid environment. Zheng, et al. [223] adopted a coupled WRF-CFD simulation to analyze the airflow and pollutant dispersion on a university campus in Shenyang, China. The wind and turbulence information simulated in WRF has been used as the initial and boundary conditions of the CFD model to perform detailed aerodynamic analysis. In contrast, the thermal environment was not simulated and analyzed in this study. Mortezazadeh, et al. [39] explored the method to integrate WRF simulation results in a CFD model to reproduce the thermal environment in the Greater Montreal Area during a heatwave in 2017. Berardi, et al. [224] selected two vulnerable locations from the Greater Toronto Area (GTA), and the results from the WRF simulation are used as inputs to the microclimate model, ENVI-met, to test the effectiveness of greenery scenarios. They found that by increasing the tree canopy in the local area, the temperature can be reduced by 0.5°C and 1.4°C at the two locations. Similarly, to study a period of extreme heat in San Jose, California, McRae, et al. [225] also integrated WRF results with ENVI-met simulations to measure the cooling effects of vegetation.

There are also attempts to incorporate the climate data from the regional climate model or CFD simulation for the whole building simulation. Wong, et al. [226] developed a multiscale simulation framework to couple WRF, OpenFOAM, and EnergyPlus for evaluating the microclimate and the building energy performance of the National University of Singapore campus. The method has been verified to estimate the energy saving of the buildings with the urban heat island measures applied in the microscale model. Shu, et al. [147] proposed using high-resolution convection-permitting climate data for city-scale overheating assessment. The data was provided to a building energy model using EnergyPlus to perform the indoor overheating assessment. It was found that the conventional regional climate model (RCM) in a coarse resolution at 25 km may highly underestimate the overheating in cities.

Resolving the interactions between global and urban climates is necessary to generate information on a scale relevant to urban overheating. The ability to produce detailed information regarding global climate change and urban areas will aid practitioners in implementing urban overheating mitigation strategies. Previous studies have done so by coupling large-scale climate models with microscale CFD models to study the local climate in extremely high resolution [227]. For example, Tumini and Rubio-Bellido [228] evaluated the climate change effect on the microclimate of a park square with its surrounding buildings in Concepcion, Chile. The future climate was obtained through a "morphing" method [131, 229] regarding the GCM scenario of A2 'medium-high' Greenhouse Gas (GHG) emissions. The microclimate simulation is conducted in ENVI-met, and an increase in the average temperature of 1.02°C, 1.60°C, and 2.70°C was found for 2020, 2050, and 2080, respectively. However, statistical downscaling methods such as that implemented by Tumini, et al. [230] are with limitations, as they can only be calculated based on historical observations and, therefore, cannot account for the potential variability in future climates [231].

Consequently, to generate data necessary to study climate change, Conry, et al. [232] used WRF to dynamically downscale climate projections in Chicago produced by the Community Climate

System Model. Subsequently, from a spatial resolution of 0.333km, the data is used to drive an ENVI-met model with a grid resolution of 2 m to study the pedestrian level thermal comfort. The added benefit of dynamically downscaling to such a degree provides a robust source of spatially averaged initial conditions for the microscale CFD model.

Undoubtedly, climate change will significantly impact the urban environment, building energy consumption for heating and cooling [233], air pollution, and human health and well-being. For instance, many researchers [34, 234-236] analyzed the change in building energy use due to climate change under various global warming scenarios. By gradually dynamically downscaling GCM climate data to a regional scale and finally to a neighborhood scale through CFD models, climate data suitable for building simulations can be produced. Subsequently, this data is input to EnergyPlus to calculate heating and cooling loads for buildings in Madrid, Milan, and London, where results indicate a relative decrease in heating energy demand while a significant increase in cooling should be expected. A similar procedure is used by San José, et al. [237] to generate climate data to study the effects of climate change on air pollution and human health in London.

Additionally, the downscaled microscale data was validated against existing air quality stations in the city, which showed good agreement between the model and observed data. Subsequent analyses showed that concentrations of atmospheric pollutants would not change significantly in the future. However, the rise in temperatures is a significant concern regarding human morbidity.

1.2.6 Overheating evaluation method

Evaluating overheating risks inside and outside buildings requires the determination of appropriate overheating criteria [27, 40, 99, 238, 239]. There have been many reviews focusing on the various aspects of overheating criteria which provide a good scope when evaluating overheating under different scenarios [4, 27, 28, 30, 32]. This section of the review will cover the most commonly employed methods for assessing indoor and outdoor overheating, and also outline crucial criteria for studying overheating in future research.

The *PMV/PPD* thermal comfort model [240] (*PMV* stands for predicted mean vote and *PPD* stands for predicted percentage dissatisfied) developed by Fanger and the two-node model developed by Gagge [241], [242] is widely applied to the overheating assessment. According to various standards such as EN [243], ISO [244], ASHARE [245], and CIBSE [246], different *PMV/PPD* static comfort limits were suggested under different building operation types. Due to the difficulty of measuring *PMV* in various indoor environments, some standards convert the *PMV/PPD* ranges into operative temperature scales. In CIBSE TM52 [247], the *PMV/PPD* ranges were based on specific relative humidity (=50%), air velocity (<0.1m/s), metabolic rate (1.2 met), and clothing factor (0.5 clo for summer). Accordingly, the temperature thresholds of the residential building are determined as 26 °C and 28 °C for the living room and bedroom, respectively. With the threshold temperature, the overheating risks could then be evaluated by the hours of exceedance [247], overheating degree hour [248, 249], and heat exposure index [250]. Besides, Robinson and Haldi [251], [252] also developed a mathematical model for predicting overheating risk under various environmental conditions, considering the analogy between the charging and discharging of human's tolerance to overheating stimuli. Compared with the data from the field survey, the application of this analytical model provided encouraging results.

Based on Hamdy, et al. [20] and Rahif, et al. [27], a climate change-sensitive overheating evaluation method based on Indoor Overheating Degree, Ambient Warmness Degree (AWD) and Overheating Escalation Factor was proposed for a multi-zonal and climate change-sensitive overheating assessment. The Indoor Overheating Degree index is the summation of the temperature difference between the indoor operative temperature and a preferred comfort temperature averaged over the total number of zonal occupied hours, as shown in Equation (1.1).

$$IOD = \frac{\sum_{z=1}^{Z}\sum_{i=1}^{N_{occ}(z)}[\left(T_{fr,i,z} - TL_{comf,i,z}\right)^{+} \times t_{i,z}]}{\sum_{z=1}^{Z}\sum_{i=1}^{N_{occ}(z)} t_{i,z}} \tag{1.1}$$

Where, z is the building zone counter, i is the occupied hour counter, t is the time step (typically it is 1 hour), Z is the total number of zones in a building, $N_{occ}(z)$ is the total occupied hours in a given calculation period, $T_{fr,i,z}$ is the free-running indoor operative temperature at the time step i in the zone z, and $TL_{comf,i,z}$ is the comfort temperature limits at the time step i in the zone z, $\left(T_{fr,i,z} - TL_{comf,i,z}\right)^{+}$ is the positive differences between $T_{fr,i,z}$ and $TL_{comf,i,z}$ and only positive differences are taken into summation. Both static and adaptive temperature limits can be used as the thresholds ($TL_{comf,i,z}$). The IOD allows for considering the occupancy profiles of each zone, making it possible to reflect the occupant behavior and adaptation opportunities based on the zone type by applying zone-specific comfort models. The disadvantage of IOD is its neglect of the personal and environmental factors in determining thermal comfort since it is only calculated through the operative temperature.

The Ambient Warmness Degree (AWD) averages the cooling Degree hours calculated for a base temperature of 18 °C during the summer hours when the outdoor air temperature is not lower than 18 °C. It could represent the severity of outdoor warmness. The equation of AWD is shown below:

$$AWD = \frac{\sum_{i=1}^{N}[\left(T_{a,i} - T_{b}\right)^{+} \times t_{i,z}]}{\sum_{i=1}^{N} t_{i}} \tag{1.2}$$

$$\alpha_{IOD} = \frac{IOD}{AWD} \tag{1.3}$$

Where, $T_{a,i}$ is the outdoor dry-bulb air temperature, T_b is base temperature set at 18 °C, N is the number of occupied hours such that $T_{a,i} \geq T_b$ in the summer season, and t is the time step (1 h), and $\left(T_{a,i} - T_b\right)^+$ is the positive difference between $T_{a,i}$ and T_b. Solar radiation is not considered in AWD, which means the same AWD index will be obtained under two different climates with the same temperature files but different solar irradiance levels. By coupling the IOD index and AWD index, the Overheating Escalation Factor (α_{IOD}) was established as shown in Equation (1.3). The $\alpha_{IOD} > 1$ means that indoor thermal conditions get worse when compared to outdoor thermal stress, and on the contrary, $\alpha_{IOD} < 1$ means that the building could suppress some of the outdoor thermal stress. Thus, the α_{IOD} could show the sensitivity of a building to the progressive rise in outdoor air temperature due to the impact of climate change.

To be concluded, for evaluating both indoor and outdoor overheating, the threshold temperature of the residential building is the most widely used standard for evaluating overheating not only because it is convenient and easy to apply, but also it could be easily transformed into other indexes to quantify the overheating risk under different scenarios, such as hours of exceedance, overheating degree hour, and heat exposure index. The combination of overheating criteria of Indoor Overheating Degree, Ambient Warmness Degree (AWD), and Overheating Escalation Factor has a more systematic understanding of both indoor and outdoor overheating and could reveal the impacts of climate change. However, due to its complexity, this criterion only suits limited scenarios and cannot be applied to urban-scale overheating studies which will involve complex outdoor and indoor climates.

Various overheating evaluation methods can be applied at different scales such as building, neighborhood, or city level. The choice of scale depends on the specific goals and requirements of the study, as well as available resources and data. Applying methods at the building scale allows for detailed assessments of individual building performance and tailored design solutions but can be time-consuming and may not capture broader urban microclimate interactions [4, 40, 99, 253-255]. The neighborhood scale considers interactions between buildings and the surrounding environment, better representing the actual urban microclimate experienced by occupants, but may require more computational resources and provide less detailed assessments of individual buildings [256-259]. The city scale offers a comprehensive understanding of the urban heat island effect and helps prioritize large-scale heat mitigation strategies, but requires significant computational resources and may not account for local variations in microclimate and building performance [147, 260-265]. Ultimately, each scale provides unique insights into overheating, and a combination of scales can help develop a more comprehensive understanding of the issue and inform effective mitigation strategies.

1.2.7 Conclusion

This chapter presents a systematic review of the application of climate model projections for future indoor and outdoor overheating impact assessments, divided into four primary stages. Several prominent research gaps have been identified and are summarized as follows for each stage:

- Future climate data generation: Although progress has been made in generating future climate data using downscaling methods, challenges remain in conducting high-resolution, multi-decadal urban climate simulations under various greenhouse emission scenarios. Moreover, the accuracy and versatility of statistical and dynamical downscaling methods are limited by their reliance on historical data and high computational costs, respectively.

Statistical-dynamical methods offer a promising compromise, allowing urban environments to be physically parameterized while maintaining versatility through advanced statistical and data-driven modeling techniques.

- Future climate input preparation: Bias correction and reference year data methods are crucial for improving the reliability of projected data and streamlining climate change impact assessments. However, there is a lack of consensus on the weighting of climatic variables in reference year data methods. Using thermal comfort indices like SET or UTCI instead of individual climatic variables could be a potential solution.
- Indoor climate simulation: Neighborhood-scale urban climate modeling is essential for studying future overheating. Challenges include modeling spatially dynamic indoor climate and incorporating real occupancy patterns in building energy models.
- Outdoor climate simulation: Simplifications in computational fluid dynamics (CFD) models raise concerns about accuracy and validity. Future research should focus on quantifying the sensitivity of input parameters to better understand the impacts of these simplifications.
- Overheating evaluation methods: Although widely used standards for outdoor and indoor overheating assessments exist, they fail to consider social and economic vulnerabilities. As specific populations, such as the elderly, poor, and minority groups, are disproportionately affected by extreme heat events, using thermal-only overheating standards is insufficient. A more comprehensive approach should incorporate social-economic components, such as the percentage of vulnerable populations and the accessibility of heat mitigation methods.

1.3 Challenges and Research objectives

The aim of this thesis is to evaluate the effects of climate change on multiscale urban overheating and to pinpoint outdoor heat-vulnerable zones across varying scales. There are three key challenges of this study:

1. **Future climate data (low-resolution)** VS **Outdoor heat stress or thermal comfort (high-resolution)**

   First of all, outdoor thermal comfort or heat stress evaluation requires fine resolution microclimate data. However, long-term future urban climate data are normally under global or regional scale which are too coarse for thermal comfort evaluation.

2. **Future climate data (long-term)** VS **CFD simulation (short-term)**

   To resolve the first conflict, the assessment needs to be conducted under micro-scale which requires CFD simulation. Then, the second challenge appears which is using long-term climate data as CFD simulation input. Due to the limitation of computational resource, CFD simulation could not be conducted for a long time period.

3. **Whole city urban climate (large-scale)** VS **CFD simulation (micro-scale)**

   Besides, CFD simulation could not be conducted for an entire city with a promising accuracy. Thus, another challenge would be which location should be chosen for conducting CFD simulation to represent general urban overheating. It is important to determine the best location which could represent the urban climate in general.

In alignment with these challenges, the objectives of the study have been outlined:

- Develop a comprehensive framework that integrates the application of climate model projections specifically tailored for evaluating future outdoor overheating impacts. This framework will provide a systematic approach to assess outdoor urban overheating under the impacts of climate changes;

- Address the reliability concerns related to future climate data through a statistical method. This method could capture the bias between observational and simulated climate data for current time period and then apply it to the future climate data for improving the reliability;
- Develop a statistical method to select typical and extreme future climate inputs from long-term climate data for CFD simulation. This method could significantly decrease the computational cost and labor work when simulating long-term climate data while keeping the representative features of future climate conditions by selecting typical and extreme scenarios;
- Develop a statistical method to select typical and extreme locations from entire urban area for CFD simulation. This method could significantly decrease the computational cost and labor work when simulating local urban microclimate while keeping the representative features of urban climate conditions by selecting typical and extreme scenarios;

To address the challenges and objectives above, the focuses of the following chapters are listed as below:

- **Chapter 2** – Representative future climate data for regional urban overheating assessment: This chapter applied a reference year selection method in terms of typical and extreme reference years based on future climate datasets for assessing regional urban overheating of three Canadian cities, Montreal, Toronto, and Vancouver among 2010s, 2050s, and 2090s. This chapter contains 1) Raw climate data acquisition at the mesoscale through GCM-RCMs, 2) Data processing through bias correction for improving the reliability of climate data, 3) Regional urban overheating assessment with temperature thresholds.

- **Chapter 3** – Microscale urban overheating assessment using representative future climate data through CFD simulations: This chapter assesses the effects of climate change on outdoor thermal comfort in downtown Montreal using CityFFD-CityBEM co-simulations through steady-state (Universal Thermal Climate Index - UTCI) and dynamic (Discomfort Capacitor Model - PDISC) outdoor thermal comfort models under both typical (TDD) and extreme warm (EWD) future climate scenarios.
- **Chapter 4** – Representative spatial and temporal method for assessing broader spatial and temporal scale future urban overheating: This chapter developed a representative location method to select typical and extreme locations with climatic outputs from WRF simulation of a historical heatwave. With the representative locations selected by representative location selection method, CFD simulations were performed to assess the climate change impacts on representative urban overheating using climate input of TDD and EWD from reference year method.

The framework of this thesis is shown as follow which is developed to evaluate urban overheating under regional, neighborhood scale, and neighborhood scale representing the whole city.

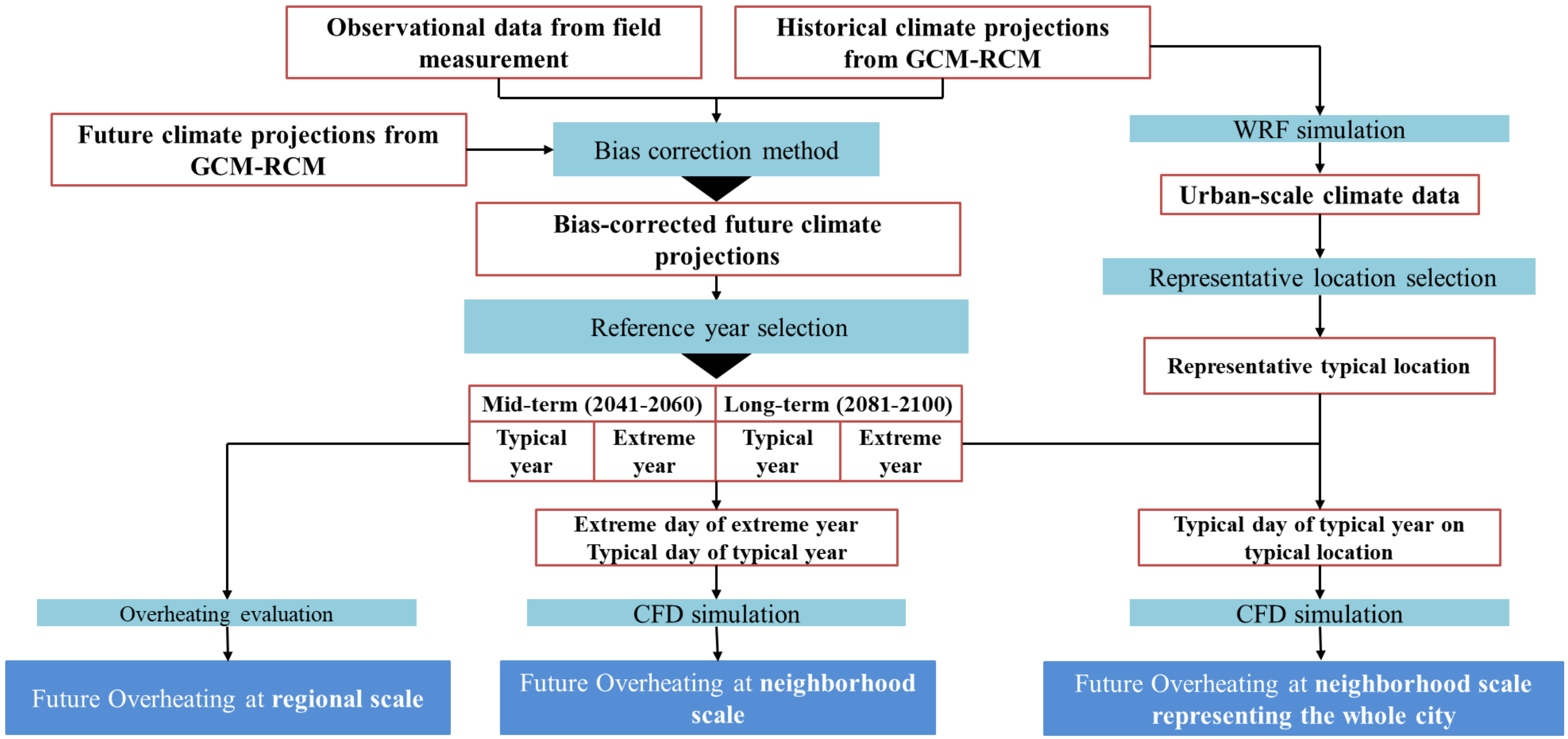

Fig. 1.12 Framework of the thesis

Chapter 2

Assessment of future overheating conditions in Canadian cities using a reference year selection method

This chapter is prepared based on published paper: Assessment of future overheating conditions in Canadian cities using a reference year selection method.

Abstract

Climate change has led to prolonged, more frequent, intense, and severe extreme weather events, such as summertime heatwaves, creating many challenges on the economy and society and human health and energy resources. For example, the 2010 and 2018 heatwave in Quebec, Canada, resulted in about 280 and 93 heat-related deaths, and there were around 500 fatalities due to overheated indoor environments in 2021 around entire Canada. Therefore, it is imperative to understand and evaluate the overheating conditions in buildings, for which selecting suitable future reference weather data under climate change is one of the first critical steps. This study evaluated a reference year selection method in terms of typical and extreme reference years based on future climate datasets to assess both outdoor and indoor overheating in the future. The future climate data were collected from the Coordinated Regional Downscaling Experiment (CORDEX) program. Three Canadian cities (Montreal, Toronto, Vancouver) were selected for the overheating evaluation during three selected periods (2001-2020, 2041-2060, 2081-2100). The CORDEX climate projections were first bias-corrected by the multivariate quantile mapping correction method with the observational data. Then, the typical and extreme reference year data were generated as well as climate data from the design summer year for comparison. The performance of the reference year selection method was evaluated by comparing the maximum, minimum, and average overheating hours for the 20-years data of each period. This study demonstrates that the multivariate quantile mapping bias correction method can improve the reliability of future climate data making it one of the most important steps for any future weather projection study. Besides, the reference year selection method could efficiently capture maximum and minimum monthly overheating hours providing the upper and lower boundary of possible outdoor and indoor overheating conditions. In contrast, neither the severest nor the typical monthly outdoor and indoor

overheating conditions could be predicted by the design summer year method. Finally, owing to the effects of climate change, average monthly overheating hours normally increase by around one time (from 50% to 150%) until the mid-term future (2041-2060) and by around two to three times (even up to nine times for some scenarios) during the long-term future (2081-2100).

Keywords: Climate change; future projection; bias correction; reference year data; urban overheating

2.1 Introduction

Due to greenhouse gas emissions, the global climate system has been significantly affected, which resulted in more intense and frequent extremely hot outdoor conditions in recent years all around the world [20, 27, 90, 143, 266]. Human daily life was affected by these extreme weather conditions in diverse aspects, including economy, health, society, energy, and infrastructure systems [5, 6, 266, 267]. In 2003, Europe experienced one of the hottest summers in the past 500 years with more than 30000 deaths [17, 18] and record-high temperatures of 20–30% above the average of June to mid-August [19]. In the Netherlands, around 2000 heat-related deaths occurred during summer with a maximum temperature of 35 °C [20]. The 2010 heatwave in Quebec, Canada, resulted in a significant increase of 33% in the crude death rate (about 280 extra deaths) [21] and the 2018 heatwave in Quebec caused 93 deaths. Although both outdoor and indoor overheating has garnered much attention during recent years in Canada, the most recent heatwave in 2021 still caused about 500 deaths across the country [22]. As a consequence of global warming, the frequencies, magnitudes, and intensities of heat events in Canada, and indeed around the globe, are expected to keep increasing in the future [25, 26]. It is expected that the deadly heatwaves would occur about 60 days annually in the mid-latitudes and affect 48%~74% of the world's population by 2100 [3].

Building environments provide shelters from weather extremes and ensure the quality of life for residents [268, 269]. This has been greatly challenged in recent decades [147, 270]. Although there are limited studies on the epidemiological evidence that high-temperature exposures indoors contribute to adverse health effects [271, 272], it could be self-evident that the above-mentioned heat-related deaths were not only caused by the intolerable outdoor conditions but also the inability of buildings to moderate extreme temperatures indoors [273]. It has also been reported that exposure to elevated indoor temperatures reduces the ability of a human body to recover from outdoor heat stress [274, 275], causing sleep fragmentation [276, 277], poor work performance [278], and possibly impairing the mental health [279, 280].

Free-running residential buildings are one of the most vulnerable building types to the risks of overheating [281]. There have been many studies assessing indoor conditions of buildings across various countries and climate zones, such as the United Kingdom [282-284], the Netherlands [20, 285, 286], Sweden [287, 288], and Canada [145, 146, 148] in respect to temperate climates, Honduras [289], Taiwan [265], and Hong Kong [143, 290] for tropical and subtropical climates. Most previous studies focused on existing overheating conditions [135, 143, 283, 288, 289]. In contrast, increasing attention started towards the future overheating scenarios [20, 287, 290], and the prediction of future overheating effects relying on building simulation models with current and future projected climatic conditions.

An essential part of future overheating assessments is to prepare projected future climate files as inputs to a building simulation model. They are usually from global climate models (GCMs), including an atmospheric model, ocean model, land surface scheme, and a sea ice model [34]. However, the major challenges of using GCMs are various existing climate models and multiple greenhouses gas emission scenarios creating many options and complexities for users to choose from. For the Coupled Model Intercomparison Project Phase 5 (CMIP5), forty GCMs from 20 research groups were proposed and publicly available [35]. The Intergovernmental Panel on Climate Change (IPCC) has four Representative Concentration Pathways (RCPs) that represent different future greenhouse gas emission scenarios, including RCP 2.6, RCP 4.5, RCP 6.0, and RCP 8.5. More recently, led by the IPCC, the energy modeling community developed a new set of emission scenarios driven by different socioeconomic assumptions, the so-called 'Shared Socioeconomic Pathways (SSPs). A number of these SSP scenarios have been selected to drive climate models as part of the Coupled Model Intercomparison Projects 6 (CMIP6). The previous RCP scenarios have been updated in CMIP6 in the form of SSP1-2.6, SSP2-4.5, SSP4-6.0, and SSP5-8.5, each of which results in similar 2100 radiative forcing levels as their predecessors in RCPs. Several new scenarios were also applied in CMIP6, such as SSP1-1.9, SSP4-3.4, SSP5-3.4OS, and SSP3-7.0, to take into account more socioeconomic drivers. Such a large number of climate models and RCP scenarios complicate the process of applying their different combinations to one specific assessment and enormous computational costs. Moreover, a building overheating assessment for future projected years is expected to cover a long-term period of at least 20-30 years [34], which results in high computational costs when evaluating every year. Therefore, one of the computationally effective solutions is to select a few reference years as the subsets of the long-term time-series climates while encompassing the uncertainties associated with future climate projections.

Reference years are one year (or a few years) prepared from the climate time series to capture aspects of interest from the long-term datasets. For building energy applications, the typical meteorological year (TMY) defined by Hall, et al. [118] is often used by combining multiple typical meteorological months (TMM). TMY was widely applied to evaluating building energy performance [112-117] as well as the overheating assessment [112-117, 142-144]. In comparison, Typical reference year (TRY), Weather Year for Energy Calculations (WYEC), and International Weather Year for Energy Calculations (IWEC) were developed by the American Society of Heating, Refrigerating, and Air-conditioning Engineers (ASHRAE). The test reference year from Hui and Lok [119] and typical meteorological year 2 (TMY2) from the National Solar Radiation Data Base (NSRDB) [291] were intended to capture typical, or average, aspects of climatic variables of the long-term datasets [125, 127, 128].

There are also reference year methods for building overheating assessments, the intention of which is to capture extreme summer conditions from long-term data as the reference datasets, like the design summer year (DSY) from Levermore and Parkinson [130], actual meteorological year (AMY) from Hong, et al. [133], summer reference year from Jentsch, et al. [134]. For a cold climate, such as Canada, several studies have focused on the overheating assessment in different cities [135, 136, 145-147]. Baba and Ge [146] evaluated the performance of existing buildings under a current extreme year and projected future climates. Their results showed that the thermal conditions of a single-family detached house built in 1964 and 1990 are more comfortable than the house built to meet the current National Energy Code of Canada for Buildings (NECB), and the overheating risk of Canadian buildings will be increased in the future. In a recent study, Chang et al. [147] evaluated the external overheating within the urban areas of Ottawa and Montreal by Weather Research and Forecasting (WRF) simulations with two resolutions (1 km and 25 km). Besides, the WRF simulation data were then used for the indoor overheating assessment by EnergyPlus simulations. It was shown that the 1-km grid resolution is essential for assessing indoor overheating conditions because the 25-km resolution could lead to an underprediction of the overheating hours in about 95% of the urban grids within either of these two cities. Studies from

Laouadi [135-137] developed a new reference year method called reference summer weather years (RSWY) to evaluate indoor overheating. This method includes generating historical climate data, developing a heat stress metric for the definition, and characterizing heat events. A modified Standard Effective Temperature (t-SET) considering both environmental and psychological factors was used to generate RSWY for selected Canadian cities. This method was also applied to evaluate future climate change impacts on indoor overheating [148].

Recently, Nik [34] developed an approach for selecting reference years for climate change impact assessment on buildings where three reference years: typical downscaled year (TDY), extreme cold year (ECY), and extreme warm year (EWY), were selected to capture the typical, coldest and warmest conditions within a climate time-series. This method aims at selecting the limited number of hourly weather data sets out of regional climate models (RCMs) without neglecting the climate uncertainties, extremes, and variations in different time scales without weighting weather parameters in time series. The selected three reference years are found to efficiently capture the range of climatic projections and building energy response from an ensemble of regional climate projections. The approach has since been applied in a wide range of studies to prepare reference datasets for building energy and building hygrothermal applications [138, 139, 141, 149].

More recently, Nik's method is also applied to the future projected changes in indoor thermal comfort and degree-days evaluation of a European city [292]. It is found that cooling degree days increase by 45% for the typical weather conditions and even up to 500% for an extreme warm July from one 30-year period to another. According to their study, the annual overheating hours can increase by up to 140% in the future time under extreme summer months in the city. In this study, the suitability of Nik [44] method towards selecting typical and extreme reference years for indoor and outdoor overheating applications is evaluated over three Canadian cities. This study, therefore, evaluates the method in an overheating context, which is a relatively less explored area of investigation of the method in the past. At the same time, the evaluation is performed over Canadian cities which have different climates than European cities over which previous overheating study [67] with the method has been performed.

The study is described in the following sections. Section 2.2 provides detailed descriptions of the tasks and workflow process of the study and includes the locations and period of time of interest, the collection of climate data, methods of data processing, building model configurations, and overheating criteria. Results and discussions of data processing, as well as the outdoor and indoor overheating conditions, are reported in Section 2.3, and the conclusions are provided in Section 2.4.

2.2 Methodology

The following steps were conducted to select reference years for the three Canadian cities in an overheating context, and evaluate future projected changes in the overheating of buildings in these locations:

Step one - Collection of observational and climate model simulation data (details described in Section 2.2.2):

The observations were collected from the airport locations for each city and for the time period of 1998-2017 from the CWEEDS database (hereafter referred to as observational time-period). The three sets of regional climate projections were collected from the Coordinated Regional Downscaling Experiment (CORDEX) program for the observational, contemporary, mid-term future, and long-term future time periods and for the grids encompassing the airport locations of the three cities.

Step two - Bias correction of climate model simulations (details described in Section 2.2.3 and 2.3.1):

The regional climate model data were used to calibrate the multivariate bias correction algorithm (MBCn) bias-correction function, which was then used to prepare bias-corrected climate simulations for the contemporary, mid-term future, and long-term future time periods.

Step three - Preparation of typical and extreme climate datasets (details described in Section 2.2.4 and 2.3.2):

The typical downscaled year (TDY), extreme warm year (EWY), and extreme cold year (ECY) were prepared for the three time periods. In addition, the Design Summer Year (DSY) was selected for the same periods.

Step four - Building simulations with current and future projected climate (details described in Section 2.2.5):

The indoor environment in the single-detached home when exposed to the climate in contemporary, mid-term future, and long-term future time periods were simulated using EnergyPlus simulation software.

Step five - Assessment of future outdoor and indoor overheating (describe in Section 2.3.3):

Future overheating assessment in the cities was performed by comparing the overheating conditions in the mid-term and long-term future to those of the contemporary time period.

2.2.1 The region and time-periods of interest

Three Canadian cities were selected for the overheating assessment in this study, including Montreal (Quebec), Toronto (Ontario), and Vancouver (British Columbia). These three cities were, in 2016, the three largest urban agglomerations, by population, in Canada [293]. Demographic and geographic details of these three cities are provided in Table 2.1. For the overheating evaluation, three time periods: contemporary (2001-2020), mid-term future (2041-2060), and long-term future (2081-2100) are considered. Fig. 2.1 shows the average monthly summary of daily observations of temperature, humidity, and wind speed for the three cities collected from Environment and Climate Change Canada (ECCC) [294].

Table 2.1 Information of three selected Canadian cities

City	Latitude and longitude	Elevation above sea level (m)	City Area (km^2)	Population density ($person/km^2$)	Climate	Prevailing wind direction
Montreal	45°30′N 73°33′W	36	431.5	4,828.3	Semi-continental	West
Toronto	43°44′N 79°22′W	76.5	630.2	4434.1	Semi-continental	West
Vancouver	49°15′N 123°06′W	2	115.2	5749.9	Western maritime	East

The daily average (solid line) and daily maximum (dash line) temperature over 1981-2010 are reported in Fig. 2.1. The average temperature varies from -11.5 °C to 19.8 °C for Montreal, -3.7 °C to 22.3 °C for Toronto, and 3.6 °C to 18 °C for Vancouver. The daily maximum temperature varies from 12 ℃ to 36.1 ℃ for Montreal, 16.1 ℃ to 40.6 ℃ for Toronto, and 14.9 ℃ to 34.4 ℃ for Vancouver. The historical hottest month for three Canadian cities based on the average and maximum daily temperature is normally found in July or August. It is clear that Toronto has the highest temperature during the summer periods, and Montreal tends to have the coldest winter. Compared with Montreal and Toronto, Vancouver is more likely to have a cool summer and slightly cold winter. Besides, Toronto and Montreal are climate locations where overheating is more likely to occur as compared to Vancouver, considering the historical daily maximum temperature for these locations. Average humidity varies from 73.2% to 90.4% for Montreal, 76.1% to 89.6% for Toronto, and 81.3% to 89.2% for Vancouver. It could be found that Montreal and Toronto have similar climate patterns where wet summers and dry winters are evident, whereas Vancouver has a different climate pattern from the other two eastern Canadian locations. Regarding the wind velocity, average wind speed varies from 7.2 m/s to 12.3 m/s for Montreal, 10 m/s to 14 m/s for Toronto, and 11.2 m/s to 13.2 m/s for Vancouver. Across the twelve months, the wind speeds are higher in winter in Montreal and Toronto, whereas the difference in monthly wind speeds in Vancouver is relatively small over the twelve months.

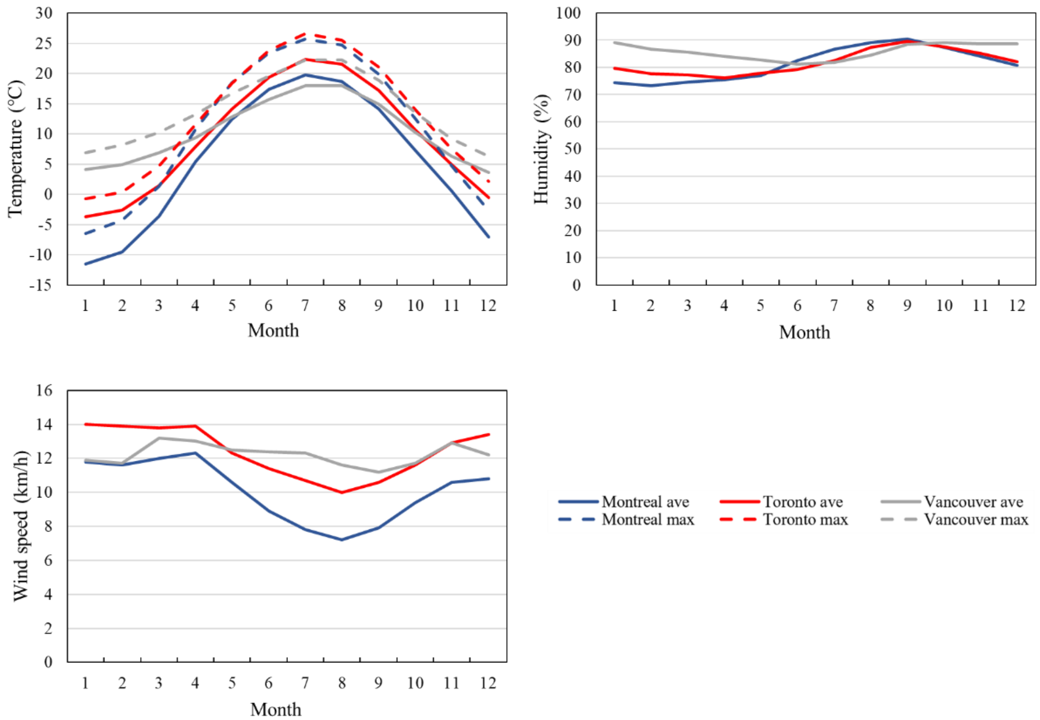

Fig. 2.1 Climatic variables of three Canadian cities from 1981 to 2010

2.2.2 Climate models and observational data

The climate data to undertake simulations during the contemporary and future periods were collected from the Coordinated Regional Downscaling Experiment (CORDEX) database [295], which provides multi-modal regional climate simulations for many state-of-the-art regional climate models (RCMs) forced by different global climate models (GCMs) [296]. A review of data available in the CORDEX is conducted, and a total of three RCM-GCM combinations are found to have three hourly climate projections with all the climatic variables for building simulations available for the North American domain. These three GCM-RCM combinations are selected for this study. The GCMs associated with the selected projections are:

(1) MPI-ESM-LR [297]: Climate projections based on the components of ECHAM6 for atmosphere and MPIOM for the ocean and JSBACH for the terrestrial biosphere, and

HAMOCC for the ocean biogeochemistry.

(2) NCC-NorESM1-M [298]: Climate projections of the first generation model developed by the Norwegian Climate Centre (NCC).

(3) MOHC-HadGEM2-ES [299]: Climate projections of the second version of the Hadley Centre Global Environment Model (HadGEM2) by the Met Office Hadley Centre (MOHC).

The regional climate models associated with all three climate simulations were the hydrostatic version of the Regional Model [300] (version REMO 2015), which dynamically downscales the GCM projections to a horizontal resolution of 0.22° (25 km). The future projections as applied in this study correspond to RCP 8.5, which represents the high range of non-climate policy scenarios [44, 301], assuming that by 2100, atmospheric concentrations of CO_2 will be three to four times higher than the pre-industrial levels. The global warming increases for RCP 8.5 are 2.0 °C (around 1.4–2.6 °C) during mid-term future and 3.7 °C (around 2.6–4.8°C) during long-term future [301]. For the selected GCM-RCM combinations, four climatic variables required for conducting building simulations were collected, including dry-bulb air temperature (tas), relative humidity (hurs), wind speed (sfcWind), and global solar radiation (rsds).

Besides, the observational data from local weather stations during the historical period are also collected. These observation data are downloaded from Canadian Weather Energy and Engineering Datasets (CWEEDS) [302] by Environment and Climate Change Canada from 1998 to 2017 for all three Canadian cities.

2.2.3 Bias correction of climate simulations

According to Maraun [36], the climate model bias is defined as 'the systematic difference between a simulated climate statistic and the corresponding real-world climate statistics'. There are various reasons for the bias in climate model simulations, and the primary among them is the coarse resolution of climate models at which several local scale climate processes cannot be resolved [91-94]. Therefore, failure to eliminate the bias from climate model simulations can result in an inaccurate assessment of overheating in the cities over contemporary and future projected time periods.

Based on the literatures [36, 92, 100-102], it could be found that bias-correction is performed frequently when using climate model projections for local scale impact assessments and the bias associated with climate models are significantly reduced by the bias-correction step. Many bias-correction methods such as simple scaling and additive corrections [103-105], advanced histogram equalization [101, 106, 107], and multivariate methods [108, 109] exist in the literature. In this study, climate projections are bias-corrected with the multivariate quantile mapping bias correction method: MBCn proposed by Cannon [108]. This method used an image processing technique which is N-dimensional probability density function transform, to transfer the observed continuous multivariate distribution to the corresponding multivariate distribution of variables from climate simulations [303, 304].

2.2.4 Reference year selection

Owing to the existence of multiple GCMs and RCMs, considerable uncertainties exist in future climate projections [94]. To account for the uncertainties, ideally, the ensemble of climate projections needs to be considered when performing future overheating assessments. However, this is time-consuming and computationally expensive. Furthermore, climate change assessments are performed over multidecadal timescales, which makes the task of considering climate projections from multiple GCMs and RCMs even more challenging [110, 111].

As discussed before, Nik [34] developed a method to select one typical and two extreme years of data to capture the range of climatic conditions present in an ensemble of future climate projections. Typical/extreme year data are prepared by identifying twelve typical/extreme meteorological months and combining them as one year of continuous data. For each month, the cumulative distribution function (CDF) of the outdoor air temperatures for each year is compared with the CDF outdoor air temperatures from all years, and the year with the least absolute difference between them is identified as the typical month. Extreme cold and warm year data are prepared in a similar way. However, instead of selecting the month with the least absolute difference, the month with the maximum and minimum difference between CDFs is selected as the extremely warm and cold months, respectively. They are then combined to prepare the extremely cold year and extremely warm year data.

In this study, to evaluate the performance of the reference year data method, a Design Summer Year (DSY) by Levermore and Parkinson [130] is also prepared. The DSY was introduced in 2002 [305] by CIBSE to determine the warm weather data for assessing overheating risk in naturally ventilated and passively cooled buildings with dynamic simulation programs that represent a 'near extreme' warm weather [306]. The DSY is a selected one whole-year actual weather data from the multiple-year datasets within a given time period, normally around 20 years. The procedure to identify DSY first ranks the average dry bulb temperature from April to September of each year and then selects the year that falls in the top 12.5% quartile of the rank (i.e., the 3rd warmest year in a set of 20 years), assuming a uniform probability distribution as the DSY.

2.2.5 Building model and overheating criteria

An archetype building model of a typical single-detached Canadian home created by Laouadi, et al. [135] is used in this study for the indoor simulation using EnergyPlus [307]. The home contains four thermal zones, which are the basement, first floor, second floor, and attic. Fig. 2.2 shows the geometry outline of this building. A uniform distribution of air leakage over home surfaces is considered when windows are closed. The attic space has four intentional openings with a total area of 1/150 of the attic floor surface area for ventilation. The typical internal horizontal venetian blinds and exterior applied grey screen shades were applied with an openness factor of 5%. Windows are open by 25% when the indoor temperature is higher than the outdoor temperature and a set-point temperature of 24 ºC. The window size for South and North is 2 m × 4 m, and the window size for East and West is 2 m × 2 m. Besides, there is no external obstructions around the building and no night cooling design. For brevity, this chapter does not include all the building details.

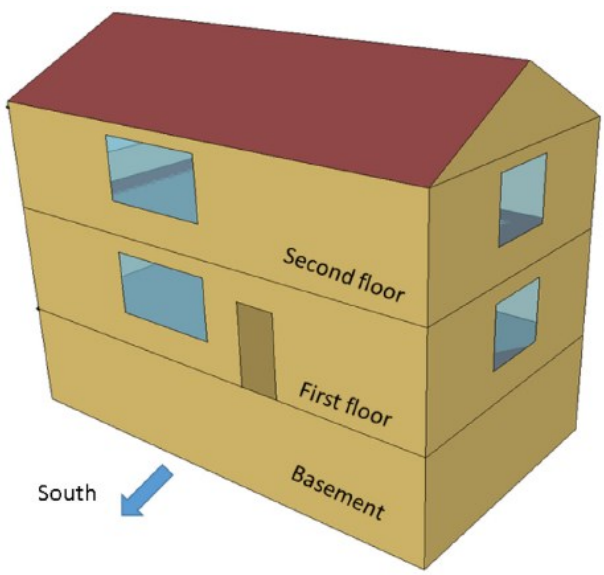

Fig. 2.2 Archetype of the single-detached house [135]

To evaluate the effects of extreme hot and cold climate conditions on the indoor temperature, the home is assumed to be free-running for the entire year. Detailed information about the characteristics of the construction is shown in Fig. 2.2. More details for all the building models can be found from in the National Building Code of Canada (2015). The numbers of people for bedroom and living room are set as three and the fraction of room occupancy will change based on the schedule (Bedroom: 0.9 for 0:00-6:00, 0 for 6:00-21:00, 0.9 for 21:00-24:00; Living room: 0 for 0:00-6:00, 0.7 for 6:00-7:00, 0.4 for 7:00-8:00, 0.3 for 8:00-16:00, 0.5 for 16:00-17:00, 0.9 for 17:00-21:00, 0 for 21:00-24:00). The solar radiation data for building simulation include three components, which are global solar radiation obtained from CORDEX database and bias-corrected using MBCn method, and direct normal and diffuse solar radiation calculated from the bias-corrected global radiation [308].

Table 2.2 Characteristics of construction practice of the single house building [135]

Envelope	2015 construction practice [309]
Roof	Asphalt shingles with attic insulation (8.2 Km^2/W)
Walls	Wood stud with Vinyl cladding (4.5 Km^2/W)
Basement wall	Insulated concrete (1.7 Km^2/W)
Basement slab	Insulated concrete (1.6 Km^2/W)
Windows with wooden frames	Double clear with low-e (U = 1.58 $W/(m^2K)$; Visible transmittance = 73%; Solar heat gain coefficient = 0.67; Window to wall ratio = 15%)

Evaluating overheating risks of buildings requires the determination of appropriate overheating criteria [27]. The *PMV/PPD* thermal comfort model [240] (*PMV* stands for predicted mean vote and *PPD* stands for predicted percentage dissatisfied) developed by Fanger is widely applied to the overheating assessment.by various standards such as EN [243], ISO [244], ASHARE [245], and CIBSE [246], suggesting different *PMV/PPD* static comfort limits under different building operation types. Due to the difficulty of measuring *PMV* in various indoor environments, some standards translate the *PMV/PPD* ranges into the operative temperature scales. In CIBSE TM52 [247], the *PMV/PPD* ranges is translated by assuming specific relative humidity (=50%), air velocity (<0.1m/s), metabolic rate (1.2 met), and clothing factor (0.5 clo for summer). Accordingly, the temperature thresholds of the residential building are determined as 26 ℃ and 28 ℃ for the living room and bedroom, respectively. With the thresholds temperature, the overheating risks could then be evaluated by the hours of exceedance [247], indoor overheating degree [20], and heat exposure index [250]. Besides, Robinson and Haldi [251], [252] also developed a mathematical model for predicting overheating risk under various environmental conditions, considering the analogy between the charging and discharging of human's tolerance to overheating stimuli. Comparing with the data from the field survey, the application of this analytical model provided encouraging results.

In this work, a fixed temperature threshold value was used for the overheating assessment. For the indoor scenario, the overheating baseline temperatures are chosen as 28 ℃ for the living room and 26 ℃ for the bedroom following previous studies [246, 247, 310]. For the outdoor scenario, the threshold value is selected as 28 ℃ based on the previous work by Chang et al. [147]. The overheating hours were defined as the number of hours when the air temperature difference between the baseline and simulated temperature is greater than or equal to one degree following the concept of hours of exceedance from the guideline of CIBESE TM52 [247]:

$$h_{outOH} = \sum h_{Tout-28\geq 1} \quad (2.1)$$

$$h_{livOH} = \sum h_{Tliv-28\geq 1} \quad (2.2)$$

$$h_{bedOH} = \sum h_{Tbed-28\geq 1} \quad (2.3)$$

where, h_{outOH} is the outdoor overheating hours, h_{livOH} is the indoor overheating hour for the living room, h_{bedOH} is the indoor overheating hour for the bedroom, $h_{Tout-28\geq 1}$ is the hour of exceedance for the outdoor scenario, $h_{Tliv-28\geq 1}$is the hour of exceedance for living room, and $h_{Tbed-28\geq 1}$ is the hours of exceedance for bedroom.

2.3 Results and discussion

2.3.1 Bias correction of climate simulations

The cumulative distribution function (CDF) of observations (gray curve), raw RCM data (blue curve), and RCM data bias-corrected using MBCn method (red curve) is shown in Fig. 2.3. The results for the other two driving models, and their results share the same pattern as given in Fig. 2.3, so they are not included here for the sake of brevity. The comparison of CDFs for Toronto and Vancouver can be found in Appendix A.1. It is clear that the bias-corrected climate data shares a similar pattern to the observational data.

Here, by using the historical weather data, the importance of conducting bias correction of the projected/estimated weather data could be shown. Without the bias correction, the average errors between observational data and RCM data for Montreal are 2.78 °C for air temperature, 68.3 W/m^2 for global solar radiation, 0.9 m/s for wind speed, and 14.5% for relative humidity. With the bias correction, these errors respectively decrease to: 0.05 °C, 0.1 W/m^2, 0.001m/s and 0.01%. The MBCn bias correction method calibrated over the observational time-period is used to correct

RCM data in the future time periods. By applying this bias correction method, the reliability of future bias-corrected RCM data will be increased and therefore, for any future weather projection study, bias correction is one of the most important steps.

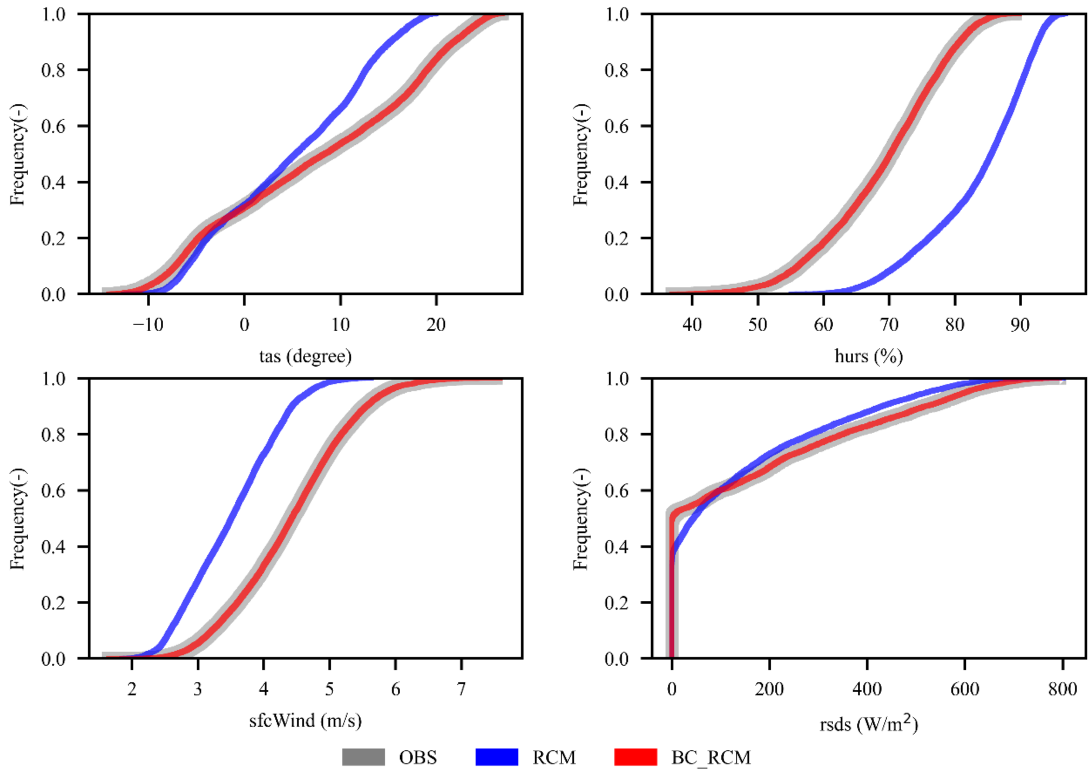

Fig. 2.3 Cumulative distribution function comparison of observational, raw RCM, and bias-corrected RCM data of dry-bulb air temperature (tas), relative humidity (hurs), wind speed (sfcWind), and global solar radiation (rsds) (City: Montreal; GCM: MPI-M-MPI-ESM-LR; Time periods: 1998-2017)

2.3.2 Assessment of selected reference years in an overheating context

As has been illustrated in Section 2.2.4, the bias-corrected climate data generated were used to obtain reference year climate data. Here, an example case for Montreal is given, whose data were collected from the contemporary climate data set term, using three driving models (MPI, NCC, MOHC). Then, the reference years (TDY, EWY, ECY) were generated by combining the reference calendar months from the selected year and the designated driving model as shown in Fig. 2.3. In Fig. 2.4, a comparison is given of the distribution of outdoor temperature between the original 20-years and reference year data sets from three driving models. The reference year climate data sets are single-year data as shown by the blue curve (extreme cold year), black curve (typical downscaled year), and red curve (extreme warm year). The yellow curve represents the temperature distribution of the DSY for the same time period. It is obvious that the temperature distribution of TDY is similar to that of the general distribution for the 20-year data set for all three driving models which means TDY can represent the general temperature distribution of 20-year data. Besides, the distribution of ECY and EWY provides the upper and lower boundary for the 20-year data set. Therefore, the reference year datasets could be used to represent both the general trend of multiple years temperature distribution as well as its upper and lower temperature limit.

Table 2.3 Selected years and models for reference year climate data sets in Montreal for all time periods

		EWY		TDY		ECY	
		Year	model	year	model	year	model
	Jan	2019	NCC	2012	MOHC	2007	MPI
2010s	Feb	2011	NCC	2019	MOHC	2019	MPI
	Mar	2015	NCC	2008	MPI	2017	MPI

	Apr	2018	MPI	2007	MOHC	2002	MPI
	May	2008	MPI	2012	MPI	2019	NCC
	Jun	2014	MPI	2015	MOHC	2018	NCC
	Jul	2020	MPI	2015	MOHC	2003	NCC
	Aug	2020	MPI	2002	MOHC	2016	NCC
	Sep	2020	MOHC	2017	MOHC	2009	NCC
	Oct	2003	MOHC	2012	MPI	2011	MPI
	Nov	2020	NCC	2020	MOHC	2013	MPI
	Dec	2012	NCC	2007	MOHC	2013	MOHC
2050s	Jan	2044	NCC	2052	MOHC	2049	MPI
	Feb	2051	NCC	2042	MOHC	2058	MOHC
	Mar	2059	NCC	2056	MOHC	2058	MPI
	Apr	2044	MOHC	2043	MPI	2046	MPI
	May	2055	MOHC	2057	MPI	2046	NCC
	Jun	2054	MOHC	2059	MOHC	2050	NCC
	Jul	2051	MOHC	2043	MPI	2051	NCC
	Aug	2051	MOHC	2055	MPI	2049	NCC

	Sep	2051	MOHC	2055	MPI	2041	NCC
	Oct	2041	MOHC	2055	MOHC	2043	MPI
	Nov	2058	NCC	2052	MOHC	2056	MPI
	Dec	2056	NCC	2056	MOHC	2041	MPI
2090s	Jan	2088	NCC	2098	MOHC	2089	MPI
	Feb	2097	NCC	2098	MOHC	2096	MPI
	Mar	2088	NCC	2087	MOHC	2085	MPI
	Apr	2085	MOHC	2095	MOHC	2083	MPI
	May	2086	MOHC	2092	MOHC	2086	NCC
	Jun	2082	MOHC	2082	MPI	2087	NCC
	Jul	2082	MOHC	2085	MPI	2081	NCC
	Aug	2097	MOHC	2088	MPI	2088	NCC
	Sep	2082	MOHC	2088	MOHC	2099	MPI
	Oct	2087	MOHC	2099	MPI	2094	MPI
	Nov	2093	MOHC	2084	MOHC	2092	MPI
	Dec	2086	NCC	2096	MOHC	2090	MPI

A similar trend could also be found for the other time periods and the other Canadian cities. The temperature distribution for DSY is more similar to that of the TDY that might be because DSY is generated as the third-warmest year. Compared with DSY, the EWY would likely capture a relatively extreme hot climate with the same temperature database. On the contrary, ECY would represent a relatively extreme cold climate. More detailed information of the nonparametric comparison for three Canadian cities over the three time periods investigated in this study can be found in Appendix A.2.

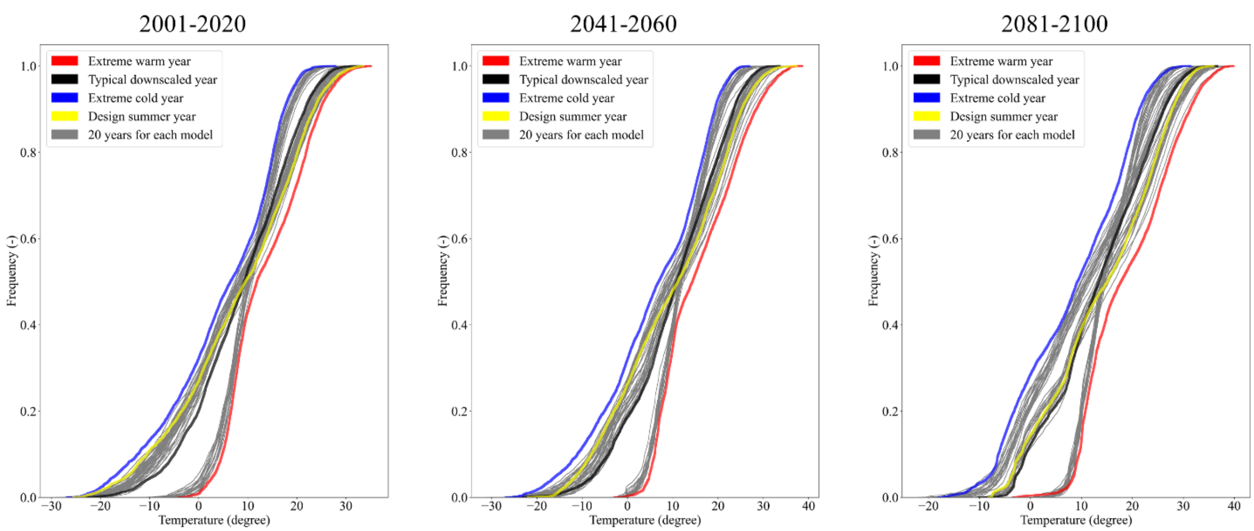

Fig. 2.4 Cumulative distribution function comparison of the hourly temperature from 20 years, DSY and 1-year reference year climate data sets of TDY, ECY, and EWY in Montreal for the contemporary term, mid-term and long-term future

The validation of the selected reference years is performed by comparing monthly outdoor and indoor overheating hours over the summer season from: 1) the data from the entire 20-years; 2) data from the three reference years: TDY, ECY, EWY; and 3) data from DSY. The cumulative yearly outdoor overheating hours of TDY (black line), EWY (red line), ECY (blue line), DSY (yellow line), and 20-year climate data (gray lines) for Montreal is presented in Fig. 2.5 while the results for Toronto and Vancouver are presented in Appendix B.1. It can be seen that the ECY and EWY are able to encompass the range of yearly overheating values simulated in the entire 20-year climate data. This is consistently observed for both contemporary and future time-periods, and the three cities.

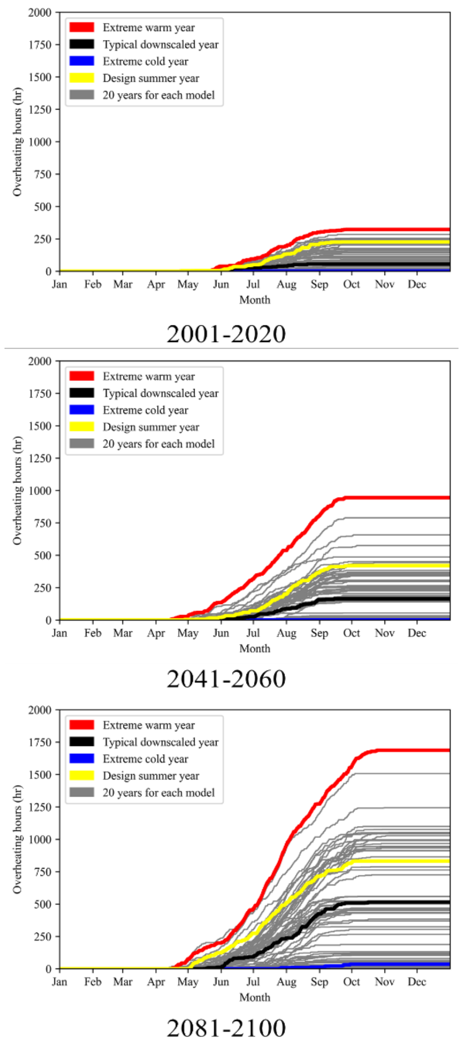

Fig. 2.5 The yearly outdoor overheating hours of TDY, EWY, ECY, DSY, and 20-year climate data for Montreal

Table 2.4 presents outdoor overheating hours during the summer months from the reference years: TDY, ECY, EWY, DSY along with the maximum (max.), minimum (min.), and average (avg.) yearly 20-year values. The results for Toronto and Vancouver can be found in Appendix B.2. In general, the maximum overheating values over the 20-years are close to the values of EWY for all cities and time-periods. The maximum outdoor overheating hours found in 20-years data of three Canadian cities considering both contemporary and future time-periods is 532 hours (Toronto, July, 2081-2100) which is same as the maximum outdoor overheating hours found in the synthesizing data (EWY, Toronto, July, 2081-2100).

The average differences in overheating hours between TDY and average yearly 20-year values are 32.61% for Montreal, 1.89% for Toronto, and 47.31% for Vancouver. The average differences in in overheating hours between EWY and maximum yearly 20-year values are 9.5% for Montreal, 8.83% for Toronto, and 22.51% for Vancouver. The average differences in overheating hours between ECY and min. yearly 20-year values are relatively small, generally less than 10 hours. On the other hand, the differences between DSY and max. yearly 20-year values are larger than 20% in most cases, and in some cases even larger than 60%.

Table 2.4 Outdoor overheating hours during the summer months in Montreal from TDY, ECY, EWY, entire 20-year data, and DSY.

Time periods	**Model**	**May**	**June**	**July**	**August**	**September**
2010s	ECY	0	1	0	0	0
	TDY	3	24	13	15	0
	EWY	36	56	99	107	22
	20-year (max.)	36	74	123	107	65

	20-year (avg.)	4	21	37	26	7
	20-year (min.)	0	0	0	0	0
	DSY	2	45	83	79	14
2050s	ECY	0	0	0	0	0
	TDY	2	23	63	68	7
	EWY	103	184	219	271	136
	20-year (max.)	103	184	219	271	136
	20-year (avg.)	10	34	74	78	26
	20-year (min.)	0	0	0	0	0
	DSY	16	51	129	169	51
2090s	ECY	0	0	8	5	23
	TDY	12	80	146	186	83
	EWY	123	264	494	316	290
	20-year (max.)	161	264	494	347	290
	20-year (avg.)	27	82	165	168	70

20-year (min.)	0	0	3	0	0
DSY	123	150	238	203	106

Above results suggest that TDY, EWY and ECY could efficiently capture average, maximum and minimum monthly outdoor overheating conditions simulated in the entire 20-year data. The EWY and ECY are able to provide upper and lower boundaries of possible outdoor overheating conditions in the cities. The EWY is able to better capture outdoor overheating conditions than the DSY and hence is more suitable to represent extreme overheating conditions in the cities.

To assess the efficacy of the reference year selection method in indoor overheating context, this study firstly simulated the indoor temperature in a free-running single house building model and compared indoor overheating from the entire 20-years climate data with the TDY, EWY, ECY, and DSY reference years. Fig. 2.6 reports the yearly cumulative indoor overheating hours for Montreal whereas the results for Toronto and Vancouver can be found in Appendix B.3. The results for basement and attic are not presented in this chapter as these areas are typically not frequently occupied by the home occupants as compared to other areas.

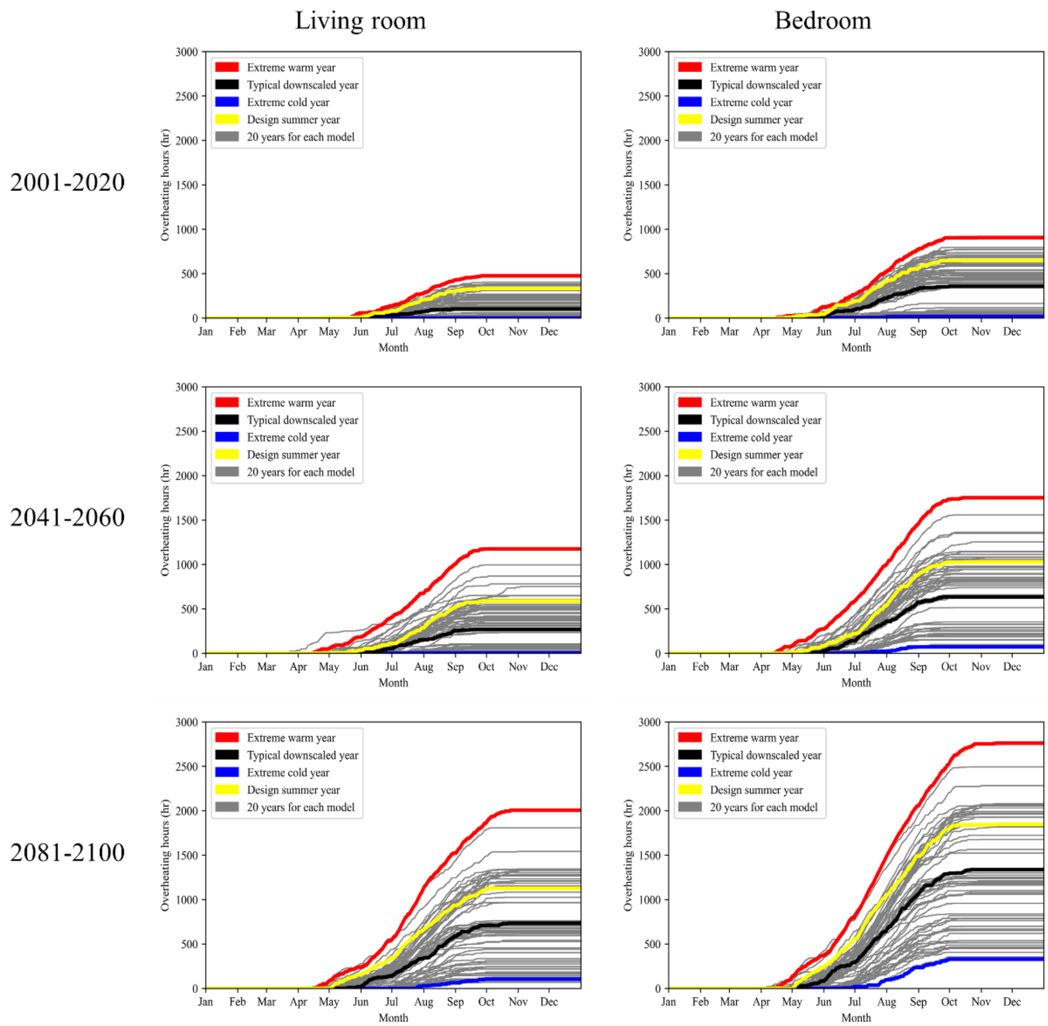

Fig. 2.6 Yearly cumulative indoor overheating hours in Montreal of reference year, DSY, and 20-years climate data

Table 2.5 presents indoor overheating hours in the living room (liv) and bedroom (bed) during the summer months from the reference years: TDY, ECY, EWY, DSY along with the maximum, minimum, and average yearly 20-year values. The results for Toronto and Vancouver can be found in Appendix B.4. The average difference between TDY and avg. yearly 20-year values is -18.42% for Montreal, -1.01% for Toronto, and 27.66% for Vancouver. The average difference in percentage between EWY and Max is 5.98% for Montreal, 2.82% for Toronto, and -9.05% for

Vancouver. On the other hand, the average difference between DSY and Max is -37.92% for Montreal, -37.42% for Toronto, and -63.73% for Vancouver.

Table 2.5 Indoor overheating hours in the living room (liv) and bedroom (bed) during the summer months in Montreal from TDY, ECY, EWY, entire 20-year data, and DSY.

Time periods	Model	May		June		July		August		September	
		Liv	Bed	Liv	Bed	Liv	Bed	Liv	Bed	Liv	Bed
2010s	ECY	0	0	1	5	0	11	0	3	0	0
	TDY	9	26	28	69	35	129	30	107	0	27
	EWY	58	101	79	135	141	260	148	250	49	131
	20-year (max.)	58	102	101	180	158	265	148	250	91	153
	20-year (avg.)	7	22	33	76	59	138	47	117	13	39
	20-year (min.)	0	0	0	0	0	2	0	2	0	0
	DSY	5	34	73	150	127	222	96	149	27	84
2050s	ECY	0	0	0	0	2	7	0	10	0	0
	TDY	1	11	22	78	64	170	66	157	4	35
	EWY	95	161	181	267	218	351	285	410	130	223
	20-year (max.)	95	162	182	267	222	354	289	412	132	225

	20-year (avg.)	93	273	327	787	773	175	84	179	26	62
	20-year (min.)	0	0	0	0	0	6	0	10	0	0
	DSY	28	69	77	138	177	317	231	350	71	137
2090s	ECY	0	0	0	21	30	78	33	136	43	94
	TDY	19	76	122	208	202	366	242	408	127	231
	EWY	154	240	313	433	577	681	393	569	348	478
	20-year (max.)	195	289	313	433	577	681	414	605	348	485
	20-year (avg.)	373	717	1117	204	225	369	228	384	99	185
	20-year (min.)	0	0	0	11	17	79	29	137	0	10
	DSY	153	240	193	317	318	487	269	443	179	311

It can be deduced from the above results that EWY and ECY are able to efficiently capture upper and lower bounds of indoor overheating hours effectively. The EWY is able to represent the upper end of the overheating spectrum more effectively than DSY. A similar conclusion could be achieved for TDY that the average difference in yearly indoor overheating hours between TDY and Ave for three Canadian cities is relatively low, only around 0.9%.

2.3.3 Use of reference years to assess future projected changes in overheating

In this section, both outdoor and indoor overheating hours of TDY and EWY of mid-term and long-term future are compared with those of contemporary term to evaluate the impacts of climate change on future overheating in the cities. Fig. 2.7 shows an example of changes in both outdoor and indoor overheating hours for Montreal among three different time periods. A similar trend is also found in Toronto and Vancouver, but due to the limit of chapter, the graphical results are not reported.

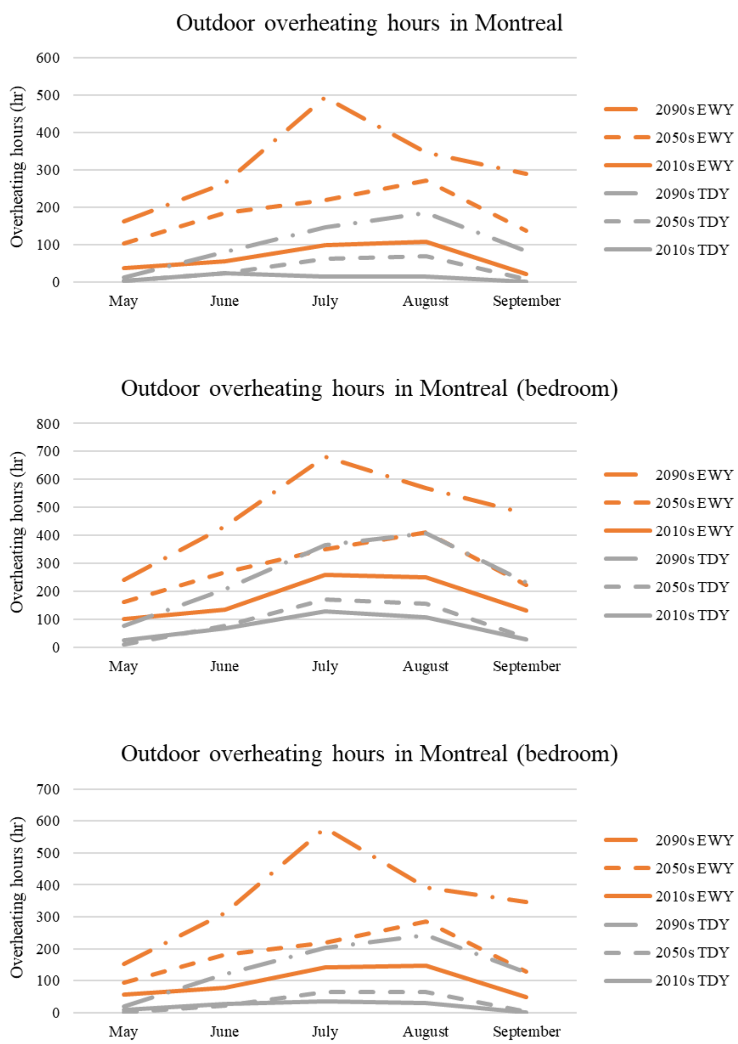

Fig. 2.7 Outdoor and indoor overheating hours of EWY and TDY for Montreal among three time periods

Due to the impacts of climate change, a similar increase trend could be found in overheating hours in the three Canadian cities according to the results shown in Table 2.4 and Table 2.5; average monthly overheating hours increase by normally around one time (from 50% to 150%) until the mid-term future and by normally around two to three times (even up to 8 times for some scenarios) during the long-term future. For instance, the most obvious increase in outdoor overheating hours among two future terms is found in Montreal; the overheating hours of TDY increase by two times by mid-term future and by nine times for long-term future and that of EWY increase by two times and three and a half times by mid-term and long-term future. In opposite, the increase in both indoor and outdoor overheating hours for Vancouver is relatively small, and only around half time by mid-term future and one time by long-term future. It could also be clearly found in Appendix B.1 and B.3 that it is more likely to find extra indoor and outdoor overheating hours appearing in the months not in the defined summer period (such as April and October) for the mid-term and long-term future.

2.4 Conclusion

This chapter evaluates outdoor extreme heat events and indoor overheating conditions for a representative residential building located in three Canadian cities (Montreal, Toronto, and Vancouver) over contemporary (2001-2020), near-term future (2041-2060), and long-term future (2081-2100) time periods. The regional climate simulations forced by three GCMs were bias-corrected with reference to historical observations recorded at the airport location of the cities. Regard that although the analysis is performed for airport locations which may not be representative of fully developed urban areas, the methodology used is generalized enough to be used in urban locations.

Thereafter, a reference year selection method is used to generate three representative climate data years: typical downscaling year (TDY), extreme cold year (ECY), and extreme warm year (EWY).

The performance of TDY, ECY, and EWY climate data sets in capturing the range of overheating conditions present in the entire 20-year long contemporary and future projected time-periods is assessed. At the same time, the projected changes from the selected reference years and 20-year datasets are compared. The results are also compared with a widely used metric of overheating: the design summer year (DSY). Based on the results, given in Sections 2.3.1, 2.3.2, and 2.3.3, following deductions from the study were obtained:

(1) The multivariate quantile mapping bias correction method is able to improve the reliability of future climate data by capturing the distribution pattern of climatic variables as well as reducing errors and therefore, for any future weather projection study, bias correction is one of the most important steps.

(2) For both outdoor/indoor overheating evaluation, EWY and ECY could efficiently capture maximum and minimum monthly overheating hours providing the upper and lower boundary of possible outdoor and indoor overheating conditions. TDY could be used to simulate the typical yearly overheating condition. The EWY captures the extreme overheating conditions better than the DSY.

(3) Owing to the effects of climate change, a similar increase could be found in both indoor and outdoor overheating hours in the three Canadian cities; average monthly overheating hours increase by normally around one time (from 50% to 150%) until the mid-term future and by normally around two to three times (even up to nine times for some scenarios) during the long-term future.

As concluded in this study, it is recommended to use an accurate and time-saving method (reference year data set) to evaluate the future outdoor and indoor overheating conditions by generating the representative year climate data as the typical and extreme scenarios. The limitations of the current work are:

(1) Only considering three Canadian cities for analysis;

(2) Only the projections from three GCMs and one RCP scenario (RCP 8.5) was considered for preparing the climate data sets;

(3) Only testing this method with the single-house building and assuming the features of the single-house building stay constant in all future years. In reality, the features of existing buildings will change based on age.

(4) Only applying a fixed temperature threshold as the indoor and outdoor overheating criteria.

Chapter 3

Evaluating climate change impacts on building level steady-state and dynamic outdoor thermal comfort in Montreal

This chapter is prepared based on published paper: Evaluating climate change impacts on building level steady-state and dynamic outdoor thermal comfort in Montreal.

Abstract

Recent decades have seen an alarming rise in urban overheating due to climate change, increasingly threatening lives worldwide. A number of studies have evaluated outdoor overheating in cities around the globe under a changing climate. The spatial scale of assessment conducted in them is coarse and is unable to reflect street-level changes in projected climate and its consequence on the thermal comfort of the population. This study assesses the effects of climate change on steady-state (Universal Thermal Climate Index - UTCI) and dynamic (Discomfort Capacitor Model - PDISC) outdoor thermal comfort in downtown Montreal using CityFFD-CityBEM co-simulations under both typical (TDD) and extreme warm (EWD) future climate scenarios. Raw future climate data for three distinct 20-year periods: 2001-2020 (2010s), 2041-2060 (2050s), and 2081-2100 (2090s) is obtained from CORDEX. The raw climate data is bias-corrected with local field measurements, followed by the selection of reference scenarios through a reference year data selection method. Thereafter, a 1.25 km by 1.25 km neighborhood of Montreal's downtown area is selected for a detailed assessment of overheating with a spatial resolution of 2 m. Our findings indicate a shift from "Slight cold stress" to "Extreme heat stress" from the 2010s to the 2090s under TDD, with "Extreme heat stress" becoming increasingly common under EWD. Additionally, PDISC analysis indicates that pedestrians will experience no discomfort walking along the route in the 2010s and 2050s under TDD conditions. However, by the 2090s, tolerable discomfort may arise after 5 minutes of walking. Under EWD conditions, intolerable thermal discomfort becomes inevitable at noon, and the duration of time for which discomfort remains tolerable is expected to be reduced from 6 minutes in the 2010s to 4 minutes in the 2090s for a brisk walk (1.7m/s).

3.1 Introduction

Driven by increased greenhouse gas emissions, the global climate system has undergone unprecedented changes, manifesting in the form of extreme weather events such as heatwaves, floods, and droughts that have widespread impacts on human societies. For instance, the 2003 European summer, one of the hottest in half a millennium, resulted in over 30,000 fatalities, while Canada's 2021 heatwave claimed around 500 lives [17, 19, 21, 22]. Such events underscore the escalating challenges associated with global warming. Projections suggest that by 2100, deadly heatwaves could affect up to 74% of the global population annually [3]. Zou, et al. [40] found that average monthly overheating hours could surge by up to nine times by the end of the 21st century. As urban environments bear the brunt of these predicted changes, a deeper understanding of urban overheating under climate change is imperative to safeguard the growing urban populations and ensure resilience in an increasingly warmer world.

According to a recent review [11] on urban overheating impact assessments under climate change, the number of studies on future overheating published in 2021 is 4 times large than that in 2010, which shows a significant increase in attention to this topic. A significant portion of previous research on future overheating has primarily centered on indoor conditions, including residential buildings [41, 140, 191, 311, 312], office structures [313-316], and public establishments [317-320]. In contrast, there are limited studies addressing future outdoor scenarios [11, 40, 99, 321, 322]. Huang, et al. [321] examined the outdoor thermal environment under the effects of climate change. Their method incorporated risk identification, evaluating facets such as thermal stress effects, exposure levels of individuals, and local vulnerability. Even though they employed ENVI-met [323] in tandem with RayMan [323] to discern the current spatial distribution of thermal stress, the future outdoor conditions were not directly simulated and scrutinized.

Zou, et al. [40], [99, 322] evaluated future outdoor overheating on three Canadian cities under two future time periods through a reference year selection method. Their study found that average monthly outdoor overheating hours normally increase by around one time (from 50% to 150%) until the mid-term future (2041–2060) and by around two to three times until long-term future (2081-2100). However, their approach oversimplified outdoor climate conditions by leveraging bias-corrected GCM-RCM data based on the local airport, which typically offer broader regional-scale projections. While RCMs downscale the course GCM data to finer regional scales, intricate details of urban microclimates still cannot be captured [66, 67, 89]. In contrast, CFD simulations could provide detailed and precise information of local urban microclimate for the target urban areas [5, 200, 324-326] with a promising grid resolution down to 1 m, allowing for a more nuanced understanding of thermal comfort, energy use, and potential overheating risks in urban settings. Additionally, CFD simulations can illustrate detailed airflow patterns, turbulence, and vortices within urban canyons, around buildings, and over other urban features, which directly influence how heat is dispersed or trapped in urban areas [326-330]. This level of detail is crucial for accurately understanding and predicting local climate conditions, which is neglected by GCM-RCM. Therefore, there's a pressing demand for research that focuses on forecasting urban overheating in designated urban regions through CFD simulations, leveraging projected climate data.

Directly evaluating future outdoor microclimates using CFD simulations presents several distinct challenges. Firstly, there is a notable lack in simulating building-level microclimate using future climate data for evaluating outdoor thermal comfort under climate change impacts. Secondly, due to the bias in future climate prediction models, the direct use of climate data as CFD simulation inputs raises concerns about their reliability. Thirdly, the vast temporal span of climate model data can be unwieldy for microscale CFD simulations, especially considering the limitations posed by computational resources. To address the aforementioned challenges, it's imperative to preprocess future climate datasets prior to their integration into CFD simulations.

Maraun [36] emphasizes that biases inherently exist in future climate simulations, arising from the systematic discrepancies between simulated climate statistics and actual climate metrics. Therefore, rectifying these biases in climate model simulations is essential for ensuring precise evaluations of both current and future urban overheating [11]. While it might be challenging to entirely eradicate these biases, employing bias-correction techniques, such as simple scaling and additive corrections [103-105], advanced histogram equalization [101, 106, 107], and multivariate approaches [108, 109], can markedly mitigate their influence on the outcomes which enhances the reliability of assessments. Moreover, to refine the temporal resolution of future climate data to align with microscale CFD simulations and to curate representative future climate scenarios, the reference year selection method [34, 40, 138] can be applied for optimizing computational efficiency. This method extracts both typical and extreme conditions from extensive climate datasets, offering a concise and representative input for CFD simulations. Although this method has been applied to evaluate yearly overheating conditions in our previous studies [40, 99, 322], it still requires further development before implementing with CFD simulation. Therefore, while data preprocessing methodologies are established, there exists a research gap in developing a cohesive workflow that integrates these techniques specifically for direct CFD simulations of future conditions.

In this chapter we aim to evaluate climate impacts on both steady-state and dynamic outdoor thermal comfort of Montreal downtown areas through CFD simulation. Section 3.2.1 briefly describes the study region and its historical climate conditions. Section 3.2.2 illustrates the procedure of collecting and processing future climate data, including raw future climate data collection from CORDEX, bias-correction using local field measurement, and reference year data method for getting reference year scenario. Section 3.2.3 presents the process of CityFFD-CityBEM co-simulation, design of the domain, and the independence test of mesh and time step size. Two outdoor thermal comfort indices UTCI and PDISC were explained in Section 3.2.4, and then applied to evaluate the climate change impacts on outdoor overheating (Section 3.3.1 and Section 3.3.2). Fig. 3.1 shows the flow chart of the present research procedure.

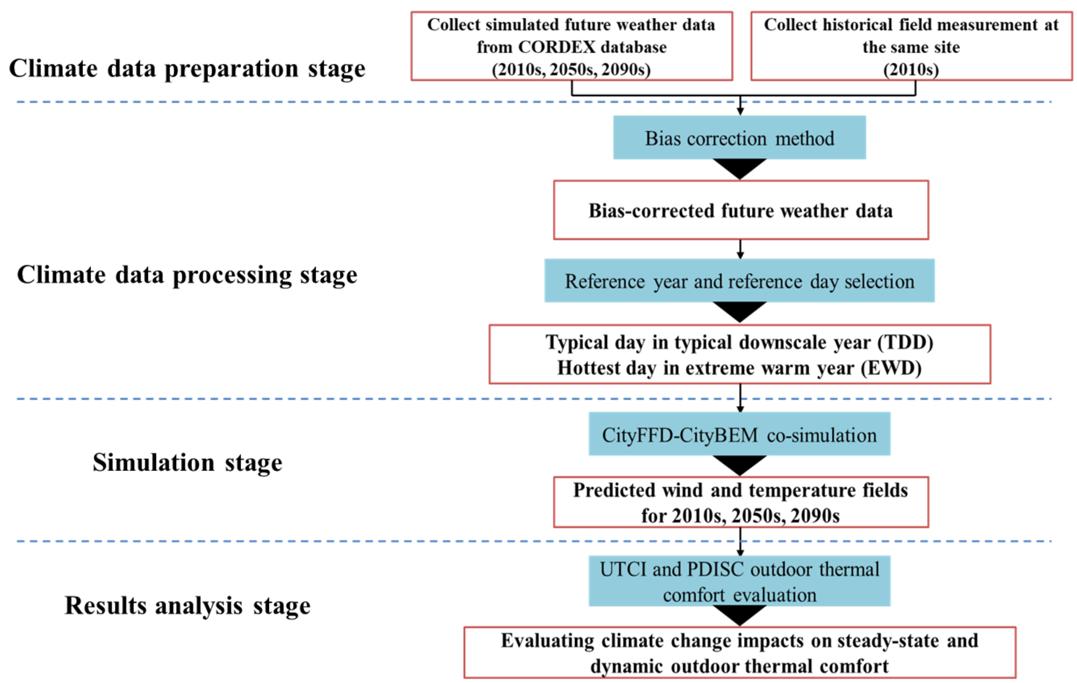

Fig. 3.1 Flow chart of the research procedure of the chapter.

3.2 Methodology

3.2.1 Study region

Montreal (Quebec, Canada) is chosen to study future outdoor thermal comfort projections. With the second largest population after Toronto and the second highest population density after

Vancouver in Canada, Montreal falls within climate zone 6A, characterized as cold and humid. Based on Zou, et al. [40], historical data from 1981 to 2010 indicate that Montreal's temperatures range from −11.5 °C to 19.8 °C, with peak daily temperatures stretching from 12 °C to 36.1 °C during summer season. The city experiences average humidity levels between 73.2% and 90.4%, while wind speeds fluctuate between 7.2 m/s and 12.3 m/s. In this study, an area of 1250 m by 1250 m inside Montreal downtown with high population and building density is selected for predicting its future thermal comfort as shown in Fig. 3.2. The black line shown in Fig. 3.2 (c) represents the selected route for dynamic thermal comfort evaluation, which will be explained in Section 3.2.4.2. The tallest building inside this area is 120 m high.

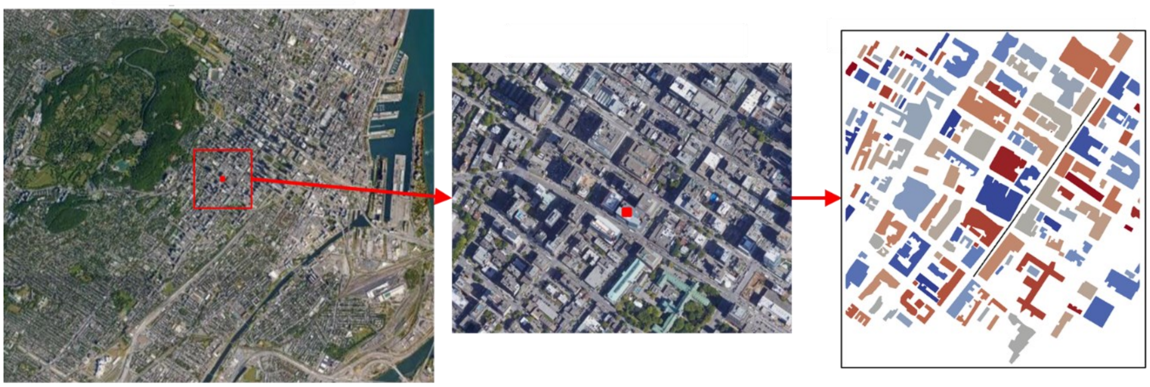

(a) **(b)** **(c)**

Fig. 3.2 Selected urban area in Montreal downtown and its building geometry. (a) Map of Montreal downtown. (b) Map of interest area. (c) Building geometry of interest area.

3.2.2 Future climate data preparation

To facilitate the assessment of outdoor thermal comfort across various temporal spans, climate data sets were gathered and prepared in Montreal for three distinct 20-year periods: 2001-2020 (2010s), 2041-2060 (2050s), and 2081-2100 (2090s). The climate data from the Coordinated Regional Downscaling Experiment (CORDEX) databased, which collects numerous combinations of regional climate models (RCMs) and global climate models (GCMs) [295]. Three GCM models were identified (MPI-ESM-LR [331], NCC-NorESM1-M [298], MOHC-HadGEM2-ES [299]) downscaled through one specific RCM model (REMO 2015 [300]), providing three-hourly climate projections encompassing the requisite climatic variables. For an in-depth understanding, our prior work [40] outlines the specifics of these combinations.

Raw climate model outputs have a known bias [100, 332]. To address this, Cannon's multivariate quantile mapping bias correction technique [108, 109] was applied which is a method rooted in the N-dimensional probability density function transform. This procedure aligns the observed continuous multivariate distribution to its climate simulation counterpart [303, 304]. Previous findings highlighted significant deviations between observed data and RCM data, which, post bias-correction, saw a dramatic reduction. This accentuates the pivotal role bias correction plays in future climate research. Additionally, given the intrinsic uncertainties in climate projections due to the variety of GCMs and RCMs, a reference year data method is integrated which is explained in a previous work [40]. Here, a typical year and two extreme years (coldest and warmest) were extrapolated to encapsulate the climatic variations inherent in future climate projections [34, 40, 99]. These typical and extreme years were formulated by amalgamating twelve representative months, identified based on their cumulative distribution function (CDF) of outdoor air temperatures. Fig. 3.3 provides a visualization of this selection, illustrating multi-year data versus the reference year data sets. For more detailed results of bias-correction as well as reference year selection methods, please refer to our former publications [40, 99, 322].

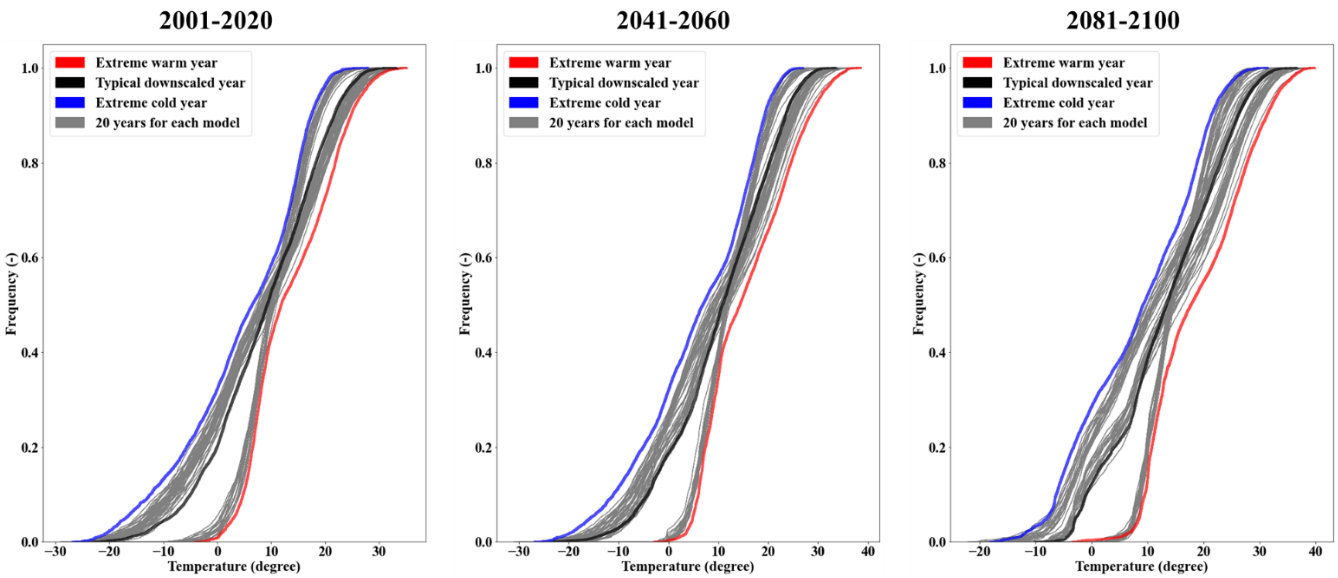

Fig. 3.3 Cumulative distribution function comparison of the hourly temperature from 20 years and 1-year reference year climate data sets of TDY, ECY, and EWY in Montreal for the contemporary term, mid-term and long-term future

Four climate variables are extracted from the future climate set for evaluating future outdoor thermal comfort which are air temperature, wind speed, humidity, and solar radiation. Two extreme and one typical condition were generated from each time periods for CFD simulation, which are the hottest day (with the maximum daily temperature) in the EWY, typical day (with the medium daily temperature) in the TDY, and coldest day (with the minimum daily temperature) in the ECY, as shown in the Fig. 3.4. The hottest day in the EWY (EWD), and typical day in the TDY (TDD), was then used as the climate input of CityFFD-CityBEM co-simulation for overheating assessment. Instead of using the hottest day of 20 years, EWD ensures the selected day represents not just an isolated extreme but a condition that aligns with projected climate trends. Moreover, the hottest day of 20 years could be an outlier not reflective of changing climate pattern. Similarly, TDD reflects not just the mean or median conditions of 20 years but also embodies the climatic conditions that characterize the typical climatic behavior over the period of interest.

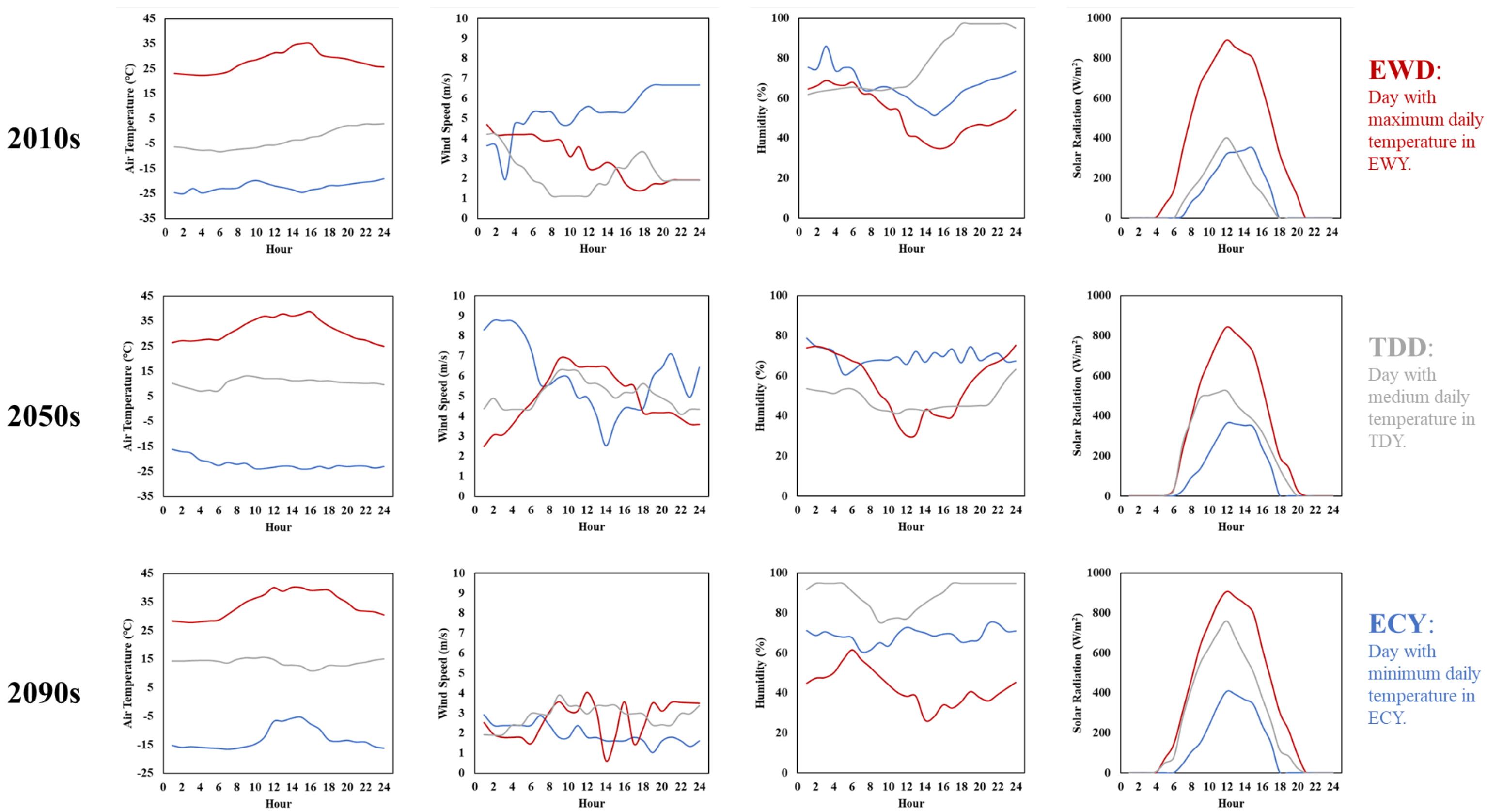

Fig. 3.4 Input climate variables of extreme and typical conditions among three time periods

3.2.3 Co-simulation by CityFFD and CityBEM

3.2.3.1 Co-simulation process

CityFFD is based on a 3D fractional step method and Fast Fluid Dynamics (FFD) solver running on the Graphics Processing Unit (GPU) to predict local microclimate features for modeling large-scale urban aerodynamics. The governing conservation equations in CityFFD are dimensionless as follows:

$$\nabla \cdot V = 0 \tag{3.1}$$

$$\frac{\partial V}{\partial t} + (V \cdot \nabla)V = -\nabla P + \left(\frac{1}{Re} + v_t\right)\nabla^2 V - \frac{Gr}{Re^2}T \tag{3.2}$$

$$\frac{\partial T}{\partial t} + (V \cdot \nabla)T = (\frac{1}{Re \cdot Pr} + \alpha_t)\nabla^2 T \tag{3.3}$$

where V, T, P and t are the velocity, temperature, pressure and time, respectively; Re, Gr and Pr are the dimensionless Reynolds number, Grashof number, and Prandtl number, respectively; and v_t and α_t are turbulence-related parameters, i.e., turbulent viscosity and turbulent thermal diffusivity. CityFFD adopts the semi-Lagrangian method for the advection term in Eqs. (3.2), (3.3). Therefore, no iteration is needed to calculate the velocity field, and computing costs are reduced.

CityBEM [212, 333-335] is an urban building energy model covering all essential heat and mass transfer mechanisms for calculating building heating/cooling loads, energy consumption, and indoor air and building surface temperature. In CityBEM, every building is represented by a single-zone model. For this study, CityBEM is utilized to simulate the surface temperature of each building. This approach provides a more accurate input for CityFFD, allowing for a more precise prediction of the urban microclimate, compared with using a constant temperature input.

In this study, the urban microclimate was modeled using a co-simulation between CityFFD and CityBEM. As illustrated in Fig. 3.5, the co-simulation process initiates with CityBEM, which uses a day's worth of weather data for initialization. After that, the building surface temperature predicted by CityBEM becomes the input for the CityFFD simulation, paired with the air temperature and wind speed taken from the weather data. The microclimate produced by CityFFD in this iteration is then assessed for spatial outdoor thermal comfort evaluation. In the subsequent iterations, rather than sourcing the air temperature and wind speed directly from the weather data file like in the first cycle, CityBEM utilizes the values simulated by CityFFD from the previous loop to model the building surface temperature for each individual structure.

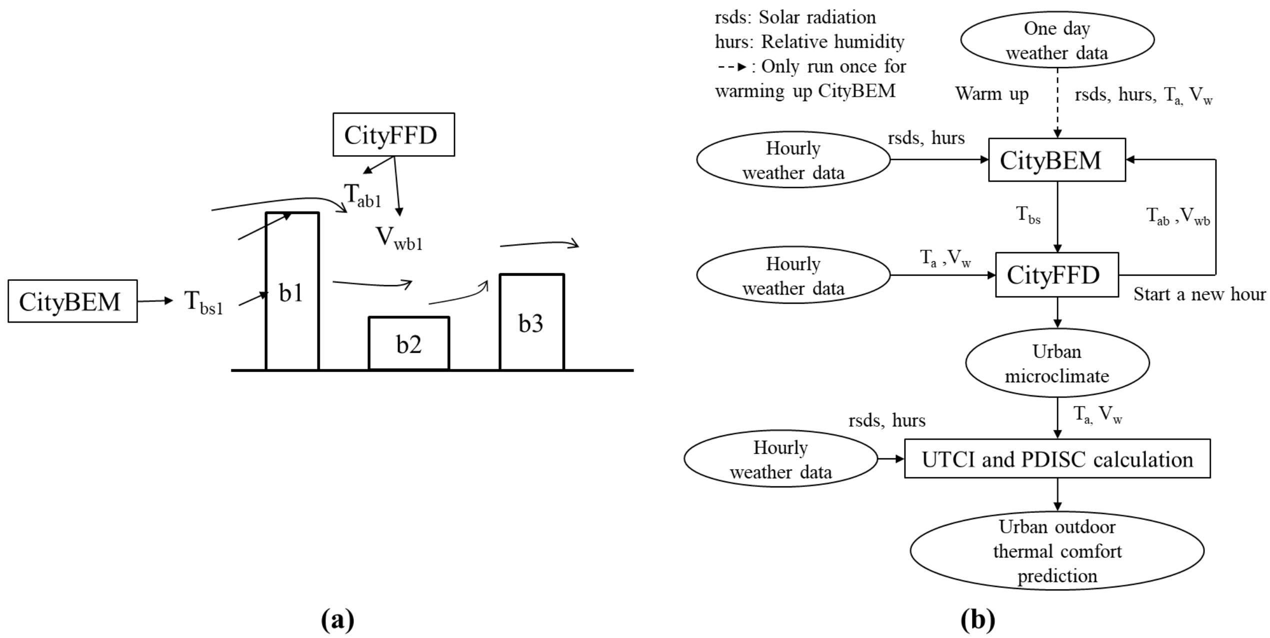

Fig. 3.5 (a) Simulated results from CityFFD and CityBEM (T_{abi} is air temperature surrounding the building i, T_{bsi} is the surface temperature on building i, V_{wbi} is the wind speed surrounding the building i) (b) Flowchart of UTCI prediction process through CityFFD and CitBEM simulation

3.2.3.2 Case design and independence test

With the building geometries in Montreal downtown area shown in Fig. 3.2, the computational domain is designed accordingly, as shown in Fig. 3.6, which follows the AIJ [196] and COST guidelines [197]. Here, H is the highest building inside domain, which is 120m.

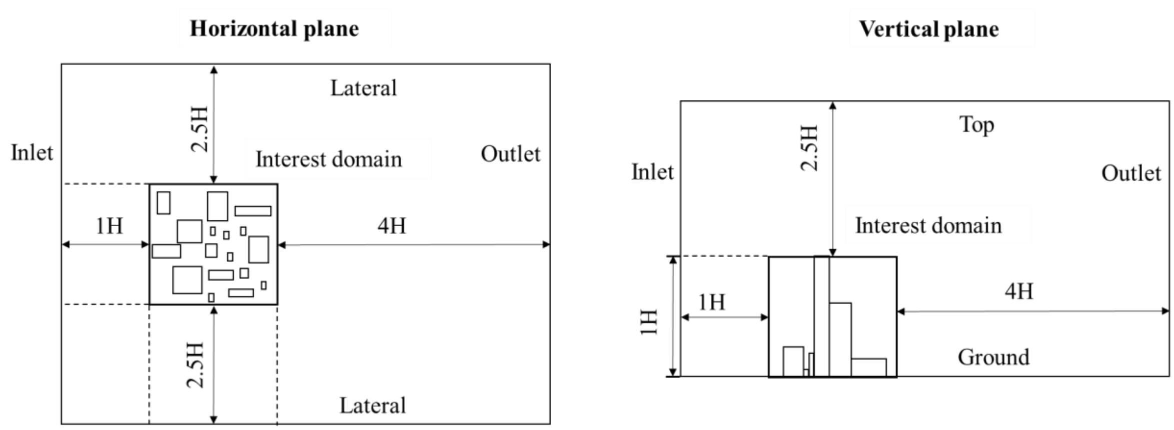

Fig. 3.6 Design of the computational domain for urban microclimate CFD simulation following AIJ [196] and COST guidelines [197] (H is the highest building inside the interest area)

To determine an appropriate mesh size and CFL number for CityFFD simulation, this study designs different combinations of mesh size and CFL number to see their impacts on numerical accuracy. The AIJ CaseF (Building complexes with complicated building shape in actual urban area (Shinjuku)) was selected for testing. There are in total 33 monitoring points inside the domain, with two points at the rooftop of high-rise buildings and the remaining ones are distributed at the height of 10 m. Here, the minimum mesh size refers to the size of the mesh inside the area of interest, where the sizes of the meshes are all constant. For the mesh size of the remaining computational domain, a growing rate of 1.2 is applied. The CFL number is calculated by wind speed, time step size, and minimum mesh size. Due to the ability of CityFFD, it could use CFL large than 1 to conduct CFD simulation with promising accuracy. Here, three CFL number were tested which are 10, 5, and 1.

Table 3.1 Independence test of mesh size and CFL number

Independence test parameters	Coarse	Medium	Fine

Minimum mesh size (m)	5 × 5 × 1	2 × 2 × 1	1 × 1 × 1
CFL (wind speed × time step size/minimum mesh size)	10	5	1

Here, Fig. 3.7 (a) and (d) are designed to compare the numerical results from different mesh and CFL design with the experimental results. Two error bars of 30 percentage were used to show the general accuracy. It could be found that, with the increasing mesh size and CFL number, the numerical results tend to be underestimated compared to experiment data. Both fine and medium design of mesh size and CFL number provide promising accuracy. From Fig. 3.7 (b), (c), (e) and (f), it is clear that the difference between fine and medium design is relatively small. Thus, to achieve a compromise between numerical accuracy and efficiency, the minimum mesh size is set to 2 m and the CFL number is set to 5 in the following CtiyFFD simulation. The validation of co-simulation between CityFFD and CityBEM inside the same domain has been done in our previous work for an entire historical heatwave period, and more details could be found in Katal, et al. [334].

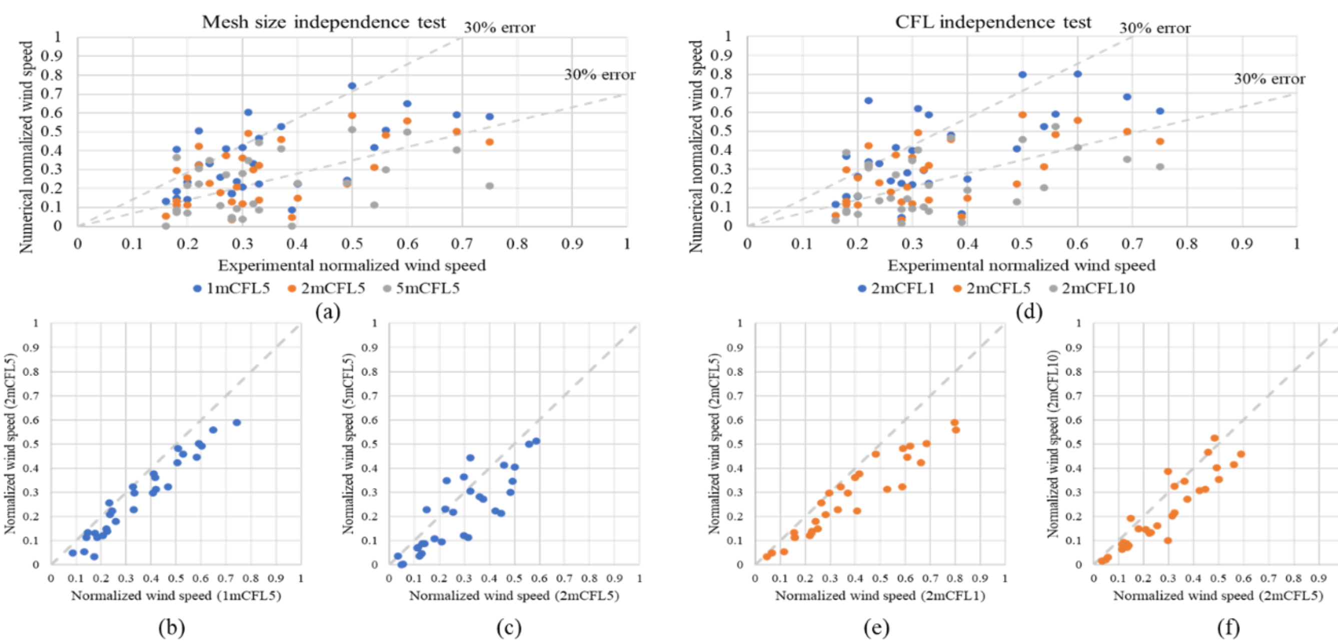

Fig. 3.7 Results of mesh and CFL independence test (mesh size = 1 m, 2 m, 5 m; CFL = 1, 5, 10). (a), (b), (c) are designed for mesh independence test. (d), (e), (f) are designed for CFL independence test.

Independence tests of mesh size and CFL number are conducted to determine appropriate mesh size and time step size which as illustrated above. In this study, considering a compromise between the numerical accuracy and computational efficiency, the horizontal mesh size is set as 2 m and the vertical mesh size is set as 1 m for the interest area. A growing ratio of 1.2 is applied for mesh design of the remaining computational domain, as shown in the following Fig. 3.8. According to the results of independence test, CFL number is set as 5 for the following simulation.

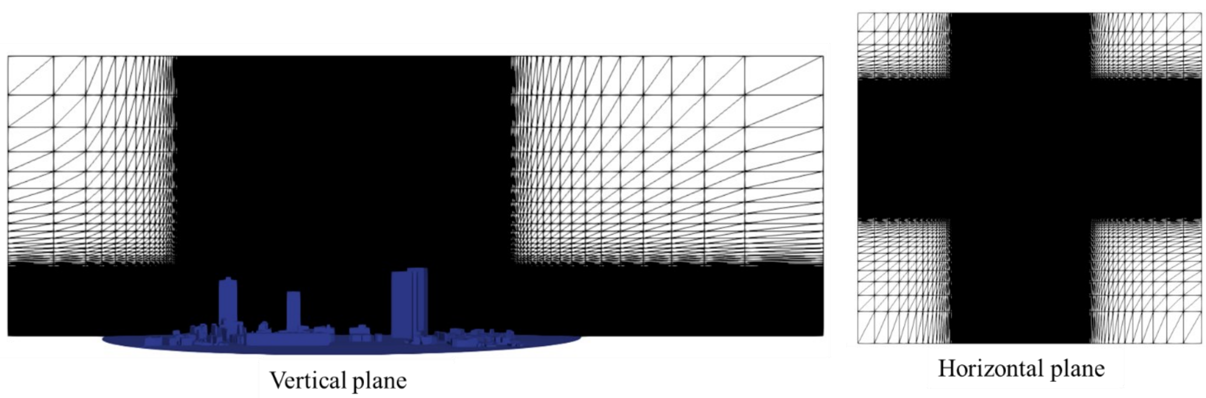

Fig. 3.8 Mesh design of computational domain.

3.2.4 Overheating evaluation index

3.2.4.1 Universal Thermal Climate Index (UTCI)

In the context of urban microclimate research, the Universal Thermal Climate Index (UTCI) would best capture the temporal variability of thermal conditions than other thermal comfort indices [336]. Compared with other thermal comfort indices having a stronger correlation with ambient air temperature, like the Heat Index (HI), Humidex, Apparent Temperature (AT), Physiological

Equivalent Temperature (PET), and Perceived Temperature (PT), UTCI is adept at accurately portraying a wide range of climates, weather scenarios, and is highly responsive to changes in environmental factors such as temperature, sunlight exposure, humidity, and particularly wind velocity [337]. The thermal stress catalogue corresponding to UTCI (˚C) values was listed in Table 3.2.

Table 3.2 Thermal stress category based on the value of UTCI.

UTCI (℃)	**Stress Category**
46 ≤ UTCI	Extreme heat stress
38 ≤ UTCI < 46	Very strong heat stress
32 ≤ UTCI < 38	Strong heat stress
26 ≤ UTCI < 32	Moderate heat stress
9 ≤ UTCI < 26	No thermal stress
0 ≤ UTCI < 9	Slight cold stress
-13 ≤ UTCI < 0	Moderate cold stress
-27 ≤ UTCI < -13	Strong cold stress
-40 ≤ UTCI < -27	Very strong cold stress
UTCI < -40	Extreme cold stress

Based on its definition [337-339], UTCI is a function of air temperature (T_a), wind speed (V_{w_10}), relative humidity (RH), and mean radiant temperature (T_{mrt}).

$$UTCI = f(T_a; V_{w\_10}; RH; T_{mrt}) \tag{3.4}$$

In addition, UTCI requires the wind speed at the elevation of 10 m above the ground. Thus, in this study, the wind speed (V_w) extracted from CFD is transformed into the wind speed at 10 m height through the power law equation:

$$\frac{V_w}{V_{w\_10}} = (\frac{h_{pd}}{h_{ref}})^{\alpha} \quad (3.5)$$

Here, V_w is the wind speed extracted from CFD at the pedestrian level height (h_{pd}) of 2 m. V_{w_10} is estimated wind speed at 10 m height (h_{ref}) for the same location, which is normally the reference height of power law wind profile. α is the exponent of power law wind profile, set as 0.3 for a dense urban area [340-342].

The mean radiant temperature (T_{mrt}) could be calculated through Equation (3.6), as a function of global temperature (T_g), wind speed (V_w) and air temperature (T_a) [336], where the global temperature (T_g) could be estimated by air temperature (T_a), wind speed (V_w) and solar radiation S_0 by equation (3.7):

$$T_{mrt} = [\left(T_g + 273.15\right)^4 + 2.47 \times 10^8 \times {V_w}^{0.6} \times \left(T_g - T_a\right)]^{0.25} - 273.15 \quad (3.6)$$

$$T_g = T_a + \frac{S_0 - 30}{0.0252 S_0 + 10.5 V_w + 25.5} \quad (3.7)$$

In these equations, the air temperature and wind speed are obtained by the co-simulation of CityFFD and CityBEM, while the solar radiation and relative humidity are directly extracted from the input climate file described in Section 3.2.2.

3.2.4.2 Dynamical thermal comfort index

The current outdoor thermal comfort indices, including the Universal Thermal Climate Index (UTCI) discussed earlier, are based on steady-state conditions and may not accurately reflect the real-world experiences of pedestrians. These experiences are often characterized by dynamic, short-term exposure to a variety of micro-environments during activities like walking and cycling for daily commutes.

To address this limitation and better quantify the thermal discomfort that accumulates during active travel, we have implemented the discomfort capacitor model *(PDISC)* [343]. The *PDISC* effectively captures the variable nature of thermal exposure and provides a more representative measure of discomfort. Details of the *PDISC* scale are presented in Table 3.3.

Table 3.3 Practical thermal discomfort scale (PDISC) and the physiological criteria (ΔT_b, change in mean body temperature) for the majority (75%) of participants.

PDISC	Behaviour impact	ΔT_b (°C)
0 – Comfortable and pleasant		
1 – Slightly uncomfortable but acceptable	Aware of but not bothered by this discomfort.	0.14
2 – Uncomfortable but tolerable	Can still live with this discomfort, but may adjust behaviour to better adapt, such as walking faster or choosing to walk in the shade if possible [344].	0.26
3 – Very uncomfortable and intolerable	Feeling of discomfort is strong enough to force a temporary stop for a break, to grab a cold drink to cool down, before considering continuing.	0.39

The change in mean body temperature is calculated as:

$$\Delta T_b = T_b - T_{b0} \tag{3.8}$$

Where, T_{b0} is the initial mean body temperature, and T_b is the real time mean body temperature. The mean body temperature combines changes in mean skin temperature (T_{skin}) and body core temperature (T_{core}) as,

$$T_b = 0.1 * T_{skin} + 0.9 * T_{core} \tag{3.9}$$

Previous experiments (Table 3.3) revealed most participants began reporting slight discomfort after a 0.14 °C increment in mean body temperature. After another 0.26 °C rise, most participants' (75%) thermal discomfort capacitor became fully charged (from 'pleasant' to 'intolerable discomfort').

This study models the experience of a pedestrian traversing a 1 km route, beginning in a state of neutral thermal comfort. The designated path, depicted as a black line in Fig. 3.2 (c), runs from the southwest to the northeast. To predict dynamic thermal comfort, we examine three walking speeds: 0.9 m/s, 1.3 m/s, and 1.7 m/s. Environmental parameters (derived in Section 3.2.2) along this route are processed with a one-minute averaging window before being fed into the JOS3 model [345].

A typical summer clothing with a total insulation value of 0.51 clo is assumed. Metabolic rates corresponding to three different walking speed are set as 2.0 Met, 2.6 Met, 4.0 Met [346]. The open-source JOS3 code [345] was used to iterate the skin and core temperature over time, with the model generating local skin and core temperature results at one minute intervals.

3.3 Results and discussion

To evaluate the climate change impacts on steady-state outdoor thermal comfort, the future climate data from the RCM (described in Section 3.2.2) is used as the input data for CityFFD-CityBEM co-simulation (described in Section 3.2.3) for simulating the urban thermal and wind field among the Montreal downtown area (described in Section 3.2.1) with the horizontal mesh resolution of 2 m. Section 3.3.1 shows the procedure of obtaining temporal and spatial historical steady-state and dynamic thermal comfort conditions with co-simulation results. Sections 3.3.2 and 3.3.3 will focus on evaluating the climate change impacts on steady-state and dynamic thermal comfort respectively, by comparing between 2010s, 2050s, and 2090s.

3.3.1 Historical outdoor thermal comfort evaluation

Fig. 3.9 shows example of the UTCI distribution at the height of 2 m of Montreal downtown area at 12 pm under extreme hot condition of 2010s (Fig. 3.9 (c)) with the simulated air temperature field (Fig. 3.9 (a)) and wind speed field (Fig. 3.9 (b)) by CityFFD-CityBEM co-simulation. The relative humidity and solar radiation are obtained from local measurement in each hour and are assumed evenly distributed among the urban area for UTCI calculation. As could be found in Fig. 3.9 (c), due to the absorption of solar radiation and heat release from the building, the temperature of building surface will be higher than that of the far flow field, and thus, the urban area close to the buildings will be significantly heated.

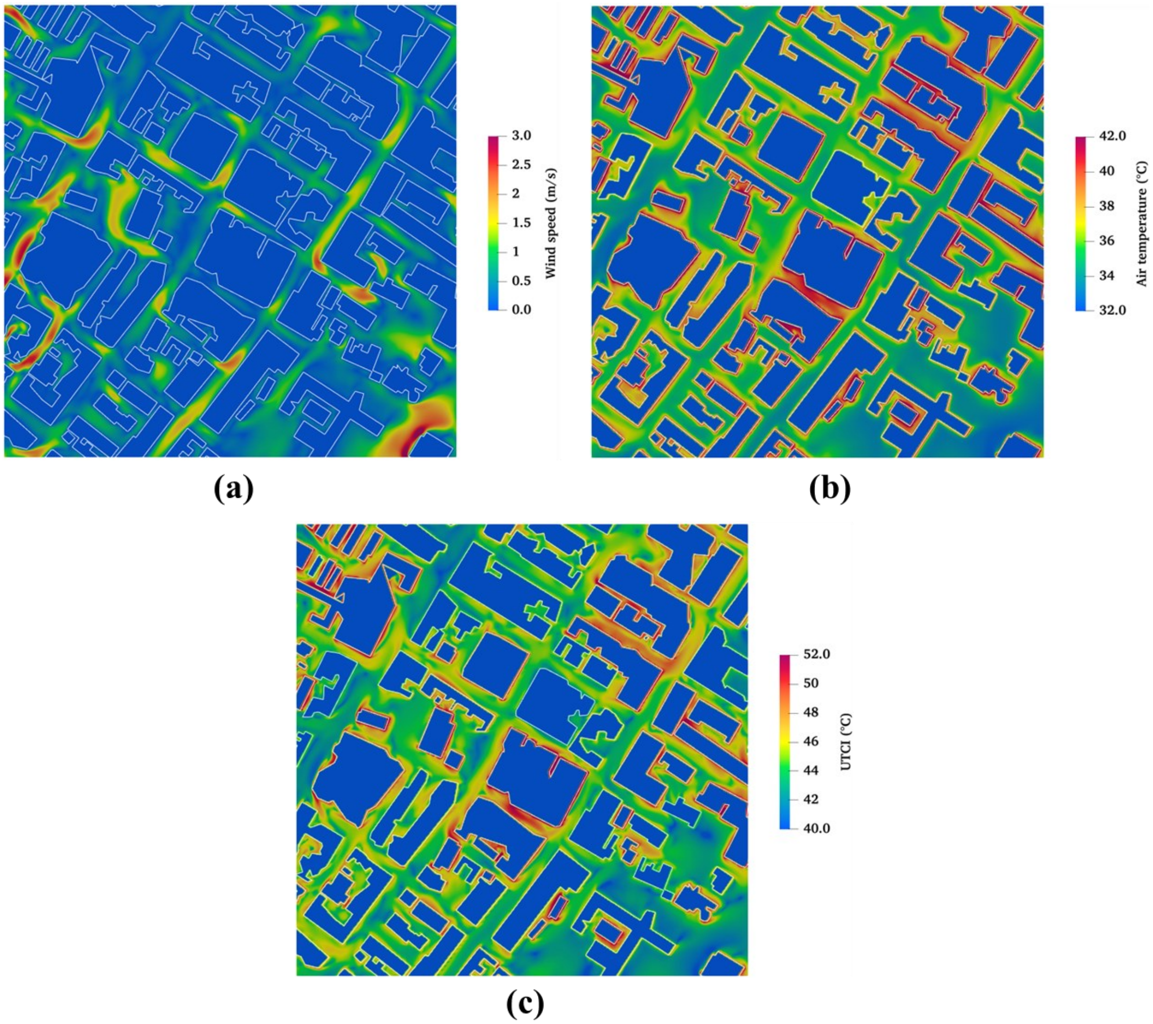

Fig. 3.9 UTCI distribution at the height of 2 m of Montreal downtown area at 12 pm under extreme hot condition of 2010s. (a) Air temperature distribution. (b) Wind speed distribution. (c) UTCI distribution.

Fig. 3.10 presents a thermal stress distribution at a height of 2 meters in downtown Montreal during a day under extreme warm conditions for the 2010s. The color bar chart represents the percentage of space, categorised by hour, that falls under various thermal stress categories, ranging from extreme cold stress to extreme heat stress. The entire downtown area is subjected to different level of heat stress (ranging from moderate to severe heat stress) for the daytime hours (from 6 am to

8pm), suggesting a substantial risk of outdoor overheating and potential discomfort for individuals exposed to these conditions. The highest level of heat stress is observed at 2pm, with 82% of the downtown area falling into the extreme heat stress category during that time.

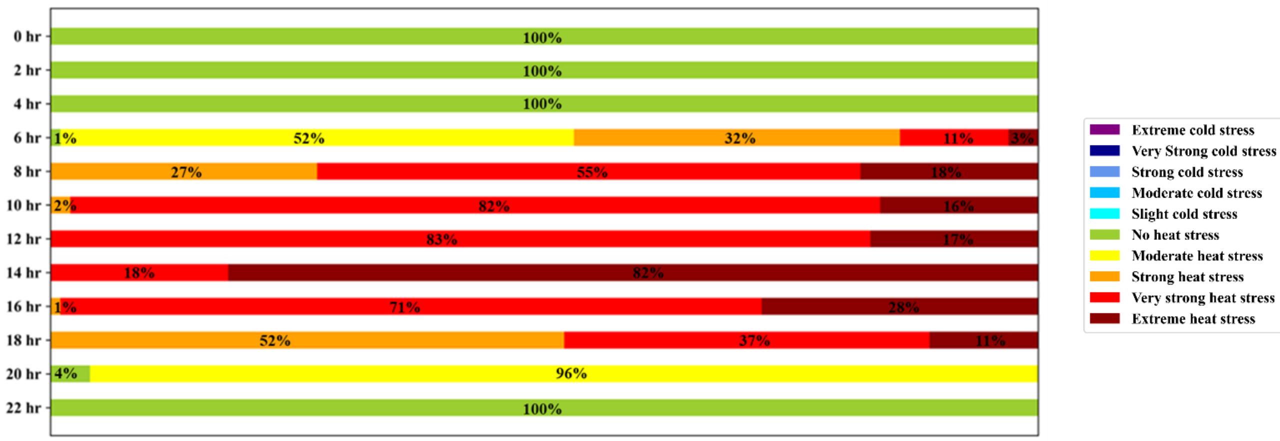

Fig. 3.10 Thermal stress distribution at the height of 2 m of Montreal downtown among the day under extreme warm condition of 2010s.

To calculate the dynamic thermal comfort index, known as PDISC, for the specified route depicted in Fig. 3.2 (c), wind velocity and air temperature data were extracted from the CityFFD-CityBEM simulation corresponding to the route, as illustrated in Fig. 3.9 (a) and (b). These simulated climatic factors, together with solar radiation and humidity, were inputted into the JOS3 model [345] to estimate the mean skin and core body temperatures experienced along the route. Subsequently, Eqs. (8) and (9) were utilized to determine the variation in average body temperature. The three PDISC levels (1-slightly uncomfortable but acceptable, 2-uncomfortable but tolerable,3-very uncomfortable and intolerable) are categorized based on the corresponding change in mean body temperature, as shown in Table 3.3 Practical thermal discomfort scale (PDISC) and the physiological criteria (ΔT_b, change in mean body temperature) for the majority (75%) of participants.. PDISC at each time step is then calculated by linear interpolation of physiological data between the two neighbouring PDISC levels. Fig. 3.11 (c) presents the change in mean body temperature and PDISC values at noon, under TDD of the 2010s for three different walking speeds: 0.9 m/s, 1.3 m/s, and 1.7 m/s.

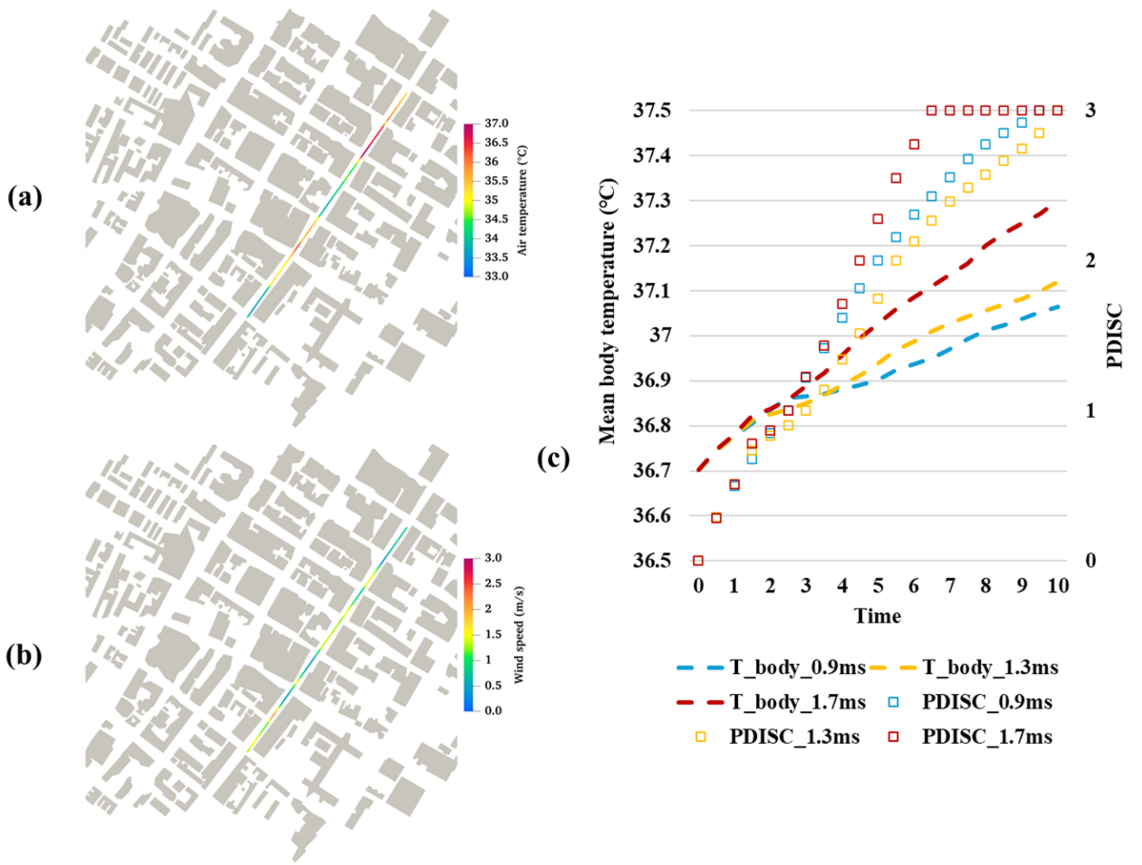

Fig. 3.11 Air temperature (a) and wind speed (b) of 1 km route inside Montreal downtown area at 12 pm under EWD of 2010s, and calculated mean skin temperature and PDISC at the route (c) under three walking speed 0.9 m/s, 1.3 m/s, and 1.7 m/s.

3.3.2 Impacts of climate change on steady-state outdoor thermal comfort

Fig. 3.12 and Fig. 3.13 highlight the UTCI distributions during three specific times of the day—9 am, 12 pm, and 5 pm—when city dwellers typically commute to work, take their lunch breaks, and return home. These times represent the peak outdoor activity periods for most residents. In the

2010s TDD, the downtown Montreal area predominantly experiences "Slight cold stress" in the early morning and late afternoon, and even midday shows no heat stress, denoting a comfortable environment for outdoor activities. Moving into the 2050s TDD, slight cold stress was replaced by neutral no heat stress conditions, indicating a noticeable warming trend in the local climate possibly attributed to climate change effects. By the 2090s TDD, however, there is a significant change towards warmer conditions. Moderate to severe heat stress cover most of downtown at 9 am and 12 pm, with instances of "Very strong and Extreme heat stress"(in red) occurs locally, signaling an increased risk of severe overheating.

Analyzing the early morning hours of EWD across the decades, we see a stark rise in "Extreme heat stress" from less than 20% in the 2010s to over 40% in the 2050s, soaring nearly to 75% by the 2090s. This trend is a clear indication of intensifying heat stress conditions. At midday, "Extreme heat stress" becomes the primary condition in the 2050s EWD and 2090s EWD, while this only covered less than 20% of the areas in the 2010s. Lastly, for the late afternoon, a marked escalation in "Very strong heat stress" is evident when comparing the 2010s to the 2050s, with the 2090s showing more than half of the area grappling with "Extreme heat stress." These findings underscore a dramatic shift towards higher thermal stress inside Montreal downtown area due to climate change.

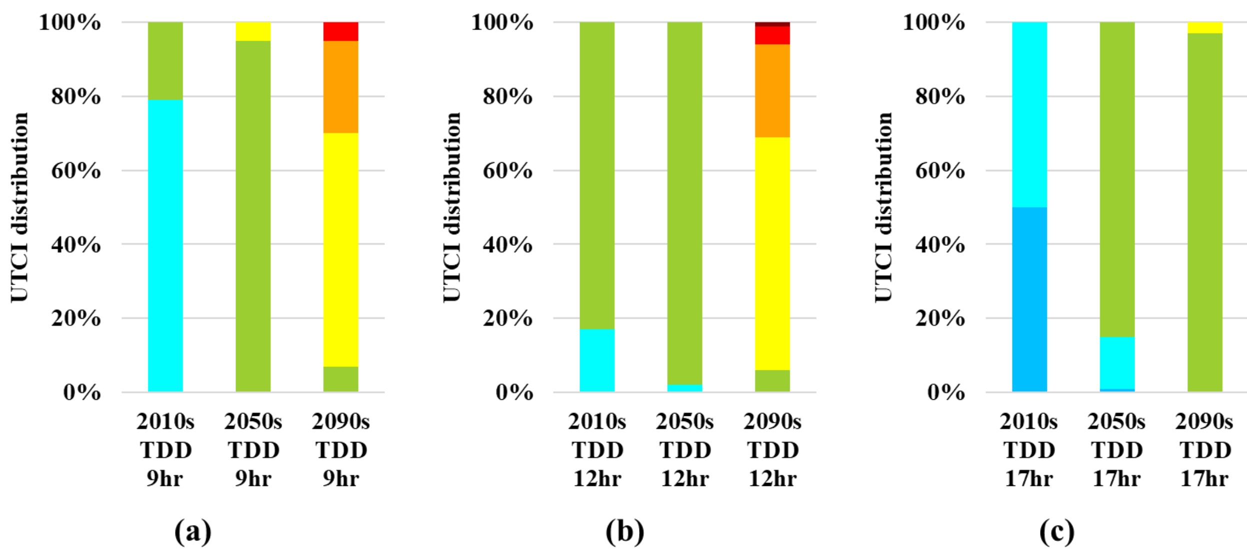

Fig. 3.12 Comparison of UTCI distribution at three selected hours (a) 9 am, (b) 12 pm, and (c) 17 pm under TDD for 2010s, 2050s and 2090s.

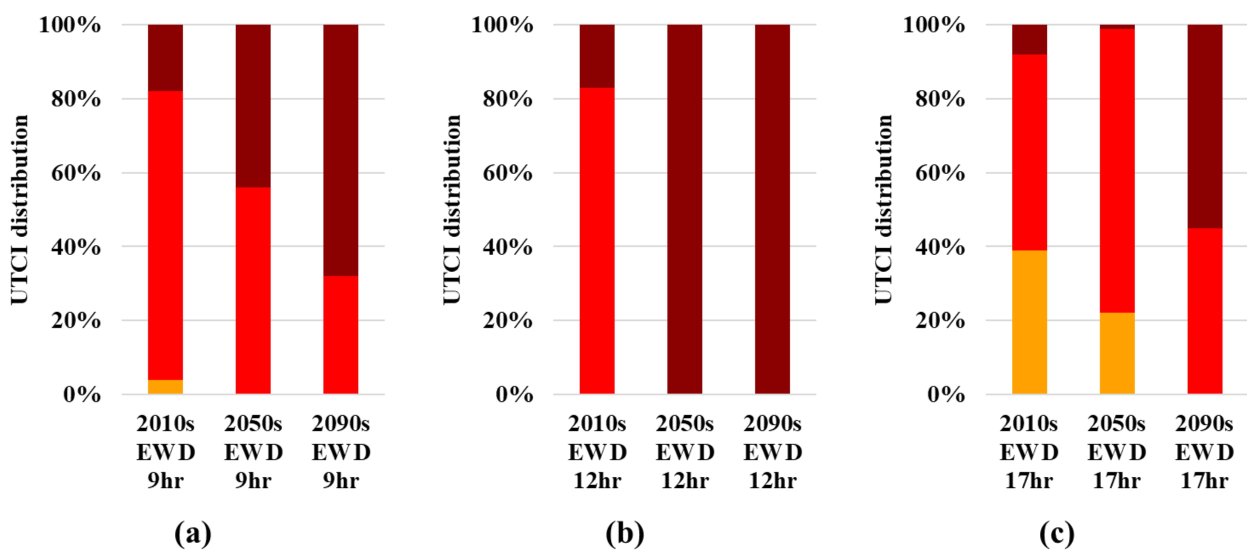

Fig. 3.13 Comparison of UTCI distribution at three selected hours (a) 9 am, (b) 12 pm, and (c) 17 pm under EWD for 2010s, 2050s and 2090s.

Comparing the TDD and EWD conditions within the same time period highlights the importance of considering both average and worst-case scenarios. The TDD conditions suggest a baseline level of heat stress that urban dwellers may frequently encounter, with a noticeable increase in thermal discomfort from the 2010s to the 2090s. The EWD conditions, representing more extreme temperature events, exhibit an even more significant increase in "Extreme heat stress" across all examined hours. This underscores the necessity of including both typical and extreme scenarios in urban overheating studies, as the EWD conditions could have catastrophic health implications if not adequately prepared for. In conclusion, the analysis demonstrates a trend of increasing outdoor overheating due to climate change, with significant implications for urban living and public health. It highlights the need for adaptive measures tailored to both typical and extreme conditions to ensure a resilient urban future.

3.3.3 Impacts of climate change on dynamic outdoor thermal comfort

Universal Thermal Climate Index (UTCI) considers steady-state conditions and may not fully capture the complex and dynamic nature of real-world pedestrian experiences which is often fluctuating and short-term. The analysis of the Practical Discomfort Scale (PDISC) vividly illustrates the impact of climate change on outdoor pedestrian dynamic thermal comfort. Under TDD conditions, pedestrians will not encounter any discomfort along the route during the 2010s and 2050s, regardless of walking speed. However, by the 2090s, pedestrians are likely to feel slightly uncomfortable halfway through the route and may reach tolerable discomfort by the route's end, depending on the walking speed. Under EWD conditions which represent extreme scenarios (Fig. 3.14), the discomfort experienced by pedestrians becomes more severe and also intensified more rapidly. The data from the 2010s to the 2090s demonstrates a significant reduction in the amount of time before pedestrians begin to feel discomfort when walking in downtown area, and this is consistent across different walking speed.

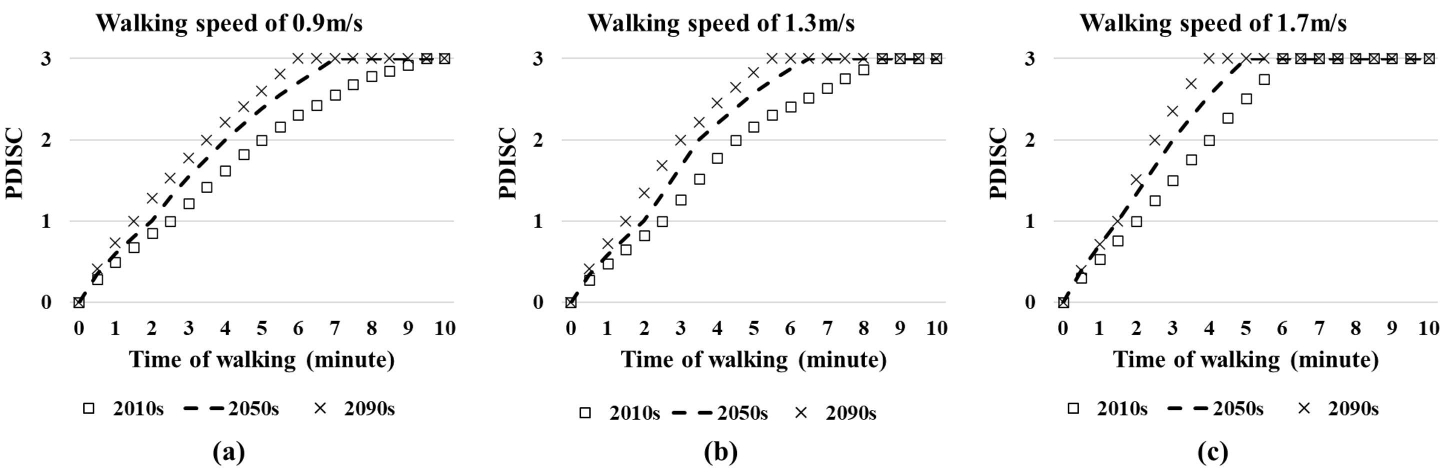

Fig. 3.14 Comparison of PDISC at 12 pm under EWD for 2010s, 2050s and 2090s with walking speed of (a) 0.9 m/s, (b) 1.3 m/s, and (c) 1.7 m/s.

The evaluation of dynamic thermal comfort begins by examining the time it takes to reach the '1-Slightly uncomfortable but acceptable' level during various periods and at different walking speeds. In the 2010s, pedestrians walking at 0.9 m/s began to feel slight discomfort after approximately 2.5 minutes, which decreased to 2 minutes in the 2050s and further to 1.5 minutes in the 2090s. At a faster walking speed of 1.3 m/s, the time to reach slight discomfort remains consistent across the 2010s, 2050s, and 2090s. However, at 1.7 m/s, this period shortens to 2 minutes in the 2010s and to merely 1.5 minutes for both the 2050s and 2090s. Over time, from the 2010s to the 2090s, there is a consistent reduction of approximately half a minute to reach this level of discomfort, across all walking speed.

In the case of '2 – Uncomfortable but tolerable' conditions, the influence of climate change on dynamic thermal comfort is more pronounced. At 0.9 m/s, the time taken to become this tolerable discomfort decreases from 5 minutes in the 2010s to 4 minutes in the 2050s, and to 3.5 minutes in the 2090s. For a walking speed of 1.3 m/s, this duration shortens from 4.5 minutes in the 2010s to

3.5 minutes in the 2050s, and further to 3 minutes in the 2090s. At 1.7 m/s, the time reduces from 4 minutes in the 2010s to 3 minutes in the 2050s and to 2.5 minutes in the 2090s. As we move from the 2010s to the 2050s, there's a general reduction of one minute to reach tolerable discomfort, and from the 2050s to the 2090s, there is a further half-minute reduction.

The trend is even more stark when considering the '3 – Very uncomfortable and intolerable' category. At 0.9 m/s, the time to reach this intolerable discomfort decreases from 9.5 minutes in the 2010s to 7 minutes in the 2050s, and to 6 minutes in the 2090s. At 1.3 m/s, it takes 8.5 minutes in the 2010s but drops to 6.5 minutes in the 2050s and 5.5 minutes in the 2090s. Finally, at the speed of 1.7 m/s, the duration shortens from 6 minutes in the 2010s to 5 minutes in the 2050s and 4 minutes in the 2090s, indicating an average decrease of about two minutes to reach this intolerable discomfort, with an additional minute's reduction as we progress from the 2050s to the 2090s.

To conclude, under the EWD, discomfort evolve much slower in 2010s, allowing pedestrians more time to adapt their behavior or seek relief. However, with each successive decade, the onset of discomfort occurs increasingly earlier, suggesting that the individuals' capacity to adaptive maybe overwhelmed by the rapid progression climate change. By the 2090s, even at this slowest walking pace, discomfort escalates to intolerable levels within only 6 minutes (around 300 meters), emphasizing an urgent need for proactive cooling strategies to mitigate these effects.

3.4 Conclusion

This chapter aims to evaluate climate impacts on both steady-state and dynamic outdoor thermal comfort of an urban area, i.e., Montreal downtown, through CityFFD-CityBEM simulations with a spatial resolution of 2 m. As detailly presented in our previous publication, raw future climate data obtained from CORDEX is bias-corrected with local field measurements, followed by the selection of reference year scenarios through the reference year data method. This research represents an initial effort to predict future steady-state and dynamic thermal comfort at the neighborhood scale by simulating the outdoor urban microclimate. The climate change impacts on steady-state and dynamic thermal comfort in downtown Montreal are quantified by conducting comparisons across the 2010s, 2050s, and 2090s.

A 1.25 km by 1.25 km of Montreal downtown area is selected, due to its high population and building density, for performing CityFFD-CityBEM co-simulation with prepared future climate inputs. Based on the independence test of mesh size and CFL number for CityFFD simulation, the minimum mesh size is set to 2 m and the CFL number is set to 5. Two outdoor thermal comfort indices UTCI and PDISC were applied to evaluate the climate change impacts on future outdoor overheating.

The results of our study clearly illustrate the profound impact of climate change on both steady-state and dynamic aspects of outdoor thermal comfort, particularly during typical commuting times (9 am, 12 pm, and 17 pm) in downtown Montreal. Under the typical condition (TDD), early mornings (9 am) and late afternoons (17 pm) in the 2010s were characterized by "Slight cold stress," transitioning to "No thermal stress" by midday (12 pm), indicating comfortable conditions for outdoor activities. However, by the 2050s, a shift towards warmer conditions emerges, with "No heat stress" observed throughout the day, culminating in "Extreme heat stress" instances by the 2090s, highlighting a significant increase in overheating risks. The trend towards heightened thermal stress is further accentuated under extreme weather conditions (EWD), with "Extreme heat stress" becoming more prevalent across all time periods, showing an escalating threat of severe overheating.

This escalation is also quantified through the dynamic thermal comfort analysis, revealing a marked decrease in the amount of time before pedestrians begin to feel discomfort when walking at various speeds, from the 2010s through to the 2090s. Pedestrians will experience no discomfort walking along the route in the 2010s and 2050s under TDD conditions. However, by the 2090s, tolerable discomfort may arise after 5 minutes of walking. Under EWD conditions, intolerable thermal discomfort becomes inevitable at noon, and the duration of time for which discomfort remains tolerable is expected to be reduced from 6 minute in 2010s to 4 minute in 2090s for a brisk walk. This consistent reduction in discomfort onset times—regardless of walking speed/across all walking speed—underscores the urgency for strategic urban cooling design interventions.

This study also acknowledges a few limitations that merit attention for future research. Firstly, because of lack of future city terrain information, it is assumed that no alterations in urban terrain and building morphology over time, overlooking potential developments or renovations that could impact thermal comfort. The focus on a single route for the Practical Discomfort Scale (PDISC) analysis may also limit the generalizability of our findings across the entire downtown area. Furthermore, the current work does not account for the potential benefits of urban greening, which might help decrease local overheating. As part of the research contributions from this study, despite of these assumptions, the proposed research method and procedure in this study will still apply, given this information would become available, and the integrated model developed, such as CityFFD-CityBEM, will be made available for other researchers upon request.

In future studies, there is a critical need to explore mitigation strategies that can address the escalating issue of overheating in urban environments. Specifically, nature-based solutions should be investigated for their effectiveness in mitigating extreme heat conditions, considering their potential to enhance urban resilience to climate change. Expanding the application of our analytical framework to other cities across different climate zones would also provide valuable insights into the varying impacts of climate change on urban thermal comfort globally. Such research would not only broaden our understanding of urban heat dynamics but also inform more holistic and adaptable urban planning and design strategies to ensure sustainable and livable cities.

Chapter 4

Assessing climate change impacts on urban overheating through Representative Methods on Spatial and Temporal Scales by implementing WRF and CityFFD

4.1 Introduction

In Chapter 2, we evaluate the climate change impacts on indoor and outdoor overheating at the regional scale. Chapter 3 assesses the impacts of climate change on outdoor overheating at the building level through CFD simulation. The reference year generation method used in the previous chapters significantly reduces labor and computational costs when processing long-term climate data, allowing for predictions of typical and extreme future overheating conditions. However, evaluations of future outdoor overheating in Chapters 2 and 3 are limited to either regional scales or specific urban areas (downtown Montreal), which may not represent the general or extreme conditions of an entire city. Thus, in this chapter, to assess climate change impacts under both representative temporal and spatial conditions, we aim to develop a representative location method. This method will help identify typical and extreme locations for more precise microclimate assessments through CFD simulation. Initially, the NARR dataset is used to perform a WRF simulation considering urban effects for the entire city during a historical heatwave. Subsequently, the representative location method is employed to select the typical and extreme hot and cold locations based on the WRF simulation output throughout the city during the heatwave. After demonstrating the significance of this representative location, we collect historical (1996-2015) and future (2080-2099) CONUS II WRF data for the entire Montreal area and select the typical location under the same heatwave period. Then, the reference year selection method is applied to obtain typical and extreme hot historical and future climate inputs for the typical location from long-term CONUS II WRF data. Finally, we perform CFD simulations for this typical location using the typical and extreme hot climate inputs. The workflow of this chapter is shown as Fig. 4.1.

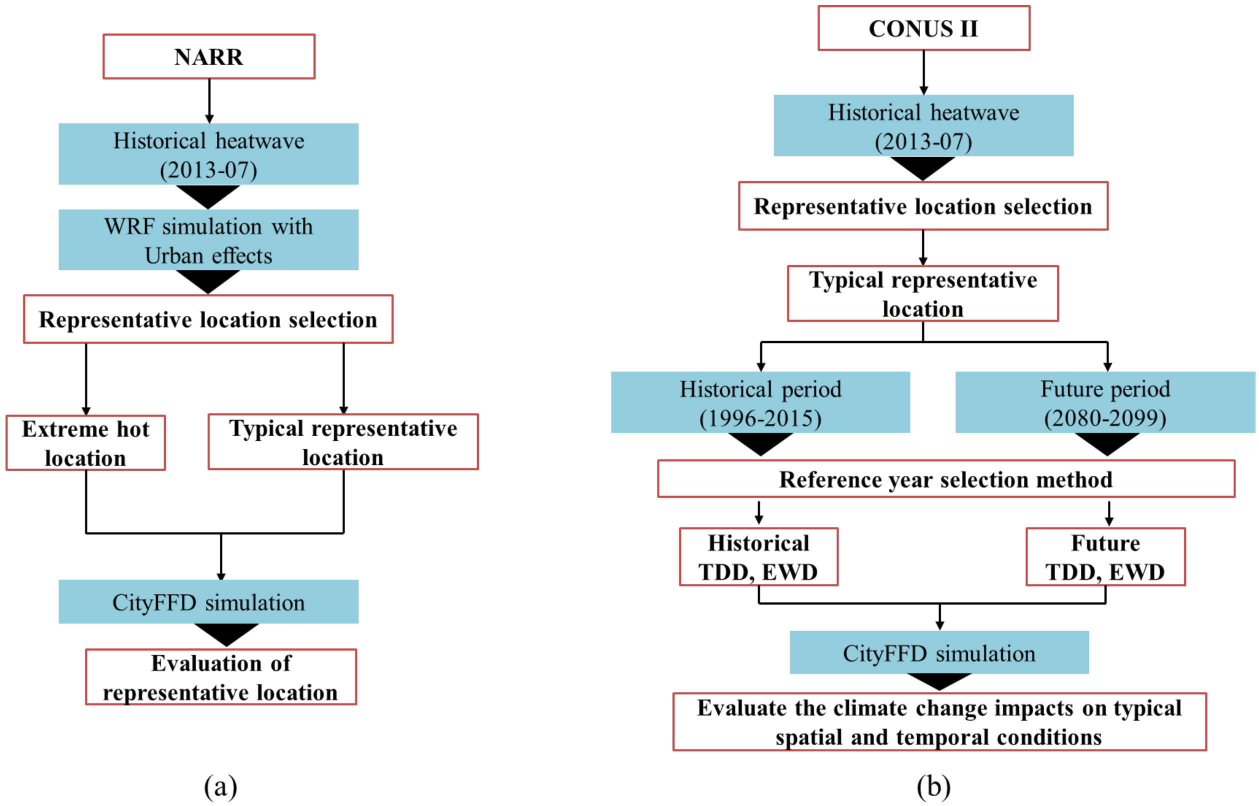

Fig. 4.1 Workflow of the chapter. (a) Demonstration of representative location method through WRF simulation using NARR input. (b) Implementing temporal and spatial representative method for predicting future urban overheating using CONUS II WRF data.

4.2 Methodology

4.2.1 Study region

The city of Montreal is selected for performing representative location selection, as shown in red box of Fig. 4.2. The detailed description of Montreal could be found in Section 2.2.1 and Section 3.2.1.

Fig. 4.2 City of Montreal for representative location selection

4.2.2 Climate data collection

- NCEP North American Regional Reanalysis (NARR)

The NCEP North American Regional Reanalysis (NARR) employs the Eta model (32 km resolution with 45 vertical layers) to produce comprehensive reanalysis products on the Eta 221 grid across 29 pressure levels. This dataset incorporates a wide range of observational inputs and is noted for its detailed three-hourly output analyses, which include additional variables to reflect accumulations or averages over the period. In this study, NARR datasets will be then used as the input climate data for WRF to simulate the urban climate of Montreal during 2013 heatwave.

Typical representative location and extreme hot location during 2013 heatwave will then be selected using WRF simulation results.

- CONUS (Continental U.S.) II High Resolution Present and Future Climate Simulation

The CONUS II simulations utilize the mean of the CMIP5 models as the boundary forcing for a high-resolution (4km) WRF model to simulate the mesoscale hydro-climate for two 20-year periods (1996-2015 and 2080-2099). These simulations are designed to capture both climate internal variability and greenhouse gas-induced changes, providing a realistic depiction of mesoscale terrain features and precipitation patterns over the CONUS. The WRF output of CONUS during 2013 heatwave will firstly be extracted for selecting typical representative location. Then, the climate data of the typical representative location will be extracted for both historical (1996-2015) and future (2080-2099) time period to perform reference year selection.

4.2.3 Numerical simulation of urban climates

4.2.3.1 WRF simulation with NARR

Urban climate modeling was conducted using the WRF model version 4.3.3 [347]. For 2013 heatwave period, simulations included a preliminary 24-hour spin-up phase; data from this phase were excluded from the analysis. As depicted in Fig. 4.3, the simulation setup featured three two-way nested domains designed for the Ottawa-Montreal region. These domains were configured with grid resolutions of 9 km, 3 km, and 1 km, corresponding to dimensions of 276 × 296, 250 × 283, and 391 × 364 grid points, respectively. The reason of using 1 km in this study could be referred to our former publication [348]. The National Centers for Environmental Prediction (NCEP) North American Regional Reanalysis (NARR) 3-hourly product (#ds608.0) [349] were used as the initial and boundary conditions for the WRF simulations.

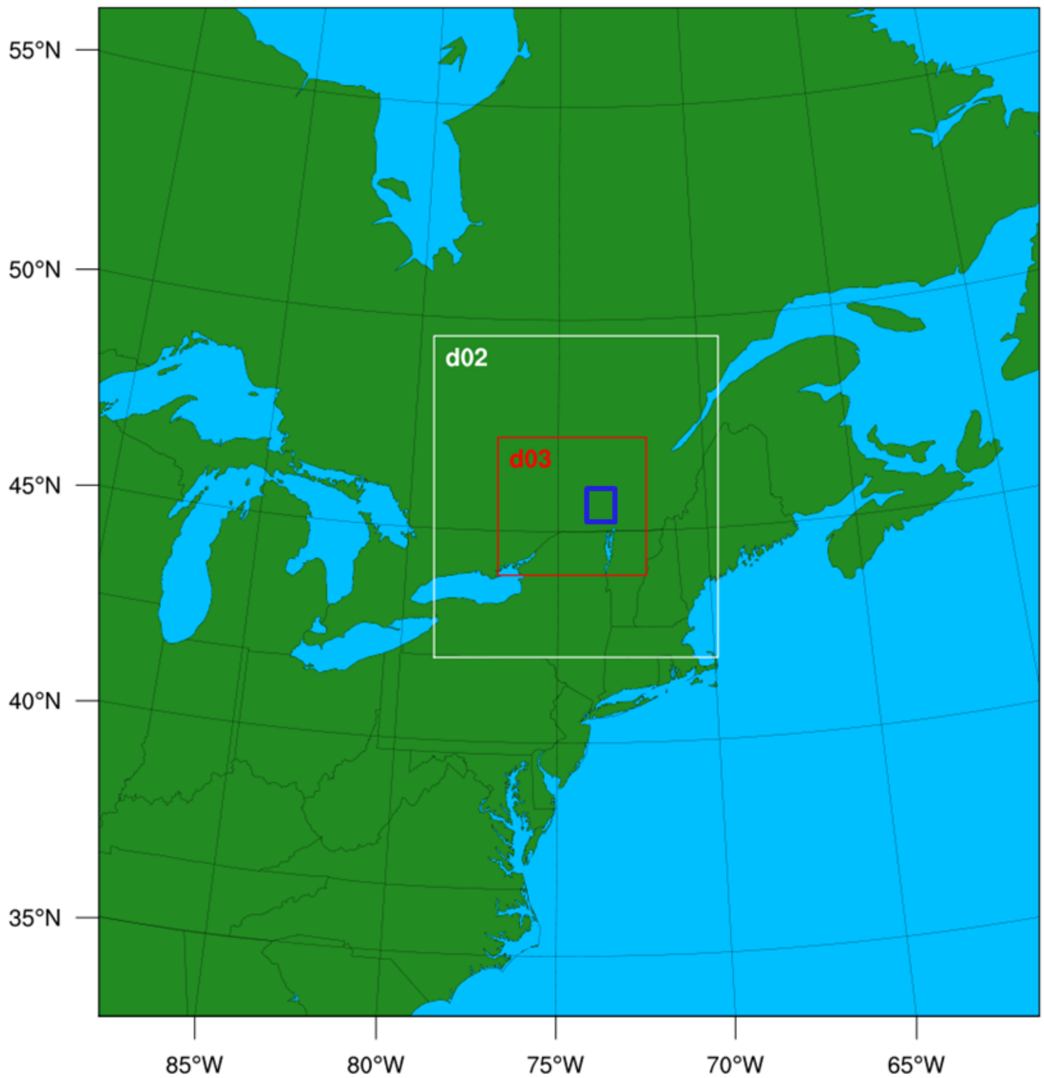

Fig. 4.3 WRF model domain for the city of Montreal (blue)

The physical options are described in Table 4.1, based on the test of the previous studies [84, 348, 350, 351], which yields the highest overall accuracy.

Table 4.2 WRF physics options

Parameterization	Option

Microphysics	WRF Single-Moment 3
Long Wave Radiation	RRTM
Short Wave Radiation	Dudhia
Surface Layer	Eta Similarity
Land Surface Model	Unified Noah
Planetary Boundary Layer	BouLac
Cumulus	Kain-Fristch (domain 1 only)
Urban	BEP + BEM

In a previous study on the Ottawa-Montreal region [77], researchers evaluated different urban parameterizations and land use datasets to find the best WRF model setup for simulating urban climate. Initially, urban areas were represented by a single urban class in the WRF model. The current study extends this by incorporating Local Climate Zones (LCZs) [352] and examining the benefits of using the multilayer urban canopy model, Building Environment Parameterization (BEP) linked with the Building Energy Model (BEM). The BEP+BEM model simulates three-dimensional heat, moisture, and momentum transfer and allows direct interactions with the planetary boundary layer. BEP effectively models complex urban phenomena such as the urban heat island effect [82]. BEM, while simpler, significantly enhances urban energy budget estimates by accounting for heat diffusion through buildings, radiation exchange through indoor surfaces and windows, and heat generation from occupants [353].

For detailed urban land use and land cover data, we used the 100m resolution global LCZ map created by Stewart and Oke [352]. This map categorizes urban areas into 10 built and 7 natural land cover types, developed by training random forest models across numerous global regions. The urban categories from this LCZ dataset, along with the modified IGBP MODIS Noah land-use classification [354], were input into the WRF model.

4.2.3.2 CFD simulation

Different from Chapter 3, this chapter only use CityFFD for CFD simulation. The building surface temperature and ground temperature is obtained through WRF outputs, instead of running CityBEM simulation. CityFFD is based on a 3D fractional step method and Fast Fluid Dynamics (FFD) solver running on the Graphics Processing Unit (GPU) to predict local microclimate features for modeling large-scale urban aerodynamics. The governing conservation equations in CityFFD are dimensionless as follows:

$$\nabla \cdot V = 0 \tag{4.1}$$

$$\frac{\partial V}{\partial t} + (V \cdot \nabla)V = -\nabla P + \left(\frac{1}{Re} + v_t\right)\nabla^2 V - \frac{Gr}{Re^2}T \tag{4.2}$$

$$\frac{\partial T}{\partial t} + (V \cdot \nabla)T = (\frac{1}{Re \cdot Pr} + \alpha_t)\nabla^2 T \tag{4.3}$$

where V, T, P and t are the velocity, temperature, pressure and time, respectively; Re, Gr and Pr are the dimensionless Reynolds number, Grashof number, and Prandtl number, respectively; and v_t and α_t are turbulence-related parameters, i.e., turbulent viscosity and turbulent thermal diffusivity. CityFFD adopts the semi-Lagrangian method for the advection term in Eqs. (4.2), (4.3). Therefore, no iteration is needed to calculate the velocity field, and computing costs are reduced.

4.2.4 Spatial and temporal representative method

Representative method is designed for reducing repeatable labor work as well as computational cost, however at the same time, determine the typical and extreme scenario to represent the general condition. The detailed explanation and evaluation of temporal representative method has been clearly clarified in previous Section 2.2.4 and Section 3.3.2, where typical and extreme years were formulated by amalgamating twelve representative months, identified based on their cumulative distribution function (CDF) of outdoor air temperatures. The hottest day in the EWY (EWD), and typical day in the TDY (TDD) were selected for performing CFD simulation.

Representative location method is developed following a similar logic, where typical and extreme locations were identified based on their cumulative distribution function (CDF) of outdoor air temperatures during a historical heatwave based on the WRF outputs. For each location, the cumulative distribution function (CDF) of the outdoor air temperatures of that location is compared with the CDF outdoor air temperatures from all locations, and the location with the least absolute difference between them is identified as the typical representative location. Extreme cold and hot locations are selected in a similar way. However, instead of selecting the location with the least absolute difference, the location with the maximum and minimum difference between CDFs is selected as the extreme hot and cold location, respectively. The detailed workflow of representative location method is shown in Fig. 4.4.

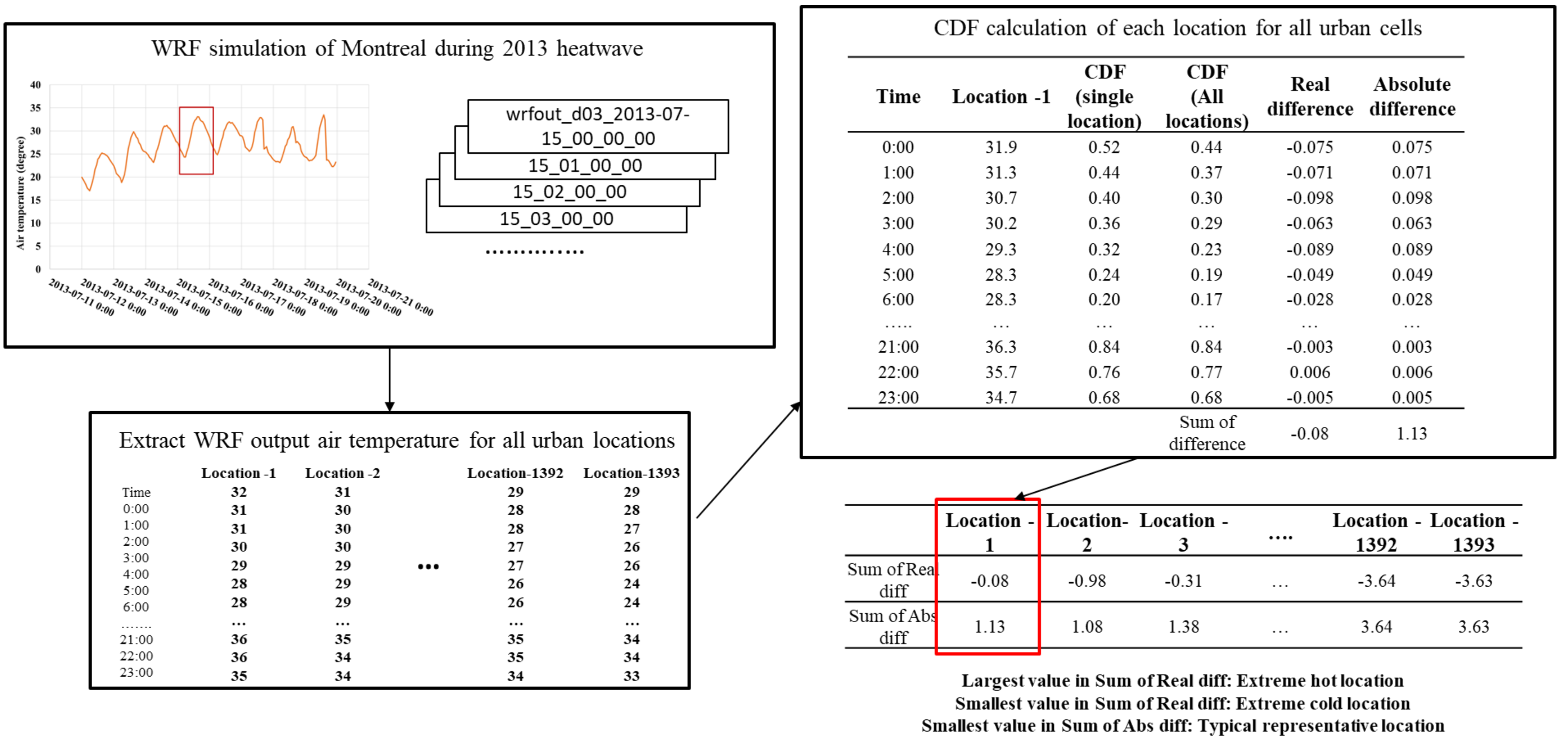

Fig. 4.4 Workflow of selecting typical representative, extreme hot, and extreme cold location with WRF outputs during 2013 heatwave

4.3 Results and discussion

4.3.1 Validation of implementing WRF and CityFFD

To assess the accuracy of using WRF outputs and CityFFD simulations for local urban microclimate evaluation, this study focuses on a specific area within downtown Montreal, depicted in Fig. 4.5. Here, field measurements were taken during the 2013 heatwave. Two sets of simulations were validated: (1) NARR+WRF+CityFFD, which involves conducting a WRF simulation with NARR input followed by a CityFFD simulation using the WRF output; (2) CONUS+CityFFD, which directly utilizes CONUS output data for the CityFFD simulation. It's important to note that urban effects are incorporated in the NARR+WRF+CityFFD simulations through the use of BEM and BEP models during the WRF simulation, whereas the CONUS dataset does not account for urban effects.

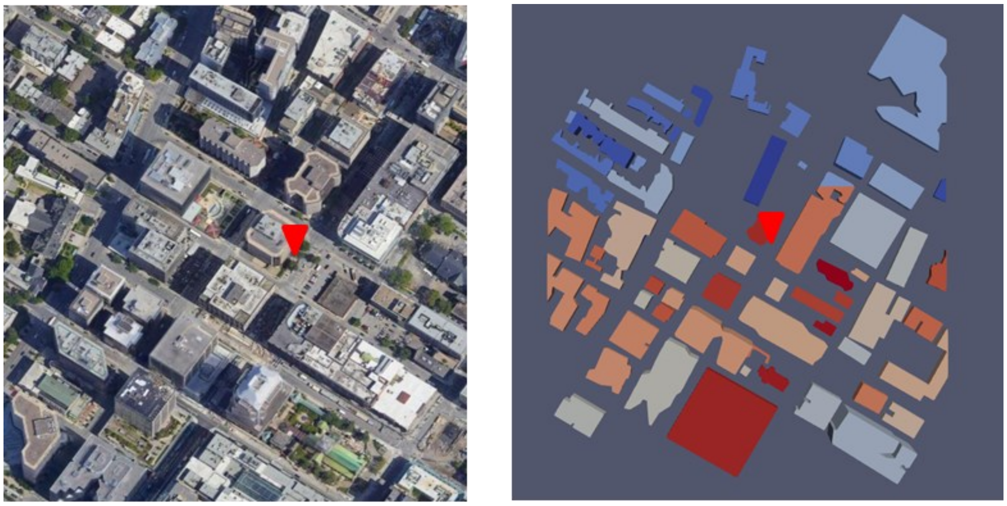

(a) (b)

Fig. 4.5 Selected urban area in Montreal downtown for validation. (a) Map of Montreal downtown. (b) Building geometry of Montreal downtown (red triangle: filed measurement site)

According to the validation results shown in Fig. 4.6, the RMSE for wind speed between CONUS+CityFFD and field measurements is 0.52 m/s, and for NARR+WRF+CityFFD it is 0.77 m/s. For air temperature, the RMSE is 4.6 ℃ for CONUS+CityFFD and 3.5 ℃ for NARR+WRF+CityFFD. Based on Yang, et al. [355], an error around 0.5 m/s in wind speed is deemed acceptable, although the air temperature prediction error in this study exceeds the recommended value of 2.5 ℃. Given that this study uses WRF outputs as inputs for CFD simulations instead of direct, real-life measurements from the local airport, it is expected and acceptable for the numerical errors to be slightly higher than the suggested value. Additionally, it is clear from the analysis that CityFFD simulations incorporating WRF outputs with urban effects tend to underestimate wind speeds in downtown areas, while concurrently overestimating air temperatures. On the other hand, CityFFD simulations using WRF outputs without urban effects show a closer alignment between predicted and actual wind speeds, but they tend to underestimate air temperatures.

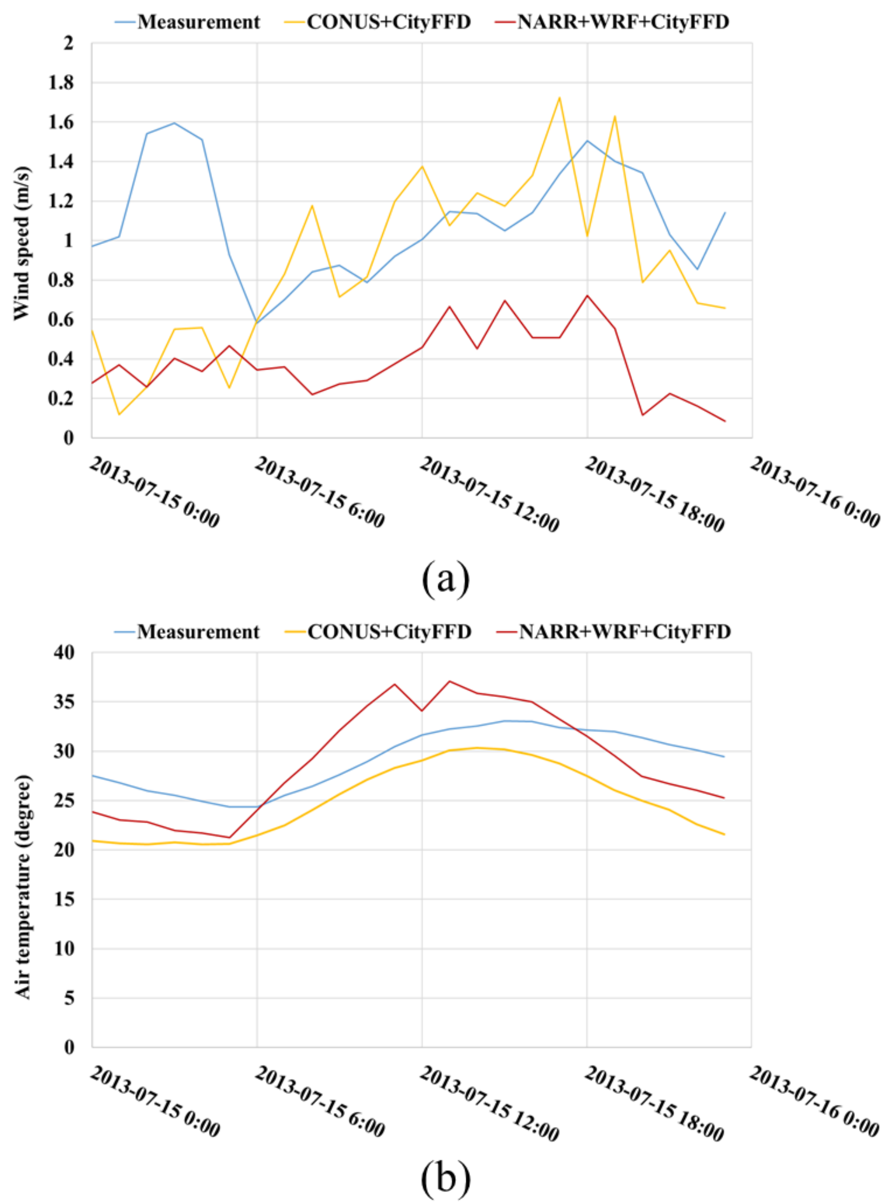

Fig. 4.6 Validation results of implementing WRF outputs and CityFFD. (a) Validation of wind speed. (b) Validation of air temperature.

4.3.2 Evaluation of representative location during heatwave with NARR+WRF+CityFFD

This section will focus on evaluating the representative location method, demonstrating the significance of selecting representative locations for accurately generating typical and extreme urban overheating conditions across the entire urban landscape. As illustrated in Section 4.2.4, the cumulative distribution function (CDF) of temperatures for all locations during the heatwave period is shown in Fig. 4.7 (a). The typical location, chosen from NARR+WRF outputs, is identified as a residential area distant from the downtown core, predominantly featuring low-rise and mid-rise residential buildings, as shown in Fig. 4.8 Fig. 4.7 (b). This selection reflects typical urban residential settings, which generally exhibit more dispersed building layouts and include natural cooling elements such as vegetation. Conversely, Fig. 4.7 (c) illustrates the selected extreme hot location within the dense downtown area of Montreal, characterized by compact high-rise and mid-rise commercial buildings. This area's urban structure, typified by its dense, heat-retaining building materials and minimal vegetative cover.

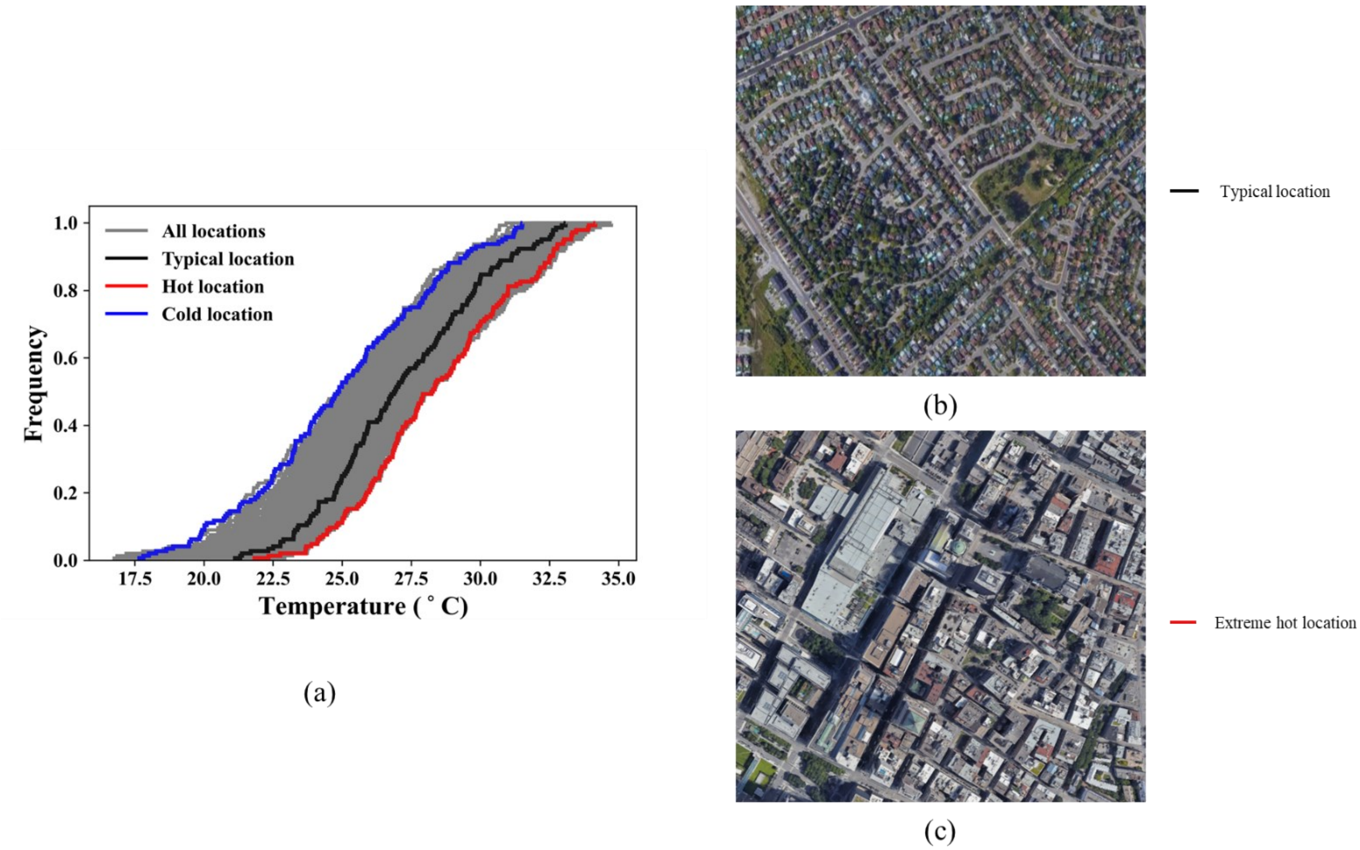

Fig. 4.7 Representative location selected from NARR+WRF. (a) cumulative density function figure of all locations (gray), typical (black), extreme hot (red), and extreme cold (blue) locations. (b) Map of typical location. (c) Map of extreme hot location.

CityFFD simulation is then conducted on the selected typical representative (Fig. 4.7 b) and extreme hot (Fig. 4.7 c) locations with the air temperature, wind speed, wind direction, and surface temperature extracted from NARR+WRF outputs. The air temperature fields of these two locations during 9 am, 12 pm, and 9 pm are shown in Fig. 4.8. It is obvious to find in figure that, the extreme hot location is generally 3 to 4 degrees higher than the typical representative location. At 9 am, the typical location exhibits relatively moderate temperatures with a uniform distribution, suggesting effective overnight cooling. Conversely, the extreme hot location demonstrates considerably higher temperatures even in the early morning, indicative of dense urban structures and heat-retaining materials such as dark pavements or building facades, which compromise the comfort levels and escalate energy consumption for cooling from the start of the day.

By noon (12 pm), as solar radiation peaks, the differences between the two locations become even more pronounced. The typical location, though warmer than in the morning, still shows cooler temperatures. In stark contrast, the extreme hot location displays a significant increase in high-temperature zones, highlighting intense solar absorption and a lack of sufficient mitigating infrastructure. By 9 pm, a substantial decrease in temperatures is found due to the absence of solar radiation. However, the extreme hot location still shows elevated temperatures compared to the typical location. This persistence of heat indicates that the built environment in the extreme hot location retains heat for longer durations. Such conditions extend the need for cooling well into the night, which can significantly impact energy consumption and resident comfort.

This detailed temporal analysis accentuates the profound differences between typical and extreme urban hot spots, emphasizing the necessity of selecting both types of locations for comprehensive urban microclimate evaluations. Such distinctions in air temperature conditions between typical and extreme locations are crucial for accurately assessing the overall urban area microclimate. Specifically, the typical location tends to maintain more moderate temperatures during a heatwave, benefiting from more effective overnight. This provides a relatively comfortable environment for residents, reducing the reliance on energy-intensive cooling systems. In contrast, the extreme hot location exhibits significantly elevated temperatures throughout the day, failing to dissipate the heat effectively even during night-time hours. The elevated temperatures at these hot spots directly impact residents' thermal comfort, potentially exacerbating health risks during heatwaves and leading to increased energy consumption for air conditioning. Such conditions underline the importance in identifying and focusing on these extreme conditions.

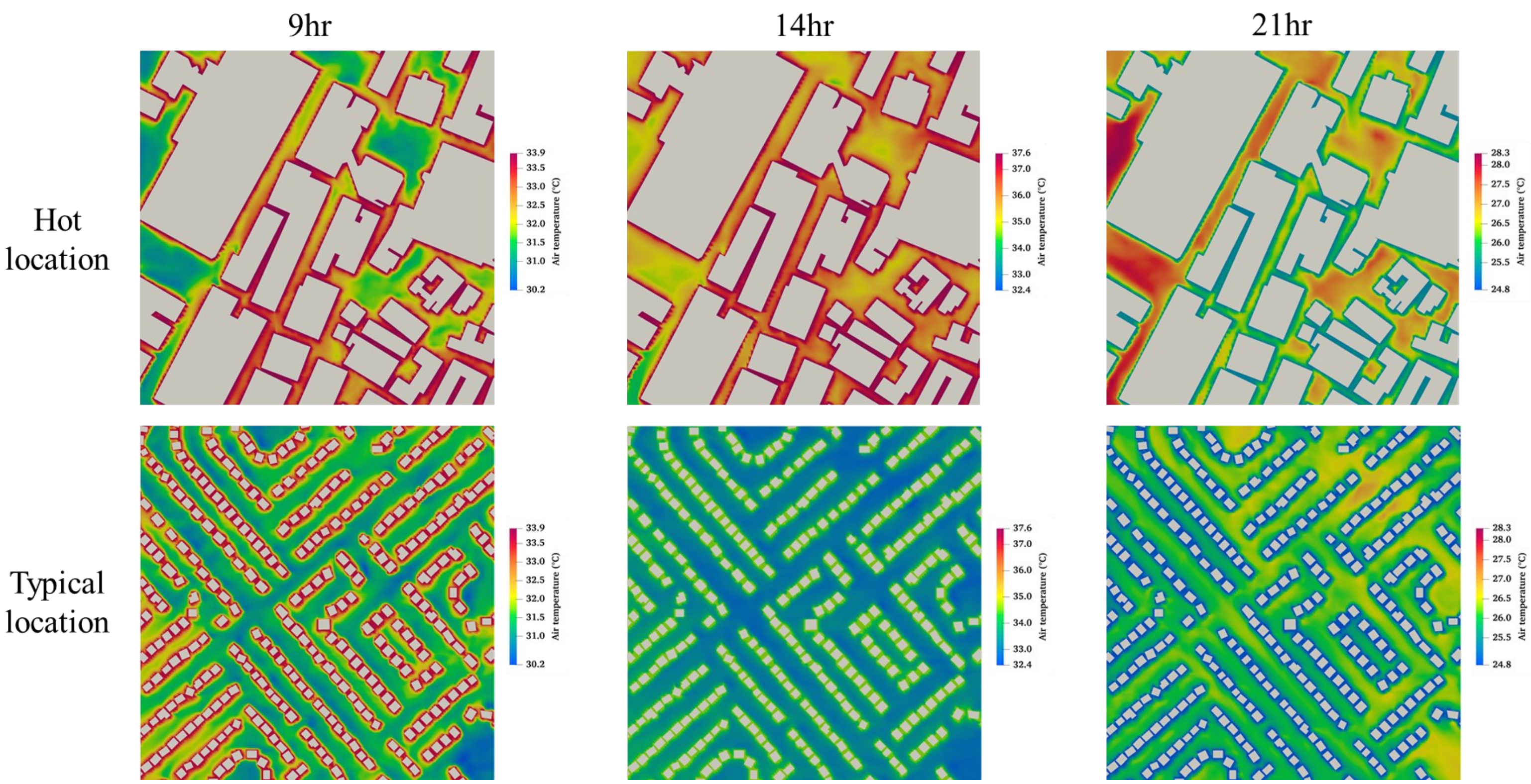

Fig. 4.8 Simulated air temperature distribution of typical representative and extreme hot location on 2013 July 15th 9 am, 14 pm, 21 pm

4.3.3 Evaluate climate change impacts on typical spatial and temporal conditions

The typical representative location is firstly selected using outputs from CONUS during 2013 heatwave. The CDF figure of all locations, and the selected typical representative location is shown in Fig. 4.9. The selected typical location is an industrial area, with less dense low-rise and mid-rise industrial buildings.

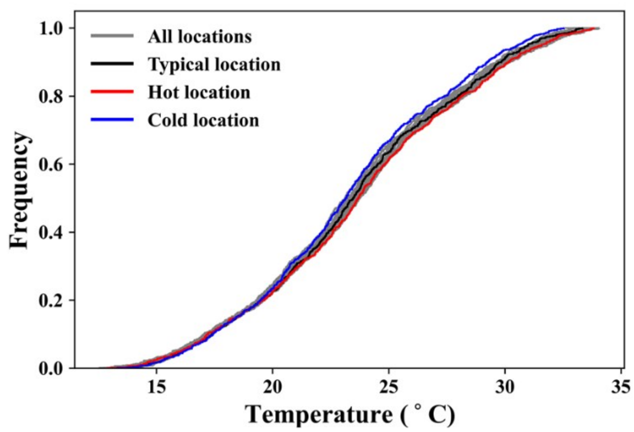

(a)

(b)

Fig. 4.9 Typical representative location selected from CONUS. (a) cumulative density function figure of all locations (gray), typical (black), extreme hot (red), and extreme cold (blue) locations. (b) Map of typical location.

With selected typical representative location, the climate data at this location is extracted for both historical (1996-2015) and future (2080-2099) period from CONUS datasets. The reference year selection method is then conducted to select typical (TDD) and extreme hot (EWD) scenario for CFD simulation, as described in Section 3.2.2. Here, CDF figures are generated in Fig. 4.10 to show the representative years generated from both historical and future period. It could be found that the typical downscaled year could represent the general condition of multiple years.

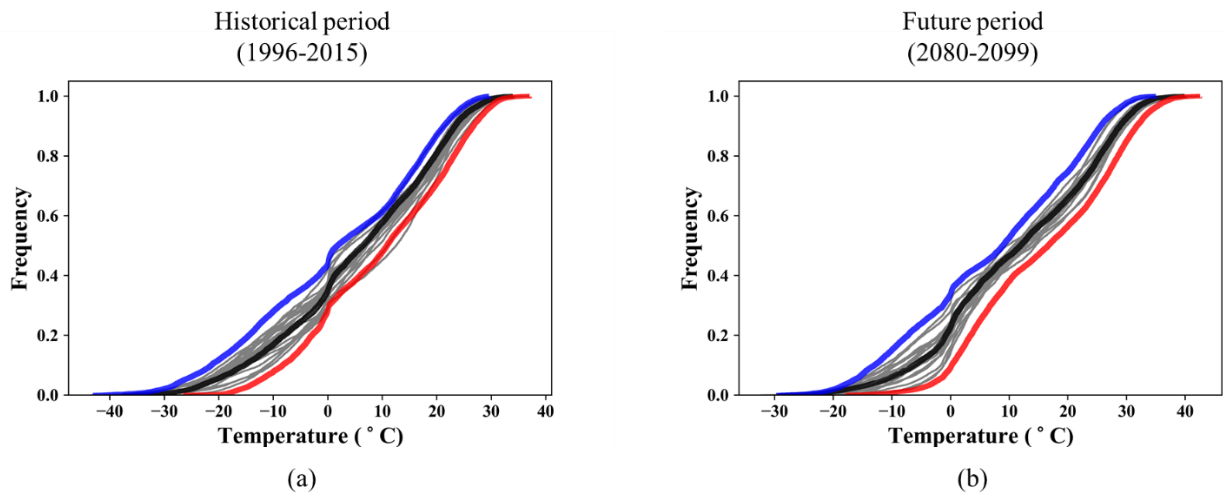

Fig. 4.10 Cumulative density function figure for reference year selection – typical downscaled year (black), extreme hot year (red), extreme cold year (blue). (a) Historical period (1996-2015). (b) Future period (2080-2099)

With the typical representative location selected through representative location method and TDD and EWD generated by reference year method, CityFFD simulation is conducted to predict urban microclimate under typical (TDD) and extreme hot (EWD) conditions for historical and future time periods on the typical location of Montreal. With the UTCI calculation method mentioned in Section 3.2.4.1, the simulated wind and temperature field are then used for UTCI calculation with relative humidity from climate files, as well as radiation field calculated by Grasshopper Ladybug.

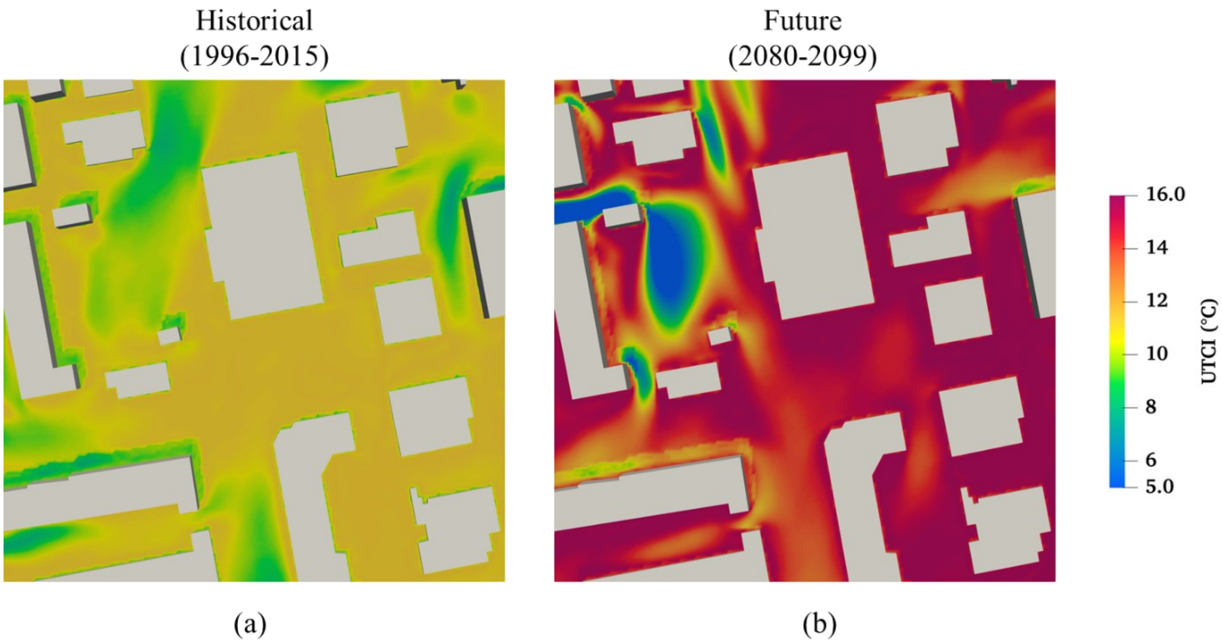

Fig. 4.11 Outdoor UTCI prediction under TDD for (a) historical and (b) future period.

The UTCI values depicted in Fig. 4.11 and Fig. 4.12 illustrate the impacts of climate change on urban thermal comfort under typical and extreme warm conditions. Fig. 4.11 (a) with its cooler and more uniform UTCI values ranging from 6°C to 12°C, may represent a slightly cool weather conditions in the historical period. In contrast, Fig. 4.11 (b) shows a significant increase in UTCI values, reaching up to 16°C, with a notable spatial diversity including warmer regions compared with the historical period. Under EWD condition during historical period, UTCI values range from 40.3°C to 45°C, the urban environment suffers from a relatively strong thermal state, allowing residents to conduct limited outdoor activities with low health risks. Conversely, the extreme warmth condition showcases UTCI values escalating from 65°C to an alarming 72°C, indicative of severe thermal stress that could drastically inhibit outdoor human activity, escalate cooling energy demands, and exacerbate public health risks.

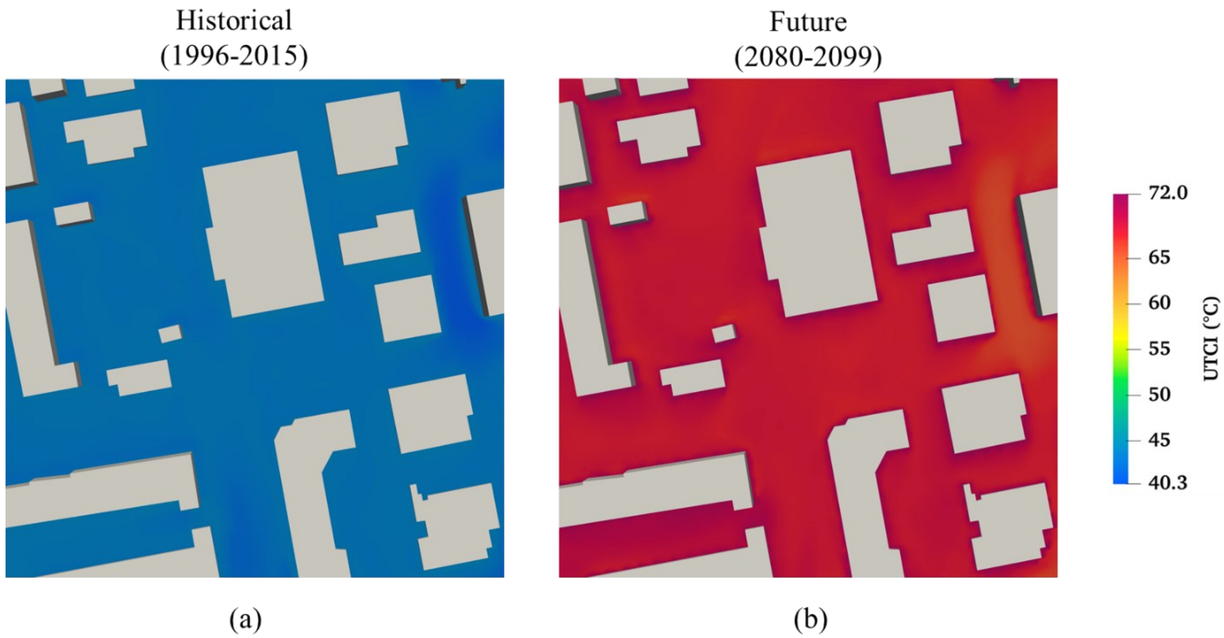

Fig. 4.12 Outdoor UTCI prediction under EWD for (a) historical and (b) future period.

Fig. 4.13 presented outdoor thermal stress distributions for historical and projected future scenarios under TDD and EWD, with the UTCI results from Fig. 4.11 and Fig. 4.12. The analysis reveals a pronounced shift towards higher thermal stress categories in the future scenarios for both typical and extreme conditions. Specifically, the complete change from 'very strong heat stress' to 'extreme heat stress' under EWD indicates a significant rise in days where the thermal conditions could potentially compromise human health and comfort. This escalation in heat stress categories suggests an exacerbation of heat effects due to increasing mean temperatures.

Furthermore, the comparison between typical and extreme conditions underscores the critical importance of selecting reference years that encompass both average and extreme climatic events. This approach is essential for accurately assessing the range of potential future thermal environments and their implications for urban planning and public health. By incorporating both TDD and EWD into climate impact studies, researchers and policymakers can better prepare for the increasing frequency and intensity of extreme heat events. This dual-focus methodology supports the development of more effective adaptation and mitigation strategies, aiming to enhance urban resilience against the adverse effects of climate change and safeguard public health in the face of escalating urban heat stress.

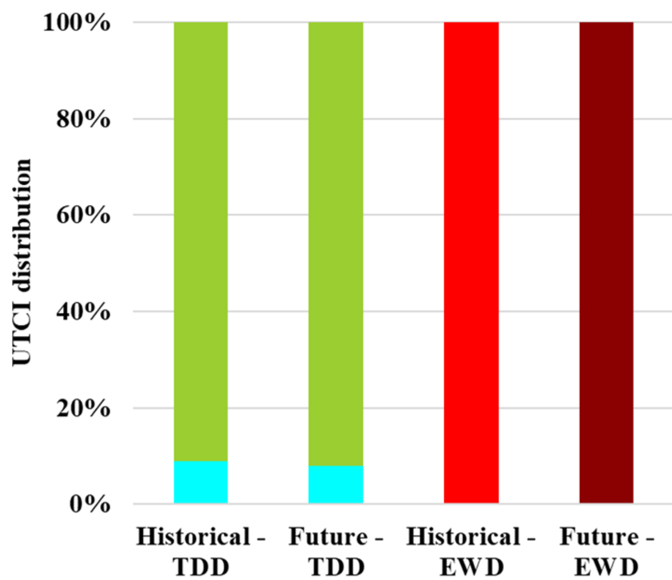

UTCI (°C)	Stress Category
46 ≤ UTCI	Extreme heat stress
38 ≤ UTCI < 46	Very strong heat stress
32 ≤ UTCI < 38	Strong heat stress
26 ≤ UTCI < 32	Moderate heat stress
9 ≤ UTCI < 26	No thermal stress
0 ≤ UTCI < 9	Slight cold stress
-13 ≤ UTCI < 0	Moderate cold stress
-27 ≤ UTCI < -13	Strong cold stress
-40 ≤ UTCI < -27	Very strong cold stress
UTCI < -40	Extreme cold stress

Fig. 4.13 UTCI thermal stress distribution for TDD and EWD under historical and future time periods

4.4 Conclusion

The research presented in this chapter meticulously assesses the impacts of climate change on urban overheating, utilizing a spatial and temporal representative method to integrate Weather Research and Forecasting (WRF) model with the City Fluid Dynamics (CityFFD) simulation. Two groups of simulation are performed in this study which are NARR+WRF+CityFFD and CONUS+CityFFD. Section 4.3.2 focuses on the evaluation of representative method under a historical heatwave period using NARR+WRF+CityFFD and Section 4.3.3 targets on evaluating climate change impacts on typical microclimate with the numerical results from CONUS+CityFFD. Here are the main conclusions:

- Selecting typical representative location and extreme hot location is necessary for comprehensive urban outdoor overheating evaluations: The typical location tends to maintain more moderate temperatures during a heatwave while the extreme hot location exhibits significantly elevated temperatures throughout the day.
- An obvious increase in general UTCI values as well as thermal stress condition is found for the typical location under climate change impacts: UTCI increases from 8 °C to mostly around 15 °C under TDD, and increases from around 42 °C to around 70°C under EWD which indicates a complete change from 'very strong heat stress' to 'extreme heat stress'

The study shows the effectiveness of using detailed urban microclimate simulations to predict general urban microclimate conditions among the whole urban area. These findings highlight the critical role of selecting appropriate reference years and locations for accurately simulating and predicting urban heat conditions, a methodological approach that enhances the capacity to forecast and mitigate the adverse effects of climate change on urban settings.

Chapter 5

Conclusion and future work

5.1 Major research outcome

5.1.1 Multiscale numerical assessment of urban overheating under climate projections: a review

This section presents a systematic review of the application of climate model projections for future indoor and outdoor overheating impact assessments, divided into four primary stages: (1) Mesoscale raw future climate data generation using GCM-RCMs; (2) Local-scale future climate input preparation through bias-correction and reference year data generation; (3) Microscale indoor and outdoor simulations with building performance models or computational fluid dynamics (CFD) software; (4) Overheating evaluation based on various overheating criteria. These stages are essential for advancing our understanding of overheating and informing future studies in this area. Key research gaps illustrated by this review include challenges in generating climate data, improving projected data reliability, and addressing indoor/outdoor climate simulation complexities. Additionally, incorporating social-economic factors into overheating evaluation methods is crucial for a comprehensive assessment. Although the focus is future urban overheating assessment, the general methodologies and procedure of future climate projections may also apply to other building performance simulations considering the climate change impacts. Notable research gaps were then identified as avenues for future research. Several prominent research gaps have been identified and are summarized as follows for each stage:

- Future climate data generation: Although progress has been made in generating future climate data using downscaling methods, challenges remain in conducting high-resolution, multi-decadal urban climate simulations under various greenhouse emission scenarios. Moreover, the accuracy and versatility of statistical and dynamical downscaling methods are limited by their reliance on historical data and high computational costs, respectively. Statistical-dynamical methods offer a promising compromise, allowing urban environments to be physically parameterized while maintaining versatility through advanced statistical and data-driven modeling techniques.
- Future climate input preparation: Bias correction and reference year data methods are crucial for improving the reliability of projected data and streamlining climate change impact assessments. However, there is a lack of consensus on the weighting of climatic variables in reference year data methods. Using thermal comfort indices like SET or UTCI instead of individual climatic variables could be a potential solution.
- Indoor climate simulation: Neighborhood-scale urban climate modeling is essential for studying future overheating. Challenges include modeling spatially dynamic indoor climate and incorporating real occupancy patterns in building energy models.
- Outdoor climate simulation: Simplifications in computational fluid dynamics (CFD) models raise concerns about accuracy and validity. Future research should focus on quantifying the sensitivity of input parameters to better understand the impacts of these simplifications.
- Overheating evaluation methods: Although widely used standards for outdoor and indoor overheating assessments exist, they fail to consider social and economic vulnerabilities. As specific populations, such as the elderly, poor, and minority groups, are disproportionately

affected by extreme heat events, using thermal-only overheating standards is insufficient. A more comprehensive approach should incorporate social-economic components, such as the percentage of vulnerable populations and the accessibility of heat mitigation methods.

5.1.2 Assessment of future overheating conditions in Canadian cities using a reference year selection method

This chapter evaluates outdoor extreme heat events and indoor overheating conditions for a representative residential building located in three Canadian cities (Montreal, Toronto, and Vancouver) over contemporary (2001-2020), near-term future (2041-2060), and long-term future (2081-2100) time periods. The regional climate simulations forced by three GCMs were bias-corrected with reference to historical observations recorded at the airport location of the cities. Regard that although the analysis is performed for airport locations which may not be representative of fully developed urban areas, the methodology used is generalized enough to be used in urban locations.

Thereafter, a reference year selection method is used to generate three representative climate data years: typical downscaling year (TDY), extreme cold year (ECY), and extreme warm year (EWY).

The performance of TDY, ECY, and EWY climate data sets in capturing the range of overheating conditions present in the entire 20-year long contemporary and future projected time-periods is assessed. At the same time, the projected changes from the selected reference years and 20-year datasets are compared. The results are also compared with a widely used metric of overheating: the design summer year (DSY). Based on the results, given in Sections 2.3.1, 2.3.2, and 2.3.3, following deductions from the study were obtained:

- The multivariate quantile mapping bias correction method is able to improve the reliability of future climate data by capturing the distribution pattern of climatic variables as well as reducing errors and therefore, for any future weather projection study, bias correction is one of the most important steps.

- For both outdoor/indoor overheating evaluation, EWY and ECY could efficiently capture maximum and minimum monthly overheating hours providing the upper and lower boundary of possible outdoor and indoor overheating conditions. TDY could be used to simulate the typical yearly overheating condition. The EWY captures the extreme overheating conditions better than the DSY.
- Owing to the effects of climate change, a similar increase could be found in both indoor and outdoor overheating hours in the three Canadian cities; average monthly overheating hours increase by normally around one time (from 50% to 150%) until the mid-term future and by normally around two to three times (even up to nine times for some scenarios) during the long-term future.

5.1.3 Evaluating climate change impacts on building level steady-state and dynamic outdoor thermal comfort in Montreal

This chapter aims to evaluate climate impacts on both steady-state and dynamic outdoor thermal comfort of an urban area, i.e., Montreal downtown, through CityFFD-CityBEM simulations with a spatial resolution of 2 m. As detailly presented in our previous publication, raw future climate data obtained from CORDEX is bias-corrected with local field measurements, followed by the selection of reference year scenarios through the reference year data method. This research represents an initial effort to predict future steady-state and dynamic thermal comfort at the neighborhood scale by simulating the outdoor urban microclimate. The climate change impacts on steady-state and dynamic thermal comfort in downtown Montreal are quantified by conducting comparisons across the 2010s, 2050s, and 2090s.

A 1.25 km by 1.25 km of Montreal downtown area is selected, due to its high population and building density, for performing CityFFD-CityBEM co-simulation with prepared future climate inputs. Based on the independence test of mesh size and CFL number for CityFFD simulation, the minimum mesh size is set to 2 m and the CFL number is set to 5. Two outdoor thermal comfort indices UTCI and PDISC were applied to evaluate the climate change impacts on future outdoor overheating.

The results of our study clearly illustrate the profound impact of climate change on both steady-state and dynamic aspects of outdoor thermal comfort, particularly during typical commuting times (9 am, 12 pm, and 17 pm) in downtown Montreal, as listed below:

- Under the typical condition (TDD), early mornings (9 am) and late afternoons (17 pm) in the 2010s were characterized by "Slight cold stress," transitioning to "No thermal stress" by midday (12 pm), indicating comfortable conditions for outdoor activities.
- However, by the 2050s, a shift towards warmer conditions emerges, with "No heat stress" observed throughout the day, culminating in "Extreme heat stress" instances by the 2090s, highlighting a significant increase in overheating risks.
- The trend towards heightened thermal stress is further accentuated under extreme weather conditions (EWD), with "Extreme heat stress" becoming more prevalent across all time periods, showing an escalating threat of severe overheating.

This escalation is also quantified through the dynamic thermal comfort analysis, revealing a marked decrease in the amount of time before pedestrians begin to feel discomfort when walking at various speeds, from the 2010s through to the 2090s:

- Pedestrians will experience no discomfort walking along the route in the 2010s and 2050s under TDD conditions.
- However, by the 2090s, tolerable discomfort may arise after 5 minutes of walking.
- Under EWD conditions, intolerable thermal discomfort becomes inevitable at noon, and the duration of time for which discomfort remains tolerable is expected to be reduced from 6 minute in 2010s to 4 minute in 2090s for a brisk walk.
- This consistent reduction in discomfort onset times—regardless of walking speed/across all walking speed—underscores the urgency for strategic urban cooling design interventions.

5.1.4 Evaluating climate change impacts on building level steady-state and dynamic outdoor thermal comfort in Montreal

The research presented in this chapter meticulously assesses the impacts of climate change on urban overheating, utilizing a spatial and temporal representative method to integrate Weather Research and Forecasting (WRF) model with the City Fluid Dynamics (CityFFD) simulation. Two groups of simulation are performed in this study which are NARR+WRF+CityFFD and CONUS+CityFFD. Section 4.3.2 focuses on the evaluation of representative method under a historical heatwave period using NARR+WRF+CityFFD and Section 4.3.3 targets on evaluating climate change impacts on typical microclimate with the numerical results from CONUS+CityFFD. Here are the main conclusions:

- Selecting typical representative location and extreme hot location is necessary for comprehensive urban outdoor overheating evaluations: The typical location tends to maintain more moderate temperatures during a heatwave while the extreme hot location exhibits significantly elevated temperatures throughout the day.
- An obvious increase in general UTCI values as well as thermal stress condition is found for the typical location under climate change impacts: UTCI increases from 8 °C to mostly around 15 °C under TDD, and increases from around 42 °C to around 70°C under EWD which indicates a complete change from 'very strong heat stress' to 'extreme heat stress'

The study shows the effectiveness of using detailed urban microclimate simulations to predict general urban microclimate conditions among the whole urban area. These findings highlight the critical role of selecting appropriate reference years and locations for accurately simulating and predicting urban heat conditions, a methodological approach that enhances the capacity to forecast and mitigate the adverse effects of climate change on urban settings.

5.2 Limitation of the study

The limitations of work in '*Assessment of future overheating conditions in Canadian cities using a reference year selection method*' are:

- Only considering three Canadian cities – Montreal, Toronto, and Vancouver – for analysis;
- Only the projections from three GCMs and one RCP scenario (RCP 8.5) was considered for preparing the climate data sets;
- Only three GCMs are considered inside this study for urban overheating evaluation
- Only testing this method with the single-house building and assuming the features of the single-house building stay constant in all future years. In reality, the features of existing

buildings will change based on age.

- Only applying a fixed temperature threshold as the indoor and outdoor overheating criteria.

The limitations of work in '*Evaluating climate change impacts on building level steady-state and dynamic outdoor thermal comfort in Montreal*' are:

- Because of lack of future city terrain information, it is assumed that no alterations in urban terrain and building morphology over time, overlooking potential developments or renovations that could impact thermal comfort;
- The focus on a single route for the Practical Discomfort Scale (PDISC) analysis may also limit the generalizability of our findings across the entire downtown area;
- The current work does not account for the potential benefits of urban greening, which might help decrease local overheating;
- The spatial changes in relative humidity due to evaporation from greenings and local water body are not considered during CFD simulation.

The limitations of work in '*Assessing climate change impacts on urban overheating through Representative Methods on Spatial and Temporal Scales by implementing WRF and CityFFD*' are:

- Only using NARR as the input dataset for WRF simulation, some more recent reanalysis project datasets are become available in recent years.
- CONUS datasets did not consider urban effects, which limits the difference in air temperature between downtown and sub-urban areas. Thus, only typical location is selected and evaluated for assessing climate change impacts.
- When assessing climate change impacts, the change in building morphology or urban

terrain is not considered.

- Although urban greening is considered in WRF simulations, it is not considered inside CityFFD simulation which might affect the real-life detailed outdoor thermal comfort conditions.

5.3 Future work

Continuing with the current work, more efforts in the future will be devoted into the following aspects, addressing the limitation of former work and based on the research of interest:

- Expanding overheating evaluation from Canadian cities only to global main cities around the world for better understanding the climate change impacts on urban overheating;
- Considering the change in urban morphology when assessing future urban microclimate through CFD simulation;
- Expand the results of the single route for the Practical Discomfort Scale (PDISC) analysis to multiple routes for best thermal comfort route selection;
- Adding urban green infrastructures (trees, green roof, green wall, etc) inside current simulation to see how will it mitigate urban overheating;
- Conduct representative location method on different types of local climate zone to refine the classification of urban areas;
- Calculating urban morphology indices for multiple urban sites and building correlation with urban morphology indices and CFD simulation results;
- Considering the change in energy consumption for maintaining sufficient thermal comfort level under climate change impacts.

Appendix

Appendix A

A.1 Cumulative distribution function comparison of observational (gray curve), raw RCM (blue curve) and bias-corrected RCM data (red curve) of sfcWind, tas, rsds, hurs (MPI, 1998-2017)

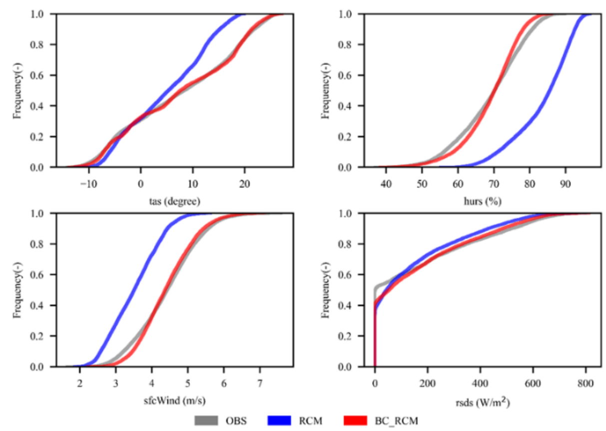

(a) Montreal

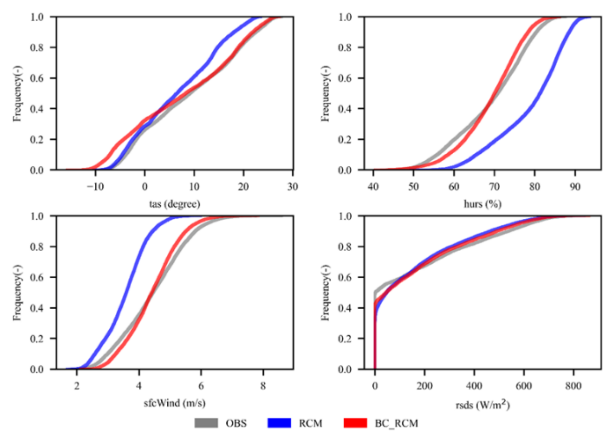

(b) Toronto

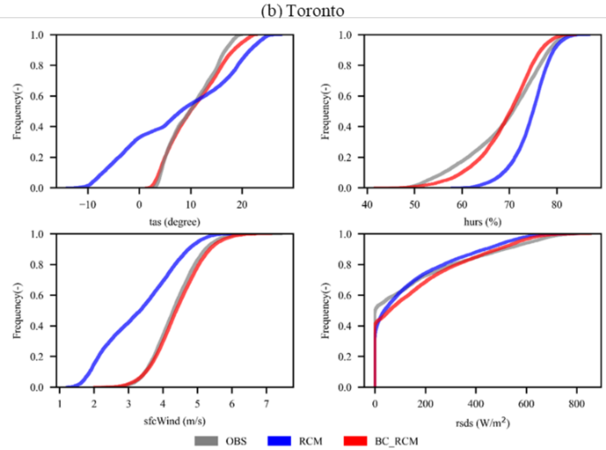

(c) Vancouver

A.2 Cumulative distribution function comparison of the hourly temperature from 20 years and reference year climate data sets of TDY, ECY and EWY

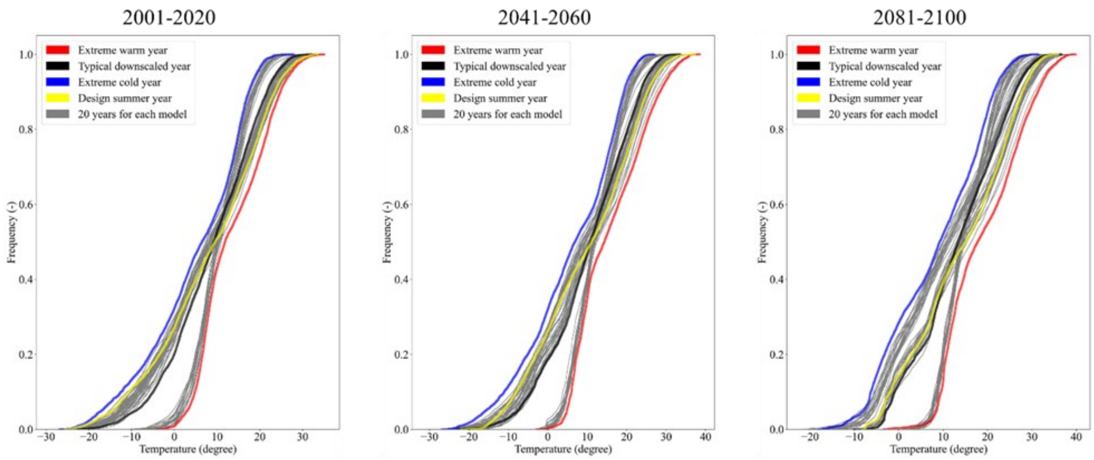

(a) Montreal

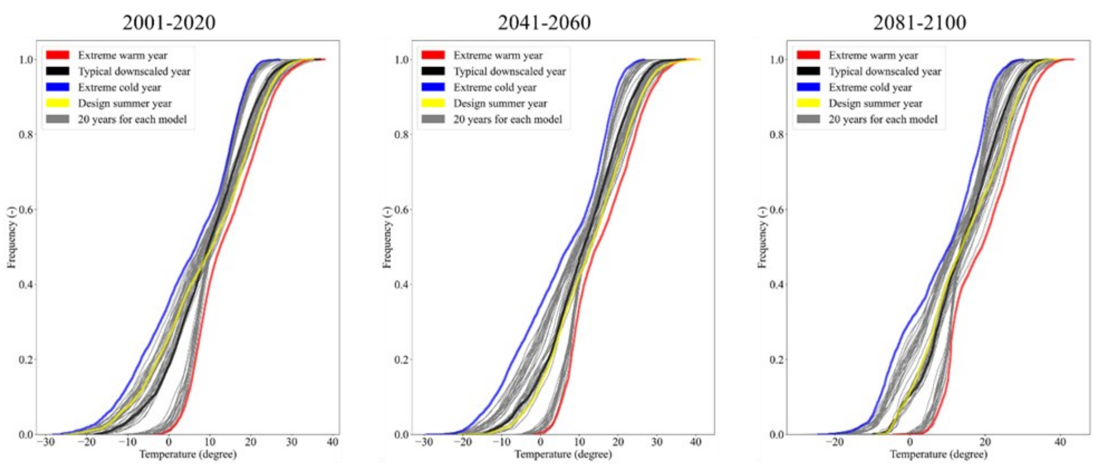

(b) Toronto

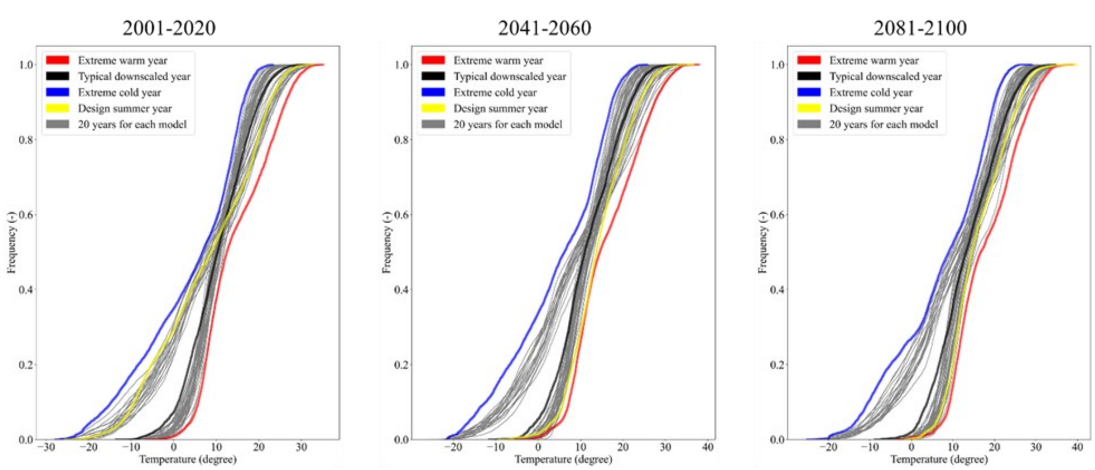

(c) Vancouver

Appendix B

B.1 Yearly cumulative outdoor overheating hours in three Canadian cities

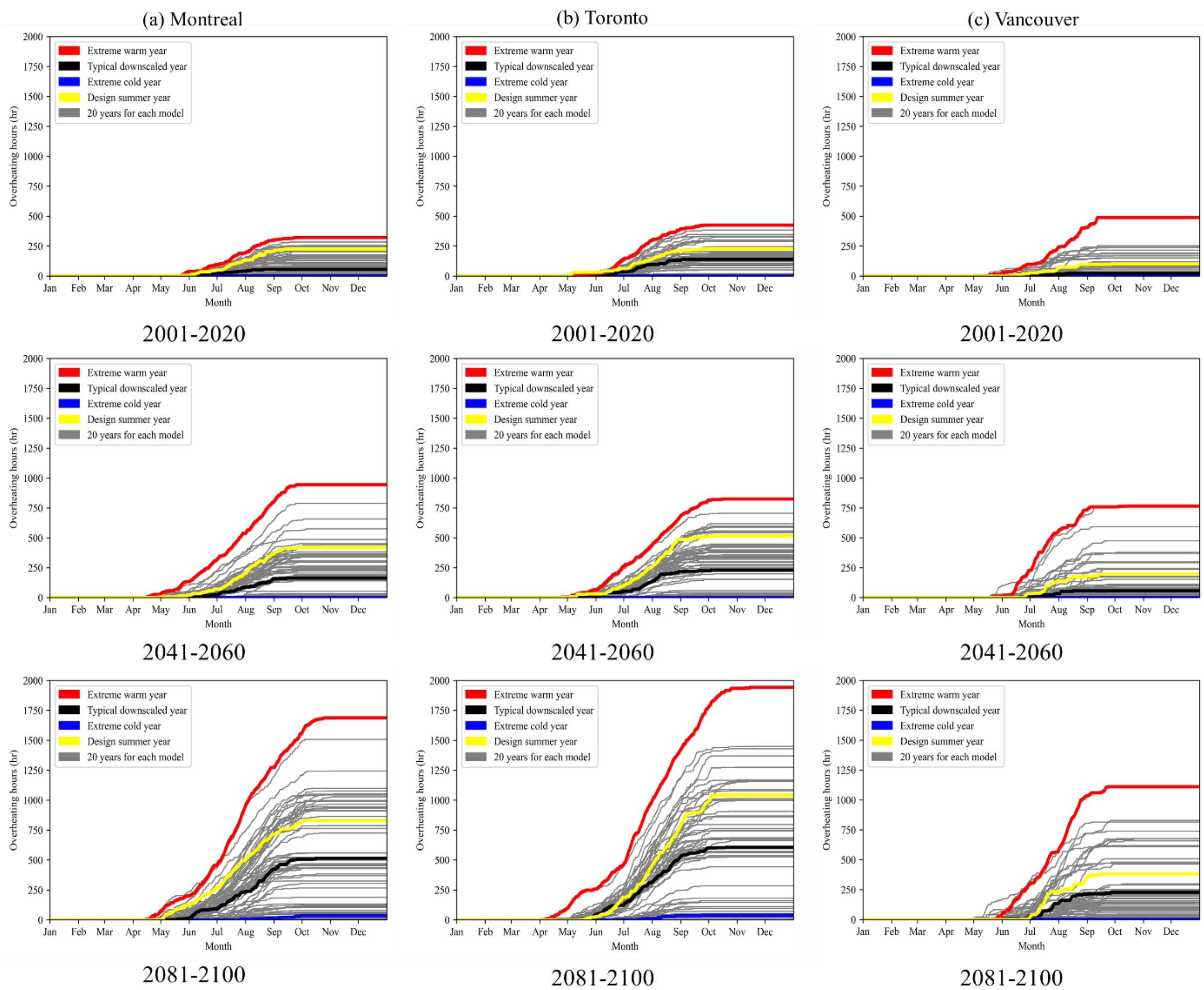

B.2 Monthly outdoor overheating hours between reference year and 20-years data sets in three Canadian cities

(a) Montreal

Time periods	Model	May	June	July	August	September
2010s	ECY	0	1	0	0	0
	TDY	3	24	13	15	0
	EWY	36	56	99	107	22

	20-year (max.)	36	74	123	107	65
	20-year (avg.)	4	21	37	26	7
	20-year (min.)	0	0	0	0	0
	DSY	2	45	83	79	14
2050s	ECY	0	0	0	0	0
	TDY	2	23	63	68	7
	EWY	103	184	219	271	136
	20-year (max.)	103	184	219	271	136
	20-year (avg.)	10	34	74	78	26
	20-year (min.)	0	0	0	0	0
	DSY	16	51	129	169	51
2090s	ECY	0	0	8	5	23
	TDY	12	80	146	186	83
	EWY	123	264	494	316	290
	20-year (max.)	161	264	494	347	290
	20-year (avg.)	27	82	165	168	70
	20-year (min.)	0	0	3	0	0
	DSY	123	150	238	203	106

(b) Toronto

Time periods	Model	May	June	July	August	September
2010s	ECY	0	0	0	0	0
	TDY	8	27	62	34	9
	EWY	21	120	154	96	31
	20-year (max.)	39	120	165	108	56
	20-year (avg.)	4	27	46	30	11
	20-year (min.)	0	0	0	0	0
	DSY	29	30	80	69	18
2050s	ECY	0	0	0	0	0
	TDY	14	39	82	83	6
	EWY	63	195	181	243	129
	20-year (max.)	69	195	206	243	133
	20-year (avg.)	12	41	93	89	30
	20-year (min.)	0	0	0	0	0
	DSY	30	72	157	227	25
2090s	ECY	0	0	9	27	3
	TDY	42	78	191	214	72
	EWY	159	208	532	429	356
	20-year (max.)	159	208	532	429	356
	20-year (avg.)	35	83	196	189	75
	20-year (min.)	0	0	5	2	0

	DSY	26	162	269	335	198

(c) Vancouver

Time periods	Model	May	June	July	August	September
2010s	ECY	0	0	0	0	0
	TDY	0	6	10	8	0
	EWY	27	69	145	162	84
	20-year (max.)	50	78	145	162	84
	20-year (avg.)	2	10	20	12	4
	20-year (min.)	0	0	0	0	0
	DSY	0	26	44	28	3
2050s	ECY	0	0	0	0	0
	TDY	0	11	22	23	0
	EWY	11	217	332	176	23
	20-year (max.)	102	217	341	191	73
	20-year (avg.)	4	21	39	31	9
	20-year (min.)	0	0	0	0	0
	DSY	0	33	108	37	21
2090s	ECY	1	0	0	0	0
	TDY	7	26	102	76	17
	EWY	49	250	278	459	75
	20-year (max.)	162	246	295	435	133

20-year (avg.)	10	31	88	74	24
20-year (min.)	0	0	0	0	0
DSY	9	22	210	122	29

B.3 Yearly cumulative indoor overheating hours in three Canadian cities

(a) Montreal

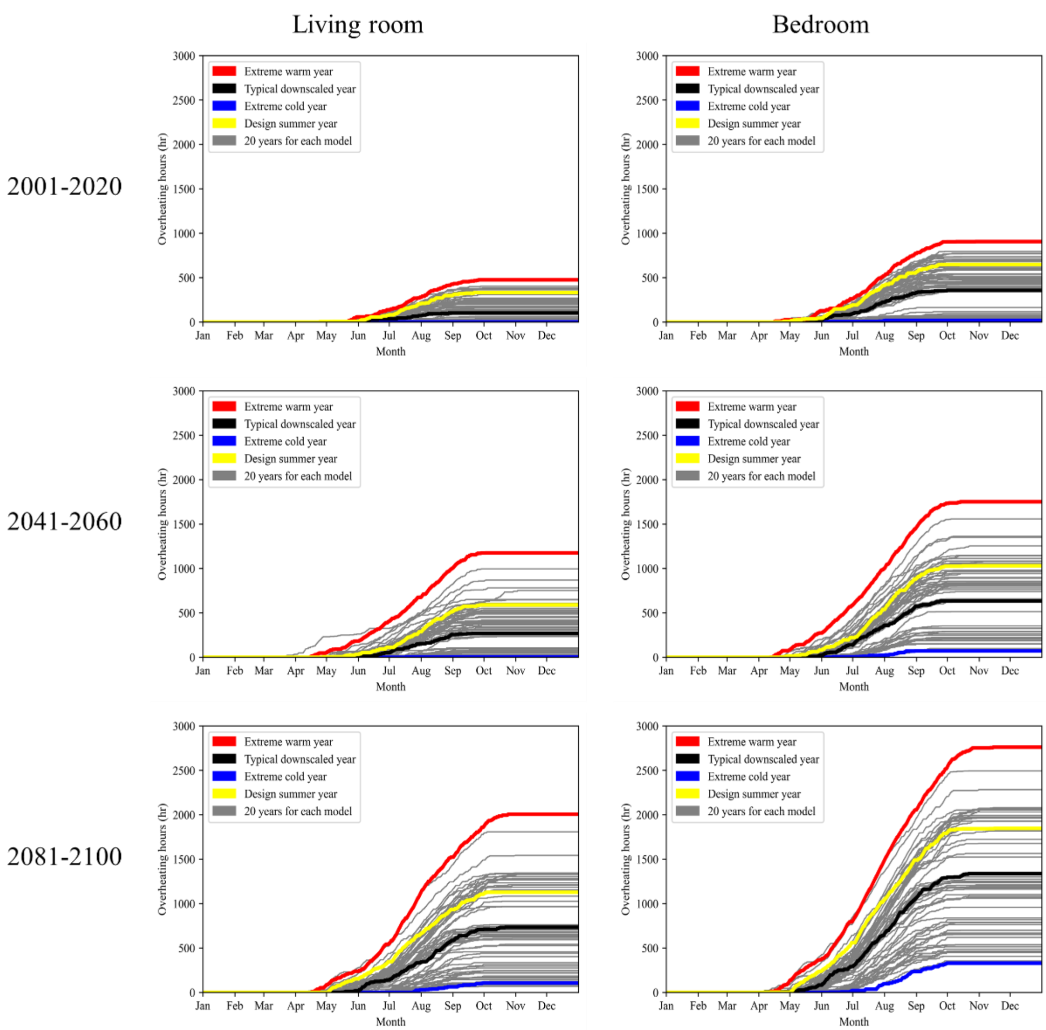

(b) Toronto

Living room Bedroom

2001-2020

2041-2060

2081-2100

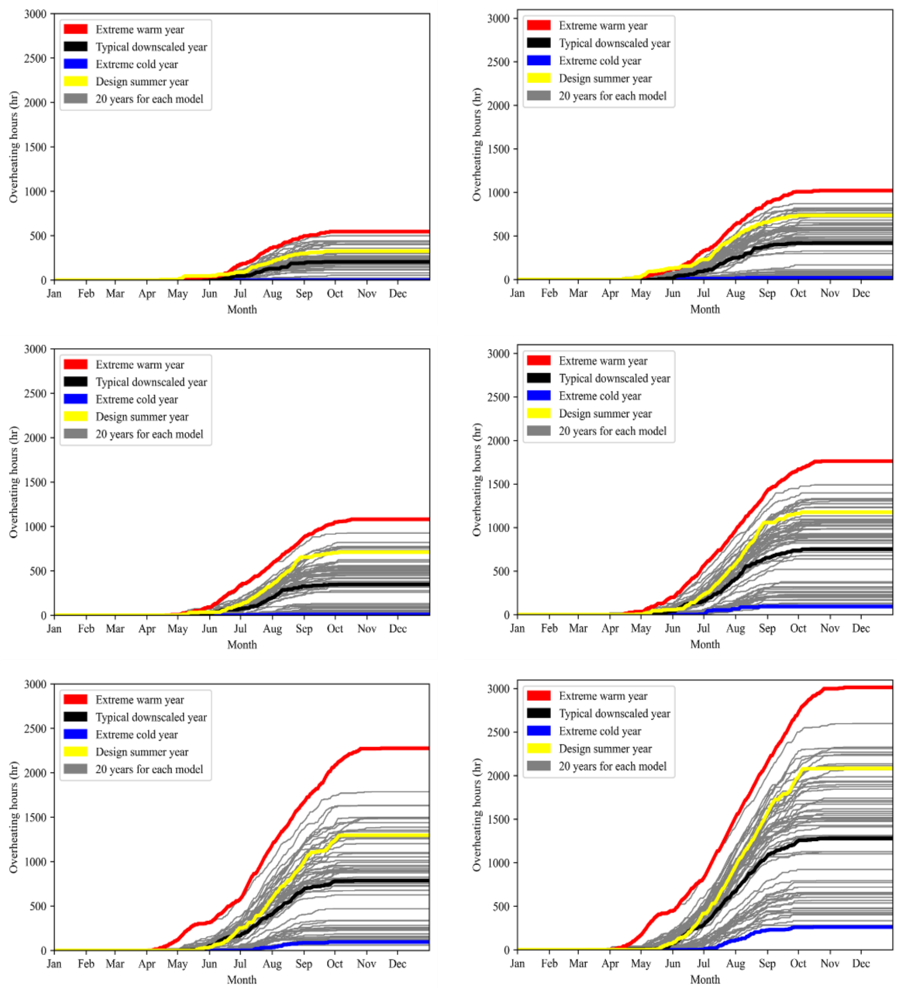

(c) Vancouver

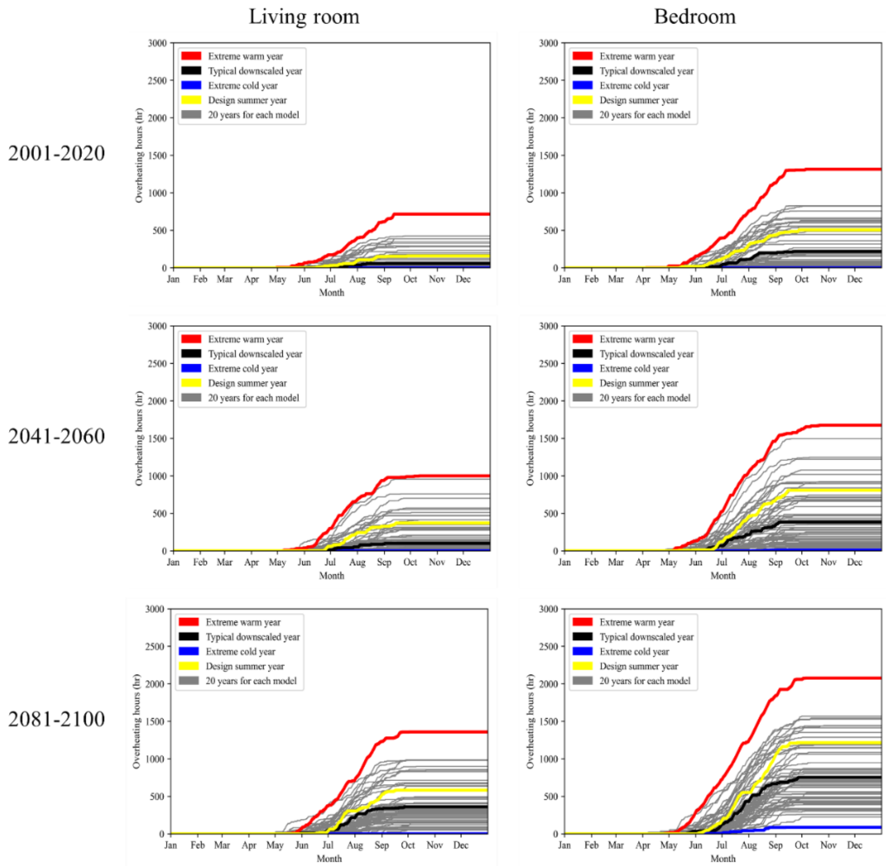

B.4 Difference in monthly indoor overheating hours between synthesizing and 20-years data sets in three Canadian cities (Liv: Living room, Bed: Bedroom)

(a) Montreal

Time periods	Model	May		June		July		August		September	
		Liv	Bed	Liv	Bed	Liv	Bed	Liv	Bed	Liv	Bed
2010s	ECY	0	0	1	5	0	11	0	3	0	0
	TDY	9	26	28	69	35	129	30	107	0	27
	EWY	58	101	79	135	141	260	148	250	49	131
	20-year (max.)	58	102	101	180	158	265	148	250	91	153
	20-year (avg.)	7	22	33	76	59	138	47	117	13	39
	20-year (min.)	0	0	0	0	0	2	0	2	0	0

	DSY	5	34	73	150	127	222	96	149	27	84
2050s	ECY	0	0	0	0	2	7	0	10	0	0
	TDY	1	11	22	78	64	170	66	157	4	35
	EWY	95	161	181	267	218	351	285	410	130	223
	20-year (max.)	95	162	182	267	222	354	289	412	132	225
	20-year (avg.)	93	273	327	787	773	175	84	179	26	62
	20-year (min.)	0	0	0	0	0	6	0	10	0	0
	DSY	28	69	77	138	177	317	231	350	71	137
2090s	ECY	0	0	0	21	30	78	33	136	43	94
	TDY	19	76	122	208	202	366	242	408	127	231
	EWY	154	240	313	433	577	681	393	569	348	478
	20-year (max.)	195	289	313	433	577	681	414	605	348	485
	20-year (avg.)	373	717	1117	204	225	369	228	384	99	185
	20-year (min.)	0	0	0	11	17	79	29	137	0	10
	DSY	153	240	193	317	318	487	269	443	179	311

(b) Toronto

Time periods	**Model**	**May**		**June**		**July**		**August**		**September**	
		Liv	**Bed**	**Liv**	**Bed**	**Liv**	**Bed**	**Liv**	**Bed**	**Liv**	**Bed**
2010s	ECY	0	11	0	0	0	4	0	6	0	0
	TDY	9	14	36	82	85	151	60	131	16	40
	EWY	31	88	141	208	183	303	135	256	48	119
	20-year (max.)	45	93	141	208	194	316	155	293	73	137

	20-year (avg.)	6	20	37	81	66	144	49	116	17	46
	20-year (min.)	0	0	0	0	0	4	0	6	0	0
	DSY	41	94	43	102	118	261	89	168	29	77
2050s	ECY	0	0	0	5	6	62	2	26	0	0
	TDY	19	41	53	118	128	255	125	240	20	83
	EWY	84	165	249	360	245	408	299	459	166	243
	20-year (max.)	94	172	249	360	269	410	299	470	166	243
	20-year (avg.)	16	39	55	114	136	261	128	243	43	88
	20-year (min.)	0	0	0	0	0	41	1	26	0	0
	DSY	34	53	90	178	224	350	307	473	47	104
2090s	ECY	0	0	0	3	35	110	50	114	9	33
	TDY	48	72	113	207	240	383	283	416	93	167
	EWY	194	277	266	378	605	697	487	633	411	568
	20-year (max.)	194	277	267	390	596	698	503	650	411	568
	20-year (avg.)	45	85	115	209	255	402	253	405	101	188
	20-year (min.)	0	0	0	3	27	110	29	114	0	2
	DSY	35	80	217	336	334	542	413	614	240	415

(c) Vancouver

Time periods	**Model**	**May**		**June**		**July**		**August**		**September**	
		Liv	**Bed**	**Liv**	**Bed**	**Liv**	**Bed**	**Liv**	**Bed**	**Liv**	**Bed**
2010s	ECY	0	0	0	0	0	0	0	0	0	0

	TDY	0	0	9	29	27	73	22	87	1	20
	EWY	57	133	108	242	227	360	214	375	102	171
	20-year (max.)	64	133	108	242	227	360	214	376	102	171
	20-year (avg.)	3	10	15	39	35	89	25	72	6	20
	20-year (min.)	0	0	0	0	0	0	0	0	0	0
	DSY	0	20	31	102	65	185	54	130	8	68
2050s	ECY	0	0	0	0	0	0	0	8	0	2
	TDY	0	10	12	57	41	149	42	129	4	37
	EWY	35	132	266	394	384	527	259	421	46	150
	20-year (max.)	119	150	264	396	397	546	256	417	97	193
	20-year (avg.)	7	19	30	64	64	149	54	135	16	47
	20-year (min.)	0	0	0	0	0	0	0	0	0	0
	DSY	0	13	59	106	183	340	85	219	45	130
2090s	ECY	1	5	0	0	0	37	0	44	0	2
	TDY	10	34	42	98	167	298	117	238	25	85
	EWY	80	280	293	437	349	514	512	604	124	216
	20-year (max.)	174	303	289	424	364	535	489	579	164	263
	20-year (avg.)	135	30	47	107	133	271	118	260	38	91
	20-year (min.)	0	0	0	0	0	37	0	44	0	0
	DSY	14	35	39	176	267	376	213	500	64	163

Reference

[1] M. De Sario, K. Katsouyanni, and P. Michelozzi, "Climate change, extreme weather events, air pollution and respiratory health in Europe," *European Respiratory Journal,* vol. 42, no. 3, pp. 826-843, 2013.

[2] S. Y. Philip *et al.*, "Rapid attribution analysis of the extraordinary heatwave on the Pacific Coast of the US and Canada June 2021," *Earth System Dynamics Discussions,* vol. 2021, pp. 1-34, 2021.

[3] C. Mora *et al.*, "Global risk of deadly heat," *Nature climate change,* vol. 7, no. 7, pp. 501-506, 2017.

[4] N. Nazarian *et al.*, "Integrated assessment of urban overheating impacts on human life," *Earth's Future,* vol. 10, no. 8, p. e2022EF002682, 2022.

[5] J. Zou, J. Liu, J. Niu, Y. Yu, and C. Lei, "Convective heat loss from computational thermal manikin subject to outdoor wind environments," *Building and Environment,* vol. 188, p. 107469, 2021.

[6] J. Zou, Y. Yu, J. Liu, J. Niu, K. Chauhan, and C. Lei, "Field measurement of the urban pedestrian level wind turbulence," *Building and Environment,* vol. 194, p. 107713, 2021.

[7] M. A. Semenov and P. Stratonovitch, "Use of multi-model ensembles from global climate models for assessment of climate change impacts," *Climate research,* vol. 41, no. 1, pp. 1-14, 2010.

[8] M. Rummukainen, "State-of-the-art with regional climate models," *Wiley Interdisciplinary Reviews: Climate Change,* vol. 1, no. 1, pp. 82-96, 2010.

[9] Y. Wang *et al.*, "Regional climate modeling: progress, challenges, and prospects," *Journal of the Meteorological Society of Japan. Ser. II,* vol. 82, no. 6, pp. 1599-1628, 2004.

[10] R. Laprise, "Regional climate modelling," *Journal of computational physics,* vol. 227, no. 7, pp. 3641-3666, 2008.

[11] J. Zou, H. Lu, C. Shu, L. Ji, A. Gaur, and L. L. Wang, "Multiscale numerical assessment of urban overheating under climate projections: a review," *Urban Climate,* vol. 49, p. 101551, 2023.

[12] A. L. Pisello, M. Saliari, K. Vasilakopoulou, S. Hadad, and M. Santamouris, "Facing the urban overheating: Recent developments. Mitigation potential and sensitivity of the main technologies," *Wiley Interdisciplinary Reviews: Energy and Environment,* vol. 7, no. 4, p. e294, 2018.

[13] Y. Toparlar, B. Blocken, B. Maiheu, and G. Van Heijst, "A review on the CFD analysis of urban microclimate," *Renewable and Sustainable Energy Reviews,* vol. 80, pp. 1613-1640, 2017.

[14] Y. Tominaga and T. Stathopoulos, "CFD simulation of near-field pollutant dispersion in the urban environment: A review of current modeling techniques," *Atmospheric environment,* vol. 79, pp. 716-730, 2013.

[15] C. B. Field and V. R. Barros, *Climate change 2014–Impacts, adaptation and vulnerability:*

Regional aspects. Cambridge University Press, 2014.

[16] S. Beck and M. Mahony, "The IPCC and the new map of science and politics," *Wiley Interdisciplinary Reviews: Climate Change,* vol. 9, no. 6, p. e547, 2018.

[17] J. Luterbacher, D. Dietrich, E. Xoplaki, M. Grosjean, and H. Wanner, "European Seasonal and Annual Temperature Variability, Trends, and Extremes Since 1500," *Science (New York, N.Y.),* vol. 303, pp. 1499-503, 04/01 2004, doi: 10.1126/science.1093877.

[18] G. Brücker, "Vulnerable populations: lessons learnt from the summer 2003 heat waves in Europe," *Eurosurveillance,* vol. 10, no. 7, pp. 1-2%P 551, 2005, doi: doi:https://doi.org/10.2807/esm.10.07.00551-en.

[19] T. E. o. E. Britannica. "European heat wave of 2003." Encyclopedia Britannica. https://www.britannica.com/event/European-heat-wave-of-2003 (accessed.

[20] M. Hamdy, S. Carlucci, P.-J. Hoes, and J. L. Hensen, "The impact of climate change on the overheating risk in dwellings—A Dutch case study," *Building and Environment,* vol. 122, pp. 307-323, 2017.

[21] R. Bustinza, G. Lebel, P. Gosselin, D. Bélanger, and F. Chebana, "Health impacts of the July 2010 heat wave in Québec, Canada," *BMC Public Health,* vol. 13, no. 1, p. 56, 2013/01/21 2013, doi: 10.1186/1471-2458-13-56.

[22] MPNRC. "Canada Heat Wave 2021 Temperature, Deaths, Reason, Map." https://www.mpnrc.org/canada-heat-wave-2021-temperature-deaths-reason-map/ (accessed.

[23] T. Salthammer, A. Schieweck, J. Gu, S. Ameri, and E. Uhde, "Future trends in ambient air pollution and climate in Germany – Implications for the indoor environment," *Building and Environment,* vol. 143, pp. 661-670, 2018, doi: 10.1016/j.buildenv.2018.07.050.

[24] M. S. Nasrin Aghamohammadi, *Urban Overheating: Heat Mitigation and the Impact on Health*. 2022.

[25] (2019). *Canada's Changing Climate Report*. [Online] Available: www.ChangingClimate.ca/CCCR2019

[26] C. B. Field, V. Barros, T. F. Stocker, and Q. Dahe, *Managing the risks of extreme events and disasters to advance climate change adaptation: special report of the intergovernmental panel on climate change*. Cambridge University Press, 2012.

[27] R. Rahif, D. Amaripadath, and S. Attia, "Review on time-integrated overheating evaluation methods for residential buildings in temperate climates of Europe," *Energy and Buildings,* vol. 252, p. 111463, 2021.

[28] D. Chen, "Overheating in residential buildings: Challenges and opportunities," *Indoor and Built Environment,* vol. 28, no. 10, pp. 1303-1306, 2019.

[29] R. S. McLeod and M. Swainson, "Chronic overheating in low carbon urban developments in a temperate climate," *Renewable and Sustainable Energy Reviews,* vol. 74, pp. 201-220, 2017.

[30] K. Yenneti *et al.*, "Urban overheating and cooling potential in Australia: An evidence-based review," *Climate,* vol. 8, no. 11, p. 126, 2020.

[31] M. Santamouris, "Recent progress on urban overheating and heat island research. Integrated assessment of the energy, environmental, vulnerability and health impact. Synergies with the global climate change," *Energy and Buildings,* vol. 207, p. 109482, 2020.

[32] S. H. Holmes, T. Phillips, and A. Wilson, "Overheating and passive habitability: indoor health and heat indices," *Building Research & Information,* vol. 44, no. 1, pp. 1-19, 2016.

[33] J. F. Nicol, J. Hacker, B. Spires, and H. Davies, "Suggestion for new approach to overheating diagnostics," *Building Research & Information,* vol. 37, no. 4, pp. 348-357, 2009.

[34] V. M. Nik, "Making energy simulation easier for future climate–Synthesizing typical and extreme weather data sets out of regional climate models (RCMs)," *Applied Energy,* vol. 177, pp. 204-226, 2016.

[35] K. E. Taylor, R. J. Stouffer, and G. A. Meehl, "An overview of CMIP5 and the experiment design," *Bulletin of the American meteorological Society,* vol. 93, no. 4, pp. 485-498, 2012.

[36] D. Maraun, "Bias correcting climate change simulations-a critical review," *Current Climate Change Reports,* vol. 2, no. 4, pp. 211-220, 2016.

[37] S. Du, X. Zhang, X. Jin, X. Zhou, and X. Shi, "A review of multi-scale modelling, assessment, and improvement methods of the urban thermal and wind environment," *Building and Environment,* p. 108860, 2022.

[38] F. Feser, B. Rockel, H. von Storch, J. Winterfeldt, and M. Zahn, "Regional climate models add value to global model data: a review and selected examples," *Bulletin of the American Meteorological Society,* vol. 92, no. 9, pp. 1181-1192, 2011.

[39] M. Mortezazadeh, Z. Jandaghian, and L. L. Wang, "Integrating CityFFD and WRF for modeling urban microclimate under heatwaves," *Sustainable Cities and Society,* vol. 66, p. 102670, 2021.

[40] J. Zou, A. Gaur, L. L. Wang, A. Laouadi, and M. Lacasse, "Assessment of future overheating conditions in Canadian cities using a reference year selection method," *Building and Environment,* p. 109102, 2022.

[41] L. A. Bugenings and A. Kamari, "Overheating in existing and renovated Danish single-and multi-family houses," *Journal of Building Engineering,* vol. 57, p. 104835, 2022.

[42] G. Flato *et al.*, "Evaluation of climate models," in *Climate change 2013: the physical science basis. Contribution of Working Group I to the Fifth Assessment Report of the Intergovernmental Panel on Climate Change*: Cambridge University Press, 2014, pp. 741-866.

[43] M. Collins *et al.*, "Long-term climate change: projections, commitments and irreversibility," in *Climate change 2013-The physical science basis: Contribution of working group I to the fifth assessment report of the intergovernmental panel on climate change*: Cambridge University Press, 2013, pp. 1029-1136.

[44] D. P. Van Vuuren *et al.*, "The representative concentration pathways: an overview," *Climatic change,* vol. 109, no. 1, pp. 5-31, 2011.

[45] M. Daniel, A. Lemonsu, M. Déqué, S. Somot, A. Alias, and V. Masson, "Benefits of explicit urban parameterization in regional climate modeling to study climate and city interactions," *Climate Dynamics,* vol. 52, no. 5, pp. 2745-2764, 2019.

[46] G. F. Garuma, "Review of urban surface parameterizations for numerical climate models," *Urban Climate,* vol. 24, pp. 830-851, 2018.

[47] V. Masson *et al.*, "City-descriptive input data for urban climate models: Model requirements, data sources and challenges," *Urban Climate,* vol. 31, p. 100536, 2020.

[48] S.-T. Chen, P.-S. Yu, and Y.-H. Tang, "Statistical downscaling of daily precipitation using support vector machines and multivariate analysis," *Journal of hydrology,* vol. 385, no. 1-4, pp. 13-22, 2010.

[49] A. Busuioc, F. Giorgi, X. Bi, and M. Ionita, "Comparison of regional climate model and statistical downscaling simulations of different winter precipitation change scenarios over Romania," *Theoretical and applied climatology,* vol. 86, no. 1, pp. 101-123, 2006.

[50] M. A. Sunyer *et al.*, "Inter-comparison of statistical downscaling methods for projection of extreme precipitation in Europe," *Hydrology and Earth System Sciences,* vol. 19, no. 4, pp. 1827-1847, 2015.

[51] C. Onyutha, H. Tabari, A. Rutkowska, P. Nyeko-Ogiramoi, and P. Willems, "Comparison of different statistical downscaling methods for climate change rainfall projections over the Lake Victoria basin considering CMIP3 and CMIP5," *Journal of Hydro-environment Research,* vol. 12, pp. 31-45, 2016.

[52] H. Von Storch and A. Navarra, *Analysis of climate variability: applications of statistical techniques*. Springer Science & Business Media, 1999.

[53] E. D. Gutmann *et al.*, "A comparison of statistical and dynamical downscaling of winter precipitation over complex terrain," *Journal of Climate,* vol. 25, no. 1, pp. 262-281, 2012.

[54] R. L. Wilby, S. P. Charles, E. Zorita, B. Timbal, P. Whetton, and L. O. Mearns, "Guidelines for use of climate scenarios developed from statistical downscaling methods," *Supporting material of the Intergovernmental Panel on Climate Change, available from the DDC of IPCC TGCIA,* vol. 27, pp. -, 2004.

[55] R. L. Wilby and C. W. Dawson, "The statistical downscaling model: insights from one decade of application," *International Journal of Climatology,* vol. 33, no. 7, pp. 1707-1719, 2013.

[56] J. Murphy, "An evaluation of statistical and dynamical techniques for downscaling local climate," *Journal of Climate,* vol. 12, no. 8, pp. 2256-2284, 1999.

[57] T. Barnett and R. Preisendorfer, "Origins and levels of monthly and seasonal forecast skill for United States surface air temperatures determined by canonical correlation analysis," *Monthly Weather Review,* vol. 115, no. 9, pp. 1825-1850, 1987.

[58] H. Von Storch, E. Zorita, and U. Cubasch, "Downscaling of global climate change estimates to regional scales: an application to Iberian rainfall in wintertime," *Journal of Climate,* vol. 6, no. 6, pp. 1161-1171, 1993.

[59] A. J. Cannon and P. H. Whitfield, "Downscaling recent streamflow conditions in British

Columbia, Canada using ensemble neural network models," *Journal of Hydrology,* vol. 259, no. 1-4, pp. 136-151, 2002.

[60] B. J. Hatchett, D. Koračin, J. F. Mejía, and D. P. Boyle, "Assimilating urban heat island effects into climate projections," *Journal of Arid Environments,* vol. 128, pp. 59-64, 2016.

[61] P. Hoffmann, O. Krueger, and K. H. Schlünzen, "A statistical model for the urban heat island and its application to a climate change scenario," *International Journal of Climatology,* vol. 32, no. 8, pp. 1238-1248, 2012.

[62] D. S. Wilks and R. L. Wilby, "The weather generation game: a review of stochastic weather models," *Progress in physical geography,* vol. 23, no. 3, pp. 329-357, 1999.

[63] M. B. Parlange and R. W. Katz, "An extended version of the Richardson model for simulating daily weather variables," *Journal of Applied Meteorology,* vol. 39, no. 5, pp. 610-622, 2000.

[64] P. Willems and M. Vrac, "Statistical precipitation downscaling for small-scale hydrological impact investigations of climate change," *Journal of hydrology,* vol. 402, no. 3-4, pp. 193-205, 2011.

[65] F. Lindberg, S. Thorsson, D. Rayner, and K. Lau, "The impact of urban planning strategies on heat stress in a climate-change perspective," *Sustainable Cities and Society,* vol. 25, pp. 1-12, 2016.

[66] R. Huth, "A circulation classification scheme applicable in GCM studies," *Theoretical and applied climatology,* vol. 67, no. 1, pp. 1-18, 2000.

[67] R. Huth, J. Kyselý, and L. Pokorná, "A GCM simulation of heat waves, dry spells, and their relationships to circulation," *Climatic Change,* vol. 46, no. 1, pp. 29-60, 2000.

[68] B. C. Hewitson and R. G. Crane, "Self-organizing maps: applications to synoptic climatology," *Climate Research,* vol. 22, no. 1, pp. 13-26, 2002.

[69] J. Corte-Real, B. Quian, and H. Xu, "Circulation patterns, daily precipitation in Portugal and implications for climate change simulated by the second Hadley Centre GCM," *Climate Dynamics,* vol. 15, no. 12, pp. 921-935, 1999.

[70] P. Hoffmann, R. Schoetter, and H. Schlünzen, "Statistical-dynamical downscaling of the urban heat island in Hamburg, Germany," *Meteorologische Zeitschrift,* vol. 27, pp. 89-109, 2018.

[71] R. W. Katz and M. B. Parlange, "Mixtures of stochastic processes: application to statistical downscaling," *Climate Research,* vol. 7, no. 2, pp. 185-193, 1996.

[72] B. Hewitson and R. Crane, "Consensus between GCM climate change projections with empirical downscaling: precipitation downscaling over South Africa," *International Journal of Climatology: A Journal of the Royal Meteorological Society,* vol. 26, no. 10, pp. 1315-1337, 2006.

[73] R. Huth, "Statistical downscaling in central Europe: evaluation of methods and potential predictors," *Climate Research,* vol. 13, no. 2, pp. 91-101, 1999.

[74] M. Vrac, M. Stein, K. Hayhoe, and X. Z. Liang, "A general method for validating statistical downscaling methods under future climate change," *Geophysical Research Letters,* vol. 34,

no. 18, 2007.

[75] S. P. Charles, B. C. Bates, and J. P. Hughes, "A spatiotemporal model for downscaling precipitation occurrence and amounts," *Journal of Geophysical Research: Atmospheres,* vol. 104, no. D24, pp. 31657-31669, 1999.

[76] N. Souverijns, "Precipitation and clouds over Antarctica from an observational and modelling perspective," 2019.

[77] A. Gaur *et al.*, "Effects of using different urban parametrization schemes and land-cover datasets on the accuracy of WRF model over the City of Ottawa," *Urban Climate,* vol. 35, p. 100737, 2021.

[78] M. P. McCarthy, M. J. Best, and R. A. Betts, "Climate change in cities due to global warming and urban effects," *Geophysical research letters,* vol. 37, no. 9, 2010.

[79] G. Mills, "Urban climatology: History, status and prospects," *Urban climate,* vol. 10, pp. 479-489, 2014.

[80] C. Milesi and G. Churkina, "Measuring and monitoring urban impacts on climate change from space," *Remote Sensing,* vol. 12, no. 21, p. 3494, 2020.

[81] H. Kusaka, M. Hara, and Y. Takane, "Urban climate projection by the WRF model at 3-km horizontal grid increment: dynamical downscaling and predicting heat stress in the 2070's August for Tokyo, Osaka, and Nagoya metropolises," *Journal of the Meteorological Society of Japan. Ser. II,* vol. 90, pp. 47-63, 2012.

[82] F. Chen *et al.*, "The integrated WRF/urban modelling system: development, evaluation, and applications to urban environmental problems," *International Journal of Climatology,* vol. 31, no. 2, pp. 273-288, 2011.

[83] F. Chen, X. Yang, and W. Zhu, "WRF simulations of urban heat island under hot-weather synoptic conditions: The case study of Hangzhou City, China," *Atmospheric research,* vol. 138, pp. 364-377, 2014.

[84] H. M. Imran, J. Kala, A. Ng, and S. Muthukumaran, "An evaluation of the performance of a WRF multi-physics ensemble for heatwave events over the city of Melbourne in southeast Australia," *Climate dynamics,* vol. 50, no. 7, pp. 2553-2586, 2018.

[85] T. M. Giannaros, D. Melas, I. A. Daglis, I. Keramitsoglou, and K. Kourtidis, "Numerical study of the urban heat island over Athens (Greece) with the WRF model," *Atmospheric Environment,* vol. 73, pp. 103-111, 2013.

[86] A. T. Hayes *et al.*, "Nature-Based Solutions (NBSs) to Mitigate Urban Heat Island (UHI) Effects in Canadian Cities," *Buildings,* vol. 12, no. 7, p. 925, 2022.

[87] C. S. B. Grimmond *et al.*, "The International Urban Energy Balance Models Comparison Project: First Results from Phase 1," (in English), *Journal of Applied Meteorology and Climatology,* vol. 49, no. 6, pp. 1268-1292, 01 Jun. 2010 2010, doi: 10.1175/2010jamc2354.1.

[88] M. Best and C. Grimmond, "Analysis of the seasonal cycle within the first international urban land-surface model comparison," *Boundary-Layer Meteorology,* vol. 146, no. 3, pp. 421-446, 2013.

[89] B. Le Roy, A. Lemonsu, and R. Schoetter, "A statistical–dynamical downscaling methodology for the urban heat island applied to the EURO-CORDEX ensemble," *Climate Dynamics,* vol. 56, no. 7, pp. 2487-2508, 2021/04/01 2021, doi: 10.1007/s00382-020-05600-z.

[90] A. Gaur, M. K. Eichenbaum, and S. P. Simonovic, "Analysis and modelling of surface Urban Heat Island in 20 Canadian cities under climate and land-cover change," *Journal of environmental management,* vol. 206, pp. 145-157, 2018.

[91] H. Von Storch and F. W. Zwiers, *Statistical analysis in climate research*. Cambridge university press, 2002.

[92] C. Teutschbein and J. Seibert, "Bias correction of regional climate model simulations for hydrological climate-change impact studies: Review and evaluation of different methods," *Journal of hydrology,* vol. 456, pp. 12-29, 2012.

[93] Y. Hui, J. Chen, C. Y. Xu, L. Xiong, and H. Chen, "Bias nonstationarity of global climate model outputs: The role of internal climate variability and climate model sensitivity," *International Journal of Climatology,* vol. 39, no. 4, pp. 2278-2294, 2019.

[94] A. Gaur and S. P. Simonovic, "Towards reducing climate change impact assessment process uncertainty," *Environmental Processes,* vol. 2, no. 2, pp. 275-290, 2015.

[95] H. R. Glahn and D. A. Lowry, "The use of model output statistics (MOS) in objective weather forecasting," *Journal of Applied Meteorology and Climatology,* vol. 11, no. 8, pp. 1203-1211, 1972.

[96] W. H. Klein, B. M. Lewis, and I. Enger, "Objective prediction of five-day mean temperatures during winter," *Journal of Atmospheric Sciences,* vol. 16, no. 6, pp. 672-682, 1959.

[97] S. Hagemann, C. Chen, J. O. Haerter, J. Heinke, D. Gerten, and C. Piani, "Impact of a statistical bias correction on the projected hydrological changes obtained from three GCMs and two hydrology models," *Journal of Hydrometeorology,* vol. 12, no. 4, pp. 556-578, 2011.

[98] R. J. Harding, G. P. Weedon, H. A. van Lanen, and D. B. Clark, "The future for global water assessment," *Journal of Hydrology,* vol. 518, pp. 186-193, 2014.

[99] J. Zou, A. Gaur, and L. L. Wang, "A Method of Selecting Future Reference Years for Indoor Overheating Assessment."

[100] A. Gaur, M. Lacasse, and M. Armstrong, "Climate data to undertake hygrothermal and whole building simulations under projected climate change influences for 11 Canadian cities," *Data,* vol. 4, no. 2, p. 72, 2019.

[101] C. Piani *et al.*, "Statistical bias correction of global simulated daily precipitation and temperature for the application of hydrological models," *Journal of hydrology,* vol. 395, no. 3-4, pp. 199-215, 2010.

[102] S. Watanabe, S. Kanae, S. Seto, P. J. F. Yeh, Y. Hirabayashi, and T. Oki, "Intercomparison of bias-correction methods for monthly temperature and precipitation simulated by multiple climate models," *Journal of Geophysical Research: Atmospheres,* vol. 117, no. D23, 2012.

[103] P. Berg, H. Feldmann, and H.-J. Panitz, "Bias correction of high resolution regional climate model data," *Journal of Hydrology,* vol. 448, pp. 80-92, 2012.

[104] D. Bannister *et al.*, "Bias correction of high-resolution regional climate model precipitation output gives the best estimates of precipitation in Himalayan catchments," *Journal of Geophysical Research: Atmospheres,* vol. 124, no. 24, pp. 14220-14239, 2019.

[105] R. Leander and T. A. Buishand, "Resampling of regional climate model output for the simulation of extreme river flows," *Journal of Hydrology,* vol. 332, no. 3-4, pp. 487-496, 2007.

[106] H. Li, J. Sheffield, and E. F. Wood, "Bias correction of monthly precipitation and temperature fields from Intergovernmental Panel on Climate Change AR4 models using equidistant quantile matching," *Journal of Geophysical Research: Atmospheres,* vol. 115, no. D10, 2010.

[107] M. Ashfaq, L. C. Bowling, K. Cherkauer, J. S. Pal, and N. S. Diffenbaugh, "Influence of climate model biases and daily-scale temperature and precipitation events on hydrological impacts assessment: A case study of the United States," *Journal of Geophysical Research: Atmospheres,* vol. 115, no. D14, 2010.

[108] A. J. Cannon, "Multivariate quantile mapping bias correction: an N-dimensional probability density function transform for climate model simulations of multiple variables," *Climate dynamics,* vol. 50, no. 1, pp. 31-49, 2018.

[109] A. J. Cannon, "Multivariate bias correction of climate model output: Matching marginal distributions and intervariable dependence structure," *Journal of Climate,* vol. 29, no. 19, pp. 7045-7064, 2016.

[110] V. M. Nik, A. S. Kalagasidis, and E. Kjellström, "Statistical methods for assessing and analysing the building performance in respect to the future climate," *Building and environment,* vol. 53, pp. 107-118, 2012.

[111] V. M. Nik, *Climate Simulation of an Attic Using Future Weather Data Sets-Statistical Methods for Data Processing and Analysis*. Chalmers Tekniska Hogskola (Sweden), 2010.

[112] A. L. Chan, T.-T. Chow, S. K. Fong, and J. Z. Lin, "Generation of a typical meteorological year for Hong Kong," *Energy Conversion and management,* vol. 47, no. 1, pp. 87-96, 2006.

[113] Y. Jiang, "Generation of typical meteorological year for different climates of China," *Energy,* vol. 35, no. 5, pp. 1946-1953, 2010.

[114] H. Li, Y. Yang, K. Lv, J. Liu, and L. Yang, "Compare several methods of select typical meteorological year for building energy simulation in China," *Energy,* vol. 209, p. 118465, 2020.

[115] O. S. Ohunakin, M. S. Adaramola, O. M. Oyewola, and R. O. Fagbenle, "Generation of a typical meteorological year for north–east, Nigeria," *Applied Energy,* vol. 112, pp. 152-159, 2013.

[116] D. Pissimanis, G. Karras, V. Notaridou, and K. Gavra, "The generation of a “typical meteorological year” for the city of Athens," *Solar Energy,* vol. 40, no. 5, pp. 405-411, 1988.

[117] S. Pusat, İ. Ekmekçi, and M. T. Akkoyunlu, "Generation of typical meteorological year for different climates of Turkey," *Renewable Energy,* vol. 75, pp. 144-151, 2015.

[118] I. Hall, R. Prairie, H. Anderson, and E. Boes, "Generation of a typical meteorological year," Sandia Labs., Albuquerque, NM (USA), 1978.

[119] S. C. M. Hui and C. Lok, "Test reference year for comparative energy study," *Hong Kong Engineer,* vol. 20, pp. 13-16, 02/01 1992.

[120] T. Kalamees and J. Kurnitski, "Estonian test reference year for energy calculations," in *Proceedings of the Estonian Academy of Sciences Engineering*, 2006, vol. 12, no. 1, pp. 40-58.

[121] T. L. Stoffel and M. D. Rymes, "Production of the weather year for energy calculations version 2 (WYEC2) data files/Discussion," *ASHRAE Transactions,* vol. 104, p. 487, 1998.

[122] L. Harriman, D. Colliver, and K. Q. Hart, "New weather data for energy calculations," *ASHRAE journal,* vol. 41, pp. 31-38, 1999.

[123] D. J. Thevenard and A. P. Brunger, "The development of typical weather years for international locations: part I, algorithms," *Ashrae Transactions,* vol. 108, p. 376, 2002.

[124] D. J. Thevenard and A. P. Brunger, "The development of typical weather years for international locations: Part II, production/Discussion," *ASHRAE Transactions,* vol. 108, p. 480, 2002.

[125] D. B. Crawley, "Which weather data should you use for energy simulations of commercial buildings?," *Transactions-American society of heating refrigerating and air conditioning engineers,* vol. 104, pp. 498-515, 1998.

[126] D. B. Crawley and Y. J. Huang, "Does it matter which weather data you use in energy simulations," *User News,* vol. 18, no. 1, pp. 2-12, 1997.

[127] ASHRAE, "International weather for energy calculations (IWEC Weather Files) User's Manual," *ASHRAE,* 2002.

[128] ASHRAE, "Weather year for energy calculations," *American Society of Heating, Refrigerating and Air-Conditioning Engineers,* 1985.

[129] K. Steemers, "Accuracy of modelled extremes of temperature and climate change and its implications for the built environment in the UK," 2004.

[130] G. Levermore and J. Parkinson, "Analyses and algorithms for new Test Reference Years and Design Summer Years for the UK," *Building services engineering research and technology,* vol. 27, no. 4, pp. 311-325, 2006.

[131] S. E. Belcher, J. N. Hacker, and D. S. Powell, "Constructing design weather data for future climates," *Building services engineering research and technology,* vol. 26, no. 1, pp. 49-61, 2005.

[132] M. J. Ren, G. Levermore, and N. Doylend, "The impact of new CIBSE weather data on natural ventilation design," *Building Services Engineering Research and Technology,* vol. 24, no. 2, pp. 83-91, 2003.

[133] T. Hong, W.-K. Chang, and H.-W. Lin, "A fresh look at weather impact on peak electricity demand and energy use of buildings using 30-year actual weather data," *Applied energy,*

vol. 111, pp. 333-350, 2013.

[134] M. F. Jentsch, M. E. Eames, and G. J. Levermore, "Generating near-extreme Summer Reference Years for building performance simulation," *Building Services Engineering Research and Technology,* vol. 36, no. 6, pp. 701-727, 2015.

[135] A. Laouadi, M. Bartko, and M. Lacasse, "A new methodology of evaluation of overheating in buildings," *Energy and Buildings,* vol. 226, p. 110360, 2020.

[136] A. Laouadi, A. Gaur, M. Lacasse, M. Bartko, and M. Armstrong, "Development of reference summer weather years for analysis of overheating risk in buildings," *Journal of Building Performance Simulation,* vol. 13, no. 3, pp. 301-319, 2020.

[137] L. Ji, A. Laouadi, C. Shu, A. Gaur, M. Lacasse, and L. L. Wang, "Evaluating approaches of selecting extreme hot years for assessing building overheating conditions during heatwaves," *Energy and Buildings,* vol. 254, p. 111610, 2022.

[138] V. M. Nik, "Application of typical and extreme weather data sets in the hygrothermal simulation of building components for future climate–A case study for a wooden frame wall," *Energy and Buildings,* vol. 154, pp. 30-45, 2017.

[139] C. Bylund Melin, C.-E. Hagentoft, K. Holl, V. M. Nik, and R. Kilian, "Simulations of moisture gradients in wood subjected to changes in relative humidity and temperature due to climate change," *Geosciences,* vol. 8, no. 10, p. 378, 2018.

[140] M. Hosseini, K. Javanroodi, and V. M. Nik, "High-resolution impact assessment of climate change on building energy performance considering extreme weather events and microclimate–Investigating variations in indoor thermal comfort and degree-days," *Sustainable Cities and Society,* vol. 78, p. 103634, 2022.

[141] A. Moazami, V. M. Nik, S. Carlucci, and S. Geving, "Impacts of future weather data typology on building energy performance–Investigating long-term patterns of climate change and extreme weather conditions," *Applied Energy,* vol. 238, pp. 696-720, 2019.

[142] J. Heckenbergerová, P. Musilek, and K. Filimonenkov, "Quantification of gains and risks of static thermal rating based on typical meteorological year," *International Journal of Electrical Power & Energy Systems,* vol. 44, no. 1, pp. 227-235, 2013.

[143] S. Liu, Y.-T. Kwok, K. Lau, and E. Ng, "Applicability of different extreme weather datasets for assessing indoor overheating risks of residential buildings in a subtropical high-density city," *Building and Environment,* vol. 194, p. 107711, 2021.

[144] A. Brambilla, J. Bonvin, F. Flourentzou, and T. Jusselme, "On the influence of thermal mass and natural ventilation on overheating risk in offices," *Buildings,* vol. 8, no. 4, p. 47, 2018.

[145] C. Tam, Y. Zhao, Z. Liao, and L. Zhao, "Mitigation Strategies for Overheating and High Carbon Dioxide Concentration within Institutional Buildings: A Case Study in Toronto, Canada," *Buildings,* vol. 10, no. 7, p. 124, 2020.

[146] F. M. Baba and H. Ge, "Overheating risk of a single-family detached house built at different ages under current and future climate in Canada," in *E3S Web of Conferences*, 2020, vol. 172: EDP Sciences, p. 02004.

[147] C. Shu *et al.*, "Added value of convection permitting climate modelling in urban overheating assessments," *Building and Environment,* vol. 207, p. 108415, 2022.

[148] A. Laouadi, M. Bartko, A. Gaur, and M. A. Lacasse, "Climate resilience buildings: guideline for management of overheating risk in residential buildings," in "Climate Resilient Buildings and Core Public Infrastructure Initiative (National Research Council of Canada. Construction); no. CRBCPI-Y4-10," National Research Council of Canada. Construction, 2021/04/01 2021.

[149] A. Perera, V. M. Nik, D. Chen, J.-L. Scartezzini, and T. Hong, "Quantifying the impacts of climate change and extreme climate events on energy systems," *Nature Energy,* vol. 5, no. 2, pp. 150-159, 2020.

[150] DOE, "Energyplus," 2020. [Online]. Available: https://energyplus.net/.

[151] E. S. R. Unit, "ESP-r," 2020. [Online]. Available: https://www.esru.strath.ac.uk//applications/esp-r/.

[152] T. E. S. Specialists, "TRNSYS," 2019. [Online]. Available: http://www.trnsys.com/support/downloads.php.html.

[153] S. Tsoka, "Optimizing indoor climate conditions in a sports building located in Continental Europe," *Energy Procedia,* vol. 78, pp. 2802-2807, 2015, doi: 10.1016/j.egypro.2015.11.630.

[154] F. M. Baba, H. Ge, R. Zmeureanu, and L. L. Wang, "Calibration of building model based on indoor temperature for overheating assessment using genetic algorithm: Methodology, evaluation criteria, and case study," *Building and Environment,* vol. 207, p. 108518, 2022, doi: 10.1016/j.buildenv.2021.108518.

[155] H. Elsharkawy and S. Zahiri, "The significance of occupancy profiles in determining post retrofit indoor thermal comfort, overheating risk and building energy performance," *Building and Environment,* vol. 172, p. 106676, 2020, doi: 10.1016/j.buildenv.2020.106676.

[156] M. Benchekroun, S. Chergui, F. Ruggiero, and S. Di Turi, "Improving the indoor climate of the traditional Ottoman houses in the Medina of Algiers," *IOP Conference Series: Materials Science and Engineering,* vol. 609, pp. 0-7, 2019, doi: 10.1088/1757-899X/609/4/042073.

[157] S. Martínez-Mariño, P. Eguía-Oller, E. Granada-Álvarez, and A. Erkoreka-González, "Simulation and validation of indoor temperatures and relative humidity in multi-zone buildings under occupancy conditions using multi-objective calibration," *Building and Environment,* vol. 200, 2021, doi: 10.1016/j.buildenv.2021.107973.

[158] A. Martínez-Ibernón, C. Aparicio-Fernández, R. Royo-Pastor, and J. L. Vivancos, "Temperature and humidity transient simulation and validation in a measured house without a HVAC system," *Energy and Buildings,* vol. 131, pp. 54-62, 2016, doi: 10.1016/j.enbuild.2016.08.079.

[159] S. Firląg and S. Murray, "Impacts of airflows, internal heat and moisture gains on accuracy of modeling energy consumption and indoor parameters in passive building," *Energy and Buildings,* vol. 64, pp. 372-383, 2013, doi: 10.1016/j.enbuild.2013.04.024.

[160] Q. Chen *et al.*, "Ventilation performance prediction for buildings: model assessment," *Building and environment,* vol. 45, no. 2, pp. 295-303, 2010.

[161] L. L. Wang and Q. Chen, "Evaluation of some assumptions used in multizone airflow network models," *Building and Environment,* vol. 43, no. 10, pp. 1671-1677, 2008.

[162] L. L. Wang, W. S. Dols, and Q. Chen, "Using CFD capabilities of CONTAM 3.0 for simulating airflow and contaminant transport in and around buildings," *Hvac&R Research,* vol. 16, no. 6, pp. 749-763, 2010.

[163] L. Wang and Q. Chen, "Theoretical and numerical studies of coupling multizone and CFD models for building air distribution simulations," *Indoor Air,* vol. 17, no. 5, pp. 348-361, 2007.

[164] S. Yan, L. L. Wang, M. J. Birnkrant, J. Zhai, and S. L. Miller, "Evaluating SARS-CoV-2 airborne quanta transmission and exposure risk in a mechanically ventilated multizone office building," *Building and Environment,* p. 109184, 2022.

[165] R. Vidhyashankar, R. Vinze, S. Nagarathinam, and V. K. Natrajan, "Modelling spatial variations in thermal comfort in indoor open-plan spaces using a whole-building simulation tool," *Journal of Building Engineering,* vol. 46, p. 103727, 2022, doi: 10.1016/j.jobe.2021.103727.

[166] P. Rohdin, A. Molin, and B. Moshfegh, "Experiences from nine passive houses in Sweden - Indoor thermal environment and energy use," *Building and Environment,* vol. 71, pp. 176-185, 2014, doi: 10.1016/j.buildenv.2013.09.017.

[167] S. Sana, A. Hayati, and M. Salmanzadeh, "Optimization of Window-to-Wall Ratio for Buildings Located in Different Climates: An IDA-Indoor Climate and Energy Simulation Study," *Energies,* vol. 14, 2021.

[168] P. Paliouras, N. Matzaflaras, R. H. Peuhkuri, and J. Kolarik, "Using measured indoor environment parameters for calibration of building simulation model - A passive house case study," *Energy Procedia,* vol. 78, pp. 1227-1232, 2015, doi: 10.1016/j.egypro.2015.11.209.

[169] I. Kistelegdi and B. Baranyai, "Dynamic Simulations Supported Indoor Climate and Energy Building Modeling," *International Journal of Engineering and Technology,* pp. 181-186, 2013, doi: 10.7763/ijet.2013.v5.537.

[170] K. Ahmed, T. Hasu, and J. Kurnitski, "Actual energy performance and indoor climate in Finnish NZEB daycare and school buildings," *Journal of Building Engineering,* vol. 56, p. 104759, 2022, doi: 10.1016/j.jobe.2022.104759.

[171] H. M. Künzel, A. Holm, D. Zirkelbach, and A. N. Karagiozis, "Simulation of indoor temperature and humidity conditions including hygrothermal interactions with the building envelope," *Solar Energy,* vol. 78, pp. 554-561, 2005, doi: 10.1016/j.solener.2004.03.002.

[172] A. Buonomano, U. Montanaro, A. Palombo, and S. Santini, "Adaptive control for building thermo-hygrometric analysis: A novel dynamic simulation code for indoor spaces with multi-enclosed thermal zones," *Energy Procedia,* vol. 78, pp. 2190-2195, 2015, doi: 10.1016/j.egypro.2015.11.316.

[173] F. Tariku, K. Kumaran, and P. Fazio, "Integrated analysis of whole building heat, air and

moisture transfer," *International Journal of Heat and Mass Transfer,* vol. 53, pp. 3111-3120, 2010, doi: 10.1016/j.ijheatmasstransfer.2010.03.016.

[174] J. Pfafferott, S. Rißmann, M. Sühring, F. Kanani-Sühring, and B. Maronga, "Building indoor model in PALM-4U: Indoor climate, energy demand, and the interaction between buildings and the urban microclimate," *Geoscientific Model Development,* vol. 14, pp. 3511-3519, 2021, doi: 10.5194/gmd-14-3511-2021.

[175] A. Ryzhov, H. Ouerdane, E. Gryazina, A. Bischi, and K. Turitsyn, "Model predictive control of indoor microclimate: Existing building stock comfort improvement," *Energy Conversion and Management,* vol. 179, pp. 219-228, 2019, doi: 10.1016/j.enconman.2018.10.046.

[176] S. Yang, M. P. Wan, W. Chen, B. F. Ng, and D. Zhai, "An adaptive robust model predictive control for indoor climate optimization and uncertainties handling in buildings," *Building and Environment,* vol. 163, p. 106326, 2019, doi: 10.1016/j.buildenv.2019.106326.

[177] F. E. Ţurcanu, C. G. Popovici, M. Verdes, V. Ciocan, and S. V. Hudişteanu, "Indoor climate modelling and economic analysis regarding the energetic rehabilitation of a church," *Energies,* vol. 13, 2020, doi: 10.3390/en13112815.

[178] W. Zhao, P. Mustakallio, S. Lestinen, S. Kilpeläinen, J. Jokisalo, and R. Kosonen, "Numerical and Experimental Study on the Indoor Climate in a Classroom with Mixing and Displacement Air Distribution Methods," *Buildings,* vol. 12, p. 1314, 2022, doi: 10.3390/buildings12091314.

[179] W. Zhang, K. Hiyama, S. Kato, and Y. Ishida, "Building energy simulation considering spatial temperature distribution for nonuniform indoor environment," *Building and Environment,* vol. 63, pp. 89-96, 2013, doi: 10.1016/j.buildenv.2013.02.007.

[180] H. Huang, S. Kato, and R. Hu, "Optimum design for indoor humidity by coupling Genetic Algorithm with transient simulation based on Contribution Ratio of Indoor Humidity and Climate analysis," *Energy and Buildings,* vol. 47, pp. 208-216, 2012, doi: 10.1016/j.enbuild.2011.11.040.

[181] L. Eriksson, G. Grozman, P. Grozman, P. Sahlin, M. H. Vorre, and L. Ålenius, "CFD-Free, Efficient, Micro Indoor Climate Prediction in Buildings," *First Building Simulation and Optimization Conference,* pp. 149-156, 2012.

[182] C. Nytsch-Geusen, K. Mathur, and L. Westermann, "Development of a real-time test bed for indoor climate simulation in a VR environment using a digital twin," *Proceedings of 14th Modelica Conference 2021, Linköping, Sweden, September 20-24, 2021,* vol. 181, pp. 263-269, 2021, doi: 10.3384/ecp21181263.

[183] L. Mba, P. Meukam, and A. Kemajou, "Application of artificial neural network for predicting hourly indoor air temperature and relative humidity in modern building in humid region," *Energy and Buildings,* vol. 121, pp. 32-42, 2016, doi: 10.1016/j.enbuild.2016.03.046.

[184] S. Ganguly, A. Ahmed, and F. Wang, "Optimised building energy and indoor microclimatic predictions using knowledge-based system identification in a historical art gallery," *Neural Computing and Applications,* vol. 32, pp. 3349-3366, 2020, doi: 10.1007/s00521-019-04224-7.

[185] A. Aliberti, L. Bottaccioli, E. Macii, S. Di Cataldo, A. Acquaviva, and E. Patti, "A non-linear autoregressive model for indoor air-temperature predictions in smart buildings," *Electronics (Switzerland),* vol. 8, pp. 1-17, 2019, doi: 10.3390/electronics8090979.

[186] H. Sözer and S. S. Aldin, "Predicting the indoor thermal data for heating season based on short-term measurements to calibrate the simulation set-points," *Energy and Buildings,* vol. 202, 2019, doi: 10.1016/j.enbuild.2019.109422.

[187] R. Kramer, J. van Schijndel, and H. Schellen, "Inverse modeling of simplified hygrothermal building models to predict and characterize indoor climates," *Building and Environment,* vol. 68, pp. 87-99, 2013, doi: 10.1016/j.buildenv.2013.06.001.

[188] A. Dodoo, "Energy and indoor thermal comfort performance of a Swedish residential building under future climate change conditions," in *E3S Web of Conferences*, 2020, vol. 172: EDP Sciences, p. 02001.

[189] M. Lei, T. van Hooff, B. Blocken, and A. Pereira Roders, "The predicted effect of climate change on indoor overheating of heritage apartments in two different Chinese climate zones," *Indoor and Built Environment,* p. 1420326X221085861, 2022.

[190] F. Fiorito *et al.*, "Adaptation of Users to Future Climate Conditions in Naturally Ventilated Historic Buildings: Effects on Indoor Comfort," *Energies,* vol. 15, 2022, doi: 10.3390/en15144984.

[191] R. Escandon, R. Suarez, A. Alonso, and G. M. Mauro, "Is indoor overheating an upcoming risk in southern Spain social housing stocks? Predictive assessment under a climate change scenario," *Building and Environment,* vol. 207, p. 108482, 2022.

[192] R. Rahif *et al.*, "Impact of climate change on nearly zero-energy dwelling in temperate climate: Time-integrated discomfort, HVAC energy performance, and GHG emissions," *Building and Environment,* vol. 223, 2022, doi: 10.1016/j.buildenv.2022.109397.

[193] B. Blocken and C. Gualtieri, "Ten iterative steps for model development and evaluation applied to Computational Fluid Dynamics for Environmental Fluid Mechanics," *Environmental Modelling & Software,* vol. 33, pp. 1-22, 2012.

[194] B. Blocken, W. Janssen, and T. van Hooff, "CFD simulation for pedestrian wind comfort and wind safety in urban areas: General decision framework and case study for the Eindhoven University campus," *Environmental Modelling & Software,* vol. 30, pp. 15-34, 2012.

[195] S. Tsoka, K. Tsikaloudaki, T. Theodosiou, and D. Bikas, "Urban warming and cities' microclimates: investigation methods and mitigation strategies—a review," *Energies,* vol. 13, no. 6, p. 1414, 2020.

[196] Y. Tominaga *et al.*, "AIJ guidelines for practical applications of CFD to pedestrian wind environment around buildings," *Journal of wind engineering and industrial aerodynamics,* vol. 96, no. 10-11, pp. 1749-1761, 2008.

[197] "The COST 732 Best Practice Guideline for CFD simulation of flows in the urban environment: a summary," *International Journal of Environment and Pollution,* vol. 44, no. 1-4, pp. 419-427, 2011, doi: 10.1504/ijep.2011.038443.

[198] S. Tsoka, A. Tsikaloudaki, and T. Theodosiou, "Analyzing the ENVI-met microclimate

model's performance and assessing cool materials and urban vegetation applications–A review," *Sustainable Cities and Society,* vol. 43, pp. 55-76, 2018/11/01/ 2018, doi: https://doi.org/10.1016/j.scs.2018.08.009.

[199] P. A. Mirzaei, "CFD modeling of micro and urban climates: Problems to be solved in the new decade," *Sustainable Cities and Society,* vol. 69, p. 102839, 2021/06/01/ 2021, doi: https://doi.org/10.1016/j.scs.2021.102839.

[200] J. Zou, "Predicting convective heat transfer from Computational Thermal Manikin in urban outdoor environments," University of Sydney, 2021.

[201] A. Martilli, "Current research and future challenges in urban mesoscale modelling," *International Journal of Climatology: A Journal of the Royal Meteorological Society,* vol. 27, no. 14, pp. 1909-1918, 2007.

[202] A. Ricci, M. Burlando, M. Repetto, and B. Blocken, "Static downscaling of mesoscale wind conditions into an urban canopy layer by a CFD microscale model," *Building and Environment,* vol. 225, p. 109626, 2022.

[203] P. A. Mirzaei and F. Haghighat, "Approaches to study Urban Heat Island – Abilities and limitations," *Building and Environment,* vol. 45, no. 10, pp. 2192-2201, 2010/10/01/ 2010, doi: https://doi.org/10.1016/j.buildenv.2010.04.001.

[204] U. K. Priya and R. Senthil, "A review of the impact of the green landscape interventions on the urban microclimate of tropical areas," *Building and Environment,* vol. 205, p. 108190, 2021/11/01/ 2021, doi: https://doi.org/10.1016/j.buildenv.2021.108190.

[205] Z. Liu, W. Cheng, C. Y. Jim, T. E. Morakinyo, Y. Shi, and E. Ng, "Heat mitigation benefits of urban green and blue infrastructures: A systematic review of modeling techniques, validation and scenario simulation in ENVI-met V4," *Building and Environment,* vol. 200, p. 107939, 2021/08/01/ 2021, doi: https://doi.org/10.1016/j.buildenv.2021.107939.

[206] N. Antoniou, H. Montazeri, M. Neophytou, and B. Blocken, "CFD simulation of urban microclimate: Validation using high-resolution field measurements," *Science of The Total Environment,* vol. 695, p. 133743, 2019/12/10/ 2019, doi: https://doi.org/10.1016/j.scitotenv.2019.133743.

[207] A. Mochida, S. Iizuka, Y. Tominaga, and I. Y.-F. Lun, "Up-scaling CWE models to include mesoscale meteorological influences," *Journal of Wind Engineering and Industrial Aerodynamics,* vol. 99, no. 4, pp. 187-198, 2011/04/01/ 2011, doi: https://doi.org/10.1016/j.jweia.2011.01.012.

[208] M. Mortezazadeh, L. L. Wang, M. Albettar, and S. Yang, "CityFFD – City fast fluid dynamics for urban microclimate simulations on graphics processing units," *Urban Climate,* vol. 41, p. 101063, 2022/01/01/ 2022, doi: https://doi.org/10.1016/j.uclim.2021.101063.

[209] M. Mortezazadeh, J. Zou, M. Hosseini, S. Yang, and L. Wang, "Estimating urban wind speeds and wind power potentials based on machine learning with city fast fluid dynamics training data," *Atmosphere,* vol. 13, no. 2, p. 214, 2022.

[210] M. Mortezazadeh and L. L. Wang, "Solving city and building microclimates by fast fluid dynamics with large timesteps and coarse meshes," *Building and Environment,* vol. 179, p.

106955, 2020.

[211] M. Mortezazadeh Dorostkar, "CityFFD–City Fast Fluid Dynamics Model for Urban Microclimate Simulations," Concordia University, 2019.

[212] A. Katal, M. Mortezazadeh, and L. L. Wang, "Modeling building resilience against extreme weather by integrated CityFFD and CityBEM simulations," *Applied Energy,* vol. 250, pp. 1402-1417, 2019.

[213] M. Vuckovic, W. Loibl, T. Tötzer, and R. Stollnberger, "Potential of Urban Densification to Mitigate the Effects of Heat Island in Vienna, Austria," *Environments,* vol. 6, no. 7, p. 82, 2019. [Online]. Available: https://www.mdpi.com/2076-3298/6/7/82.

[214] M. Vuckovic, K. Kiesel, and A. Mahdavi, "Toward advanced representations of the urban microclimate in building performance simulation," *Sustainable Cities and Society,* vol. 27, pp. 356-366, 2016/11/01/ 2016, doi: https://doi.org/10.1016/j.scs.2016.05.002.

[215] M. Demuzere, J. Kittner, and B. Bechtel, "LCZ Generator: A Web Application to Create Local Climate Zone Maps," (in English), *Frontiers in Environmental Science,* Original Research vol. 9, 2021-April-23 2021, doi: 10.3389/fenvs.2021.637455.

[216] E. E. Jeannie Evers, Emdash Editing. "GIS (Geographic Information System)." https://education.nationalgeographic.org/resource/geographic-information-system-gis (accessed.

[217] I. D. Stewart, T. R. Oke, and E. S. Krayenhoff, "Evaluation of the 'local climate zone'scheme using temperature observations and model simulations," *International journal of climatology,* vol. 34, no. 4, pp. 1062-1080, 2014.

[218] A. Shafaghat, G. Manteghi, A. Keyvanfar, H. B. I. N. Lamit, K. Saito, and D. R. Ossen, "Street Geometry Factors Influence Urban Microclimate in Tropical Coastal Cities: A Review," *Environmental & Climate Technologies,* Article vol. 17, no. 1, pp. 61-75, 2016, doi: 10.1515/rtuect-2016-0006.

[219] I. Pađen, C. García-Sánchez, and H. Ledoux, "Towards automatic reconstruction of 3D city models tailored for urban flow simulations," *Frontiers in Built Environment,* p. 141, 2022.

[220] J. Allegrini, V. Dorer, and J. Carmeliet, "Coupled CFD, radiation and building energy model for studying heat fluxes in an urban environment with generic building configurations," *Sustainable Cities and Society,* vol. 19, pp. 385-394, 2015.

[221] J. Allegrini and J. Carmeliet, "Simulations of local heat islands in Zürich with coupled CFD and building energy models," *Urban Climate,* vol. 24, pp. 340-359, 2018/06/01/ 2018, doi: https://doi.org/10.1016/j.uclim.2017.02.003.

[222] J. Allegrini and J. Carmeliet, "Coupled CFD and building energy simulations for studying the impacts of building height topology and buoyancy on local urban microclimates," *Urban Climate,* vol. 21, pp. 278-305, 2017/09/01/ 2017, doi: https://doi.org/10.1016/j.uclim.2017.07.005.

[223] Y. Zheng, Y. Miao, S. Liu, B. Chen, H. Zheng, and S. Wang, "Simulating Flow and Dispersion by Using WRF-CFD Coupled Model in a Built-Up Area of Shenyang, China," *Advances in Meteorology,* vol. 2015, p. 528618, 2015/03/23 2015, doi: 10.1155/2015/528618.

[224] U. Berardi, Z. Jandaghian, and J. Graham, "Effects of greenery enhancements for the resilience to heat waves: A comparison of analysis performed through mesoscale (WRF) and microscale (Envi-met) modeling," *Science of The Total Environment,* vol. 747, p. 141300, 2020/12/10/ 2020, doi: https://doi.org/10.1016/j.scitotenv.2020.141300.

[225] I. McRae *et al.*, "Integration of the WUDAPT, WRF, and ENVI-met models to simulate extreme daytime temperature mitigation strategies in San Jose, California," *Building and Environment,* vol. 184, p. 107180, 2020/10/15/ 2020, doi: https://doi.org/10.1016/j.buildenv.2020.107180.

[226] N. H. Wong *et al.*, "An integrated multiscale urban microclimate model for the urban thermal environment," *Urban Climate,* vol. 35, p. 100730, 2021/01/01/ 2021, doi: https://doi.org/10.1016/j.uclim.2020.100730.

[227] A. A. Wyszogrodzki, S. Miao, and F. Chen, "Evaluation of the coupling between mesoscale-WRF and LES-EULAG models for simulating fine-scale urban dispersion," *Atmospheric Research,* vol. 118, pp. 324-345, 2012/11/15/ 2012, doi: https://doi.org/10.1016/j.atmosres.2012.07.023.

[228] I. Tumini and C. Rubio-Bellido, "Measuring climate change impact on urban microclimate: A case study of concepción," *Procedia engineering,* vol. 161, pp. 2290-2296, 2016.

[229] M. F. Jentsch, P. A. B. James, L. Bourikas, and A. S. Bahaj, "Transforming existing weather data for worldwide locations to enable energy and building performance simulation under future climates," *Renewable Energy,* vol. 55, pp. 514-524, 2013/07/01/ 2013, doi: https://doi.org/10.1016/j.renene.2012.12.049.

[230] I. Tumini, E. Higueras García, and S. Baereswyl Rada, "Urban microclimate and thermal comfort modelling: strategies for urban renovation," *International Journal of Sustainable Building Technology and Urban Development,* vol. 7, no. 1, pp. 22-37, 2016/01/02 2016, doi: 10.1080/2093761X.2016.1152204.

[231] S. Thorsson, F. Lindberg, J. Björklund, B. Holmer, and D. Rayner, "Potential changes in outdoor thermal comfort conditions in Gothenburg, Sweden due to climate change: the influence of urban geometry," *International Journal of Climatology,* vol. 31, no. 2, pp. 324-335, 2011, doi: https://doi.org/10.1002/joc.2231.

[232] P. Conry, H. J. S. Fernando, L. S. Leo, A. Sharma, M. Potosnak, and J. Hellmann, "Multi-Scale Simulations of Climate-Change Influence on Chicago Heat Island," 2014. [Online]. Available: https://doi.org/10.1115/FEDSM2014-21581.

[233] H. Radhi, "Evaluating the potential impact of global warming on the UAE residential buildings – A contribution to reduce the CO2 emissions," *Building and Environment,* vol. 44, no. 12, pp. 2451-2462, 2009/12/01/ 2009, doi: https://doi.org/10.1016/j.buildenv.2009.04.006.

[234] J. M. Rey-Hernández, C. Yousif, D. Gatt, E. Velasco-Gómez, J. San José-Alonso, and F. J. Rey-Martínez, "Modelling the long-term effect of climate change on a zero energy and carbon dioxide building through energy efficiency and renewables," *Energy and Buildings,* vol. 174, pp. 85-96, 2018/09/01/ 2018, doi: https://doi.org/10.1016/j.enbuild.2018.06.006.

[235] Z. J. Zhai and J. M. Helman, "Implications of climate changes to building energy and design," *Sustainable Cities and Society,* vol. 44, pp. 511-519, 2019/01/01/ 2019, doi:

https://doi.org/10.1016/j.scs.2018.10.043.

[236] R. S. José, J. L. Pérez, L. Pérez, and R. M. Gonzalez-Barras, "Sensitivity Analysis of Building Energy Demand for Downscaled Climate Scenarios," in *2018 International Conference on Computational Science and Computational Intelligence (CSCI)*, 12-14 Dec. 2018 2018, pp. 513-518, doi: 10.1109/CSCI46756.2018.00105.

[237] R. San José, J. L. Pérez, L. Pérez, and R. M. Gonzalez Barras, "Effects of climate change on the health of citizens modelling urban weather and air pollution," *Energy,* vol. 165, pp. 53-62, 2018/12/15/ 2018, doi: https://doi.org/10.1016/j.energy.2018.09.088.

[238] L. Ji, A. Laouadi, L. Wang, and M. A. Lacasse, "Development of a bioheat model for older people under hot and cold exposures," in *Building Simulation*, 2022: Springer, pp. 1-15.

[239] L. Ji, A. Laouadi, C. Shu, L. Wang, and M. A. Lacasse, "Evaluation and improvement of the thermoregulatory system for the two-node bioheat model," *Energy and Buildings,* vol. 249, p. 111235, 2021.

[240] P. O. Fanger, "Thermal comfort. Analysis and applications in environmental engineering," *Thermal comfort. Analysis and applications in environmental engineering.,* 1970.

[241] A. P. Gagge, "An effective temperature scale based on a simple model of human physiological regulatory response," *Ashrae Trans.,* vol. 77, pp. 247-262, 1971.

[242] S. Yan, J. Xiong, J. Kim, and R. de Dear, "Adapting the two-node model to evaluate sleeping thermal environments," *Building and Environment,* vol. 222, p. 109417, 2022.

[243] E. 15251:2007, "Indoor Environmental Input Parameters for Design and Assessment of Energy Performance of Buildings Addressing Indoor Air Quality, Thermal Environment, Lighting and Acoustics."

[244] *Ergonomics of the thermal environment — Analytical determination and interpretation of thermal comfort using calculation of the PMV and PPD indices and local thermal comfort criteria. 3rd edition*, I. 7730, International Organisation for Standardization, 2005.

[245] R. American Society of Heating and E. Air-Conditioning, *ASHRAE standard thermal environmental conditions for human occupancy*. Atlanta, Ga. : The Society, [1992] ©1992, 1992.

[246] CIBSE, *TM36: Climate change and the internal environment*. 2005.

[247] CIBSE, "The limits of thermal comfort: avoiding overheating in European buildings," in "TM52," Chartered Institute of British Service Engineers, 2013.

[248] X. Li, J. Taylor, and P. Symonds, "Indoor overheating and mitigation of converted lofts in London, UK," *Building Services Engineering Research and Technology,* vol. 40, no. 4, pp. 409-425, 2019.

[249] Y. Ji, R. Fitton, W. Swan, and P. Webster, "Assessing overheating of the UK existing dwellings–A case study of replica Victorian end terrace house," *Building and Environment,* vol. 77, pp. 1-11, 2014.

[250] M. Hendel, K. Azos-Diaz, and B. Tremeac, "Behavioral adaptation to heat-related health risks in cities," *Energy and Buildings,* vol. 152, pp. 823-829, 2017.

[251] D. Robinson and F. Haldi, "Model to predict overheating risk based on an electrical

capacitor analogy," *Energy and Buildings,* vol. 40, no. 7, pp. 1240-1245, 2008.

[252] D. Robinson and F. Haldi, "An integrated adaptive model for overheating risk prediction," *Journal of Building Performance Simulation,* vol. 1, no. 1, pp. 43-55, 2008.

[253] A. Mavrogianni, M. Davies, P. Wilkinson, and A. Pathan, "London housing and climate change: impact on comfort and health-preliminary results of a summer overheating study," *Open House International,* vol. 35, no. 2, pp. 49-59, 2010.

[254] M. Vellei *et al.*, "Overheating in vulnerable and non-vulnerable households," *Building Research & Information,* vol. 45, no. 1-2, pp. 102-118, 2017.

[255] K. J. Lomas and S. M. Porritt, "Overheating in buildings: lessons from research," vol. 45, ed: Taylor & Francis, 2017, pp. 1-18.

[256] X. Xie, Z. Luo, S. Grimmond, T. Sun, and W. Morrison, "Impact of inter-building longwave radiative exchanges on building energy performance and indoor overheating," *Building and Environment,* vol. 209, p. 108628, 2022.

[257] R. Gupta and M. Gregg, "Assessing energy use and overheating risk in net zero energy dwellings in UK," *Energy and Buildings,* vol. 158, pp. 897-905, 2018.

[258] K. Williams *et al.*, "Retrofitting England's suburbs to adapt to climate change," *Building Research & Information,* vol. 41, no. 5, pp. 517-531, 2013.

[259] R. Segura *et al.*, "Observational and numerical evaluation of the pedestrian-level microclimatic effect of street trees in a highly-compact city," in *EGU General Assembly Conference Abstracts*, 2022, pp. EGU22-9195.

[260] A. Katal *et al.*, "Outdoor heat stress assessment using an integrated multi-scale numerical weather prediction system: A case study of a heatwave in Montreal," *Science of The Total Environment,* vol. 865, p. 161276, 2023.

[261] C. Shu *et al.*, "Importance of Microscale Climate Simulations in City Scale Overheating Assessments," in *Journal of Physics: Conference Series*, 2021, vol. 2069, no. 1: IOP Publishing, p. 012057.

[262] K. Gao and M. Santamouris, "The use of water irrigation to mitigate ambient overheating in the built environment: Recent progress," *Building and Environment,* vol. 164, p. 106346, 2019.

[263] H. S. Khan, M. Santamouris, P. Kassomenos, R. Paolini, P. Caccetta, and I. Petrou, "Spatiotemporal variation in urban overheating magnitude and its association with synoptic air-masses in a coastal city," *Scientific reports,* vol. 11, no. 1, p. 6762, 2021.

[264] O. Yaqubi, "Contribution to the development of a methodology to build indoor overheating vulnerability maps at the city scale integrating climate change data and urban heat island," Nantes Université, 2022.

[265] R.-L. Hwang, T.-P. Lin, and F.-Y. Lin, "Evaluation and mapping of building overheating risk and air conditioning use due to the urban heat island effect," *Journal of Building Engineering,* vol. 32, p. 101726, 2020.

[266] Y. Yau and S. Hasbi, "A review of climate change impacts on commercial buildings and their technical services in the tropics," *Renewable and Sustainable Energy Reviews,* vol.

18, pp. 430-441, 2013.

[267] O. Edenhofer, *Climate change 2014: mitigation of climate change*. Cambridge University Press, 2015.

[268] N. E. Klepeis *et al.*, "The National Human Activity Pattern Survey (NHAPS): a resource for assessing exposure to environmental pollutants," *Journal of Exposure Science & Environmental Epidemiology,* vol. 11, no. 3, pp. 231-252, 2001.

[269] A. Pisello *et al.*, "Test rooms to study human comfort in buildings: A review of controlled experiments and facilities," *Renewable and Sustainable Energy Reviews,* vol. 149, p. 111359, 2021.

[270] L. Ji, A. Laouadi, C. Shu, A. Gaur, M. Lacasse, and L. L. Wang, "Evaluating Approaches of Selecting Extreme Hot Years for Assessing Building Overheating Conditions during Heatwaves," *Energy and Buildings,* p. 111610, 2021.

[271] A. Cripps, P. Wilkinson, M. Davies, and M. Orme, *Investigation into Overheating in Homes: Literature Review*. 2012.

[272] M. Adlington and B. Ceranic, "UK Care Facilities: Is Climate Change Contributing to Overheating in Dwellings and a Cause of Concern in the Health of Vulnerable Adults," in *Sustainability in Energy and Buildings 2020*: Springer, 2021, pp. 515-525.

[273] D. Coley and T. Kershaw, "Changes in internal temperatures within the built environment as a response to a changing climate," *Building and Environment,* vol. 45, pp. 89-93, 01/31 2010, doi: 10.1016/j.buildenv.2009.05.009.

[274] S. Kovats and S. Hajat, "Heat Stress and Public Health: A Critical Review," *Annual review of public health,* vol. 29, pp. 41-55, 02/01 2008, doi: 10.1146/annurev.publhealth.29.020907.090843.

[275] P. Acharya, B. Boggess, and K. Zhang, "Assessing heat stress and health among construction workers in a changing climate: a review," *International journal of environmental research and public health,* vol. 15, no. 2, p. 247, 2018.

[276] D. J. Buysse, R. Grunstein, J. Horne, and P. Lavie, "Can an improvement in sleep positively impact on health?," *Sleep medicine reviews,* vol. 14, no. 6, pp. 405-410, 2010.

[277] Y. Wang, Y. Liu, C. Song, and J. Liu, "Appropriate indoor operative temperature and bedding micro climate temperature that satisfies the requirements of sleep thermal comfort," *Building and Environment,* vol. 92, pp. 20-29, 2015.

[278] K. Vimalanathan and T. R. Babu, "The effect of indoor office environment on the work performance, health and well-being of office workers," *Journal of environmental health science and engineering,* vol. 12, no. 1, pp. 1-8, 2014.

[279] S. Tham, R. Thompson, O. Landeg, K. Murray, and T. Waite, "Indoor temperature and health: a global systematic review," *Public Health,* vol. 179, pp. 9-17, 2020.

[280] F. Lima, P. Ferreira, and V. Leal, "A review of the relation between household indoor temperature and health outcomes," *Energies,* vol. 13, no. 11, p. 2881, 2020.

[281] D. H. Li, L. Yang, and J. C. Lam, "Impact of climate change on energy use in the built environment in different climate zones–a review," *Energy,* vol. 42, no. 1, pp. 103-112, 2012.

[282] V. Tink, S. Porritt, D. Allinson, and D. Loveday, "Measuring and mitigating overheating risk in solid wall dwellings retrofitted with internal wall insulation," *Building and Environment,* vol. 141, pp. 247-261, 2018.

[283] J. Morey, A. Beizaee, and A. Wright, "An investigation into overheating in social housing dwellings in central England," *Building and Environment,* vol. 176, p. 106814, 2020.

[284] S. M. T. Sameni, M. Gaterell, A. Montazami, and A. Ahmed, "Overheating investigation in UK social housing flats built to the Passivhaus standard," *Building and Environment,* vol. 92, pp. 222-235, 2015.

[285] I. Pollet, S. Germonpré, and A. Vens, "Residential ventilative cooling in national energy performance regulations: properties and impact on ernergy consumption and overheating," in *Healthy Buildings Europe 2015*, 2015: International Society of Indoor Air Quality and Climate (ISIAQ).

[286] T. van Hooff, B. Blocken, H. Timmermans, and J. Hensen, "Analysis of the predicted effect of passive climate adaptation measures on energy demand for cooling and heating in a residential building," *Energy,* vol. 94, pp. 811-820, 2016.

[287] A. Dodoo, L. Gustavsson, and F. Bonakdar, "Effects of future climate change scenarios on overheating risk and primary energy use for Swedish residential buildings," *Energy Procedia,* vol. 61, pp. 1179-1182, 2014.

[288] A. Dodoo and L. Gustavsson, "Energy use and overheating risk of Swedish multi-storey residential buildings under different climate scenarios," *Energy,* vol. 97, pp. 534-548, 2016.

[289] J. C. Gamero-Salinas, A. Monge-Barrio, and A. Sánchez-Ostiz, "Overheating risk assessment of different dwellings during the hottest season of a warm tropical climate," *Building and Environment,* vol. 171, p. 106664, 2020.

[290] S. Liu, Y. T. Kwok, K. K.-L. Lau, W. Ouyang, and E. Ng, "Effectiveness of passive design strategies in responding to future climate change for residential buildings in hot and humid Hong Kong," *Energy and Buildings,* vol. 228, p. 110469, 2020.

[291] W. Marion and K. Urban, "Users manual for radiation data base TMY2s derived from the 1961–1990 national solar," *National Renewable Energy Laboratory,* 1995.

[292] M. Hosseini, K. Javanroodi, and V. M. Nik, "High-resolution impact assessment of climate change on building energy performance considering extreme weather events and microclimate–Investigating variations in indoor thermal comfort and degree-days," *Sustainable Cities and Society,* p. 103634, 2021.

[293] (2018). *Population and Dwelling Count Highlight Tables, 2016 Census*. [Online] Available: https://www12.statcan.gc.ca/census-recensement/2016/dp-pd/hlt-fst/pd-pl/Table.cfm?Lang=Eng&T=801&SR=1&S=3&O=D&RPP=25&PR=0&CMA=0#tPopDwell

[294] (2021). *Canadian Climate Normals*. [Online] Available: https://climate.weather.gc.ca/climate_normals/index_e.html

[295] CORDEX. "Coordinated Regional Downscaling Experiment (CORDEX) program." https://cordex.org (accessed.

[296] F. Giorgi, C. Jones, and G. R. Asrar, "Addressing climate information needs at the regional level: the CORDEX framework," *World Meteorological Organization (WMO) Bulletin,* vol. 58, no. 3, p. 175, 2009.

[297] M. A. Giorgetta *et al.*, "Climate and carbon cycle changes from 1850 to 2100 in MPI-ESM simulations for the Coupled Model Intercomparison Project phase 5," *Journal of Advances in Modeling Earth Systems,* vol. 5, no. 3, pp. 572-597, 2013, doi: https://doi.org/10.1002/jame.20038.

[298] N. C. Centre. "WCRP CMIP5: Norwegian Climate Centre (NCC) NorESM1-M model output collection." Centre for Environmental Data Analysis. http://catalogue.ceda.ac.uk/uuid/753310df96fa4d9ca74dd33b19bdf330 (accessed.

[299] M. O. H. Centre. "WCRP CMIP5: Met Office Hadley Centre (MOHC) HadGEM2-ES model output collection." Centre for Environmental Data Analysis. http://catalogue.ceda.ac.uk/uuid/216becee8a6844ba8f8f98b9f075a635 (accessed.

[300] D. Jacob and R. Podzun, "Sensitivity studies with the regional climate model REMO," *Meteorology and Atmospheric Physics,* vol. 63, no. 1, pp. 119-129, 1997.

[301] G. Wayne, "Representative Concentration Pathways," *Skeptical science,* vol. 24, 2014.

[302] E. a. C. C. Canada. *Engineering Climate Datasets*. [Online]. Available: https://climate.weather.gc.ca/prods_servs/engineering_e.html

[303] A. Gaur, N. Bénichou, M. Armstrong, and F. Hill, "Potential future changes in wildfire weather and behavior around 11 Canadian cities," *Urban Climate,* vol. 35, p. 100735, 2021.

[304] A. Gaur, H. Lu, M. Lacasse, H. Ge, and F. Hill, "Future projected changes in moisture index over Canada," *Building and Environment,* vol. 199, p. 107923, 2021.

[305] CIBSE, "Weather, solar and illuminance data CIBSE Guide J (London:

Chartered Institution of Building Services Engineers)," 2002.

[306] J. Hacker, S. E. Belcher, and A. White, "Design Summer Years for London," 05/01 2014.

[307] D. B. Crawley *et al.*, "EnergyPlus: creating a new-generation building energy simulation program," *Energy and buildings,* vol. 33, no. 4, pp. 319-331, 2001.

[308] J. Boland, B. Ridley, and B. Brown, "Models of diffuse solar radiation," *Renewable Energy,* vol. 33, no. 4, pp. 575-584, 2008.

[309] (2015). *National Building Code of Canada 2015*. [Online] Available: https://nrc.canada.ca/en/certifications-evaluations-standards/codes-canada/codes-canada-publications/national-building-code-canada-2015

[310] V. Goncalves, Y. Ogunjimi, and Y. Heo, "Scrutinizing modeling and analysis methods for evaluating overheating risks in passive houses," *Energy and Buildings,* vol. 234, p. 110701, 2021.

[311] L. Hao, D. Herrera-Avellanosa, C. Del Pero, and A. Troi, "Overheating Risks and Adaptation Strategies of Energy Retrofitted Historic Buildings under the Impact of Climate Change: Case Studies in Alpine Region," *Applied Sciences,* vol. 12, no. 14, p. 7162, 2022.

[312] S. Alavirad, S. Mohammadi, P.-J. Hoes, L. Xu, and J. L. Hensen, "Future-Proof Energy-

Retrofit strategy for an existing Dutch neighbourhood," *Energy and Buildings,* vol. 260, p. 111914, 2022.

[313] D. Amaripadath, M. Velickovic, and S. Attia, "Performance evaluation of a nearly zero-energy office building in temperate oceanic climate based on field measurements," *Energies,* vol. 15, no. 18, p. 6755, 2022.

[314] R. Rahif, M. Hamdy, S. Homaei, C. Zhang, P. Holzer, and S. Attia, "Simulation-based framework to evaluate resistivity of cooling strategies in buildings against overheating impact of climate change," *Building and Environment,* vol. 208, p. 108599, 2022.

[315] A. T. Nguyen, D. Rockwood, M. K. Doan, and T. K. D. Le, "Performance assessment of contemporary energy-optimized office buildings under the impact of climate change," *Journal of Building Engineering,* vol. 35, p. 102089, 2021.

[316] A. O'Donovan, M. D. Murphy, and P. D. O'Sullivan, "Passive control strategies for cooling a non-residential nearly zero energy office: Simulated comfort resilience now and in the future," *Energy and Buildings,* vol. 231, p. 110607, 2021.

[317] B. Fürtön, D. Szagri, and B. Nagy, "The Effect of European Climate Change on Indoor Thermal Comfort and Overheating in a Public Building Designed with a Passive Approach," *Atmosphere,* vol. 13, no. 12, p. 2052, 2022.

[318] R. Gupta *et al.*, "Monitoring and modelling the risk of summertime overheating and passive solutions to avoid active cooling in London care homes," *Energy and Buildings,* vol. 252, p. 111418, 2021.

[319] R. Romano, "Smart Envelope for Nearly Zero Energy Schools. The Case Study of Vallisneri Secondary School in Lucca," in *Renewable Energy in the Service of Mankind Vol I: Selected Topics from the World Renewable Energy Congress WREC 2014*, 2015: Springer, pp. 723-731.

[320] M. Anderson, C. Carmichael, V. Murray, A. Dengel, and M. Swainson, "Defining indoor heat thresholds for health in the UK," *Perspectives in public health,* vol. 133, no. 3, pp. 158-164, 2013.

[321] K.-T. Huang, S.-R. Yang, A. Matzarakis, and T.-P. Lin, "Identifying outdoor thermal risk areas and evaluation of future thermal comfort concerning shading orientation in a traditional settlement," *Science of the Total Environment,* vol. 626, pp. 567-580, 2018.

[322] J. Zou, A. Gaur, and L. L. Wang, "Outdoor Overheating Evaluation in Montreal Using a Reference Year Method Among Future Time Periods," in *International Conference on Building Energy and Environment*, 2022: Springer, pp. 2767-2771.

[323] M. Bruse, "ENVI-met 3.0: updated model overview," *University of Bochum. Retrieved from: www. envi-met. com,* 2004.

[324] J. Liu and J. Niu, "CFD simulation of the wind environment around an isolated high-rise building: An evaluation of SRANS, LES and DES models," *Building and Environment,* vol. 96, pp. 91-106, 2016.

[325] B. Blocken and T. Stathopoulos, "CFD simulation of pedestrian-level wind conditions around buildings: Past achievements and prospects," *Journal of Wind Engineering and Industrial Aerodynamics,* vol. 121, pp. 138-145, 2013.

[326] B. Blocken, T. Stathopoulos, and J. Van Beeck, "Pedestrian-level wind conditions around buildings: Review of wind-tunnel and CFD techniques and their accuracy for wind comfort assessment," *Building and Environment,* vol. 100, pp. 50-81, 2016.

[327] S.-J. Mei and C. Yuan, "Urban buoyancy-driven air flow and modelling method: A critical review," *Building and Environment,* vol. 210, p. 108708, 2022.

[328] J. Allegrini, V. Dorer, and J. Carmeliet, "Buoyant flows in street canyons: Validation of CFD simulations with wind tunnel measurements," *Building and Environment,* vol. 72, pp. 63-74, 2014.

[329] S.-J. Mei, J.-T. Hu, D. Liu, F.-Y. Zhao, Y. Li, and H.-Q. Wang, "Thermal buoyancy driven canyon airflows inside the compact urban blocks saturated with very weak synoptic wind: Plume merging mechanism," *Building and Environment,* vol. 131, pp. 32-43, 2018.

[330] Y. Du, C. M. Mak, J. Liu, Q. Xia, J. Niu, and K. C. Kwok, "Effects of lift-up design on pedestrian level wind comfort in different building configurations under three wind directions," *Building and Environment,* vol. 117, pp. 84-99, 2017.

[331] M. A. Giorgetta *et al.*, "Climate and carbon cycle changes from 1850 to 2100 in MPI-ESM simulations for the Coupled Model Intercomparison Project phase 5," *Journal of Advances in Modeling Earth Systems,* vol. 5, no. 3, pp. 572-597, 2013.

[332] R. Bordoy and P. Burlando, "Bias correction of regional climate model simulations in a region of complex orography," *Journal of Applied Meteorology and Climatology,* vol. 52, no. 1, pp. 82-101, 2013.

[333] A. Katal, "Development of Multi-Scale City Building Energy Model for Urban Climate Resilience," Concordia university, 2020.

[334] A. Katal, M. Mortezazadeh, L. L. Wang, and H. Yu, "Urban building energy and microclimate modeling–From 3D city generation to dynamic simulations," *Energy,* vol. 251, p. 123817, 2022.

[335] M. Mortezazadeh, S. Yang, J. Zou, A. Katal, and S. Leroyer, "CityFFD/CityBEM–Modeling Urban Microclimate, Thermal, and Energy Performances."

[336] G. Chen, L. Rong, and G. Zhang, "Unsteady-state CFD simulations on the impacts of urban geometry on outdoor thermal comfort within idealized building arrays," *Sustainable Cities and Society,* vol. 74, p. 103187, 2021.

[337] K. Blazejczyk, Y. Epstein, G. Jendritzky, H. Staiger, and B. Tinz, "Comparison of UTCI to selected thermal indices," *International journal of biometeorology,* vol. 56, pp. 515-535, 2012.

[338] K. Błażejczyk *et al.*, "An introduction to the universal thermal climate index (UTCI)," *Geographia Polonica,* vol. 86, no. 1, pp. 5-10, 2013.

[339] G. Jendritzky, R. de Dear, and G. Havenith, "UTCI—why another thermal index?," *International journal of biometeorology,* vol. 56, pp. 421-428, 2012.

[340] J. S. Touma, "Dependence of the wind profile power law on stability for various locations," *Journal of the Air Pollution Control Association,* vol. 27, no. 9, pp. 863-866, 1977.

[341] L. Lu and K. Sun, "Wind power evaluation and utilization over a reference high-rise

building in urban area," *Energy and Buildings,* vol. 68, pp. 339-350, 2014.

[342] H. Kikumoto, R. Ooka, H. Sugawara, and J. Lim, "Observational study of power-law approximation of wind profiles within an urban boundary layer for various wind conditions," *Journal of Wind Engineering and Industrial Aerodynamics,* vol. 164, pp. 13-21, 2017.

[343] Y. Yu and R. de Dear, "Thermal respite for pedestrians in overheated urban environments–Introduction of a dynamic analysis of outdoor thermal comfort," *Sustainable Cities and Society,* vol. 86, p. 104149, 2022.

[344] V. Melnikov, V. V. Krzhizhanovskaya, and P. M. Sloot, "Models of pedestrian adaptive behaviour in hot outdoor public spaces," *Procedia Computer Science,* vol. 108, pp. 185-194, 2017.

[345] Y. Takahashi *et al.*, "Thermoregulation model JOS-3 with new open source code," *Energy and Buildings,* vol. 231, p. 110575, 2021.

[346] L. Hudie, "Ergonomics of the thermal environment Determination of metabolic rate," *Basis for the edition of the standard ISO,* vol. 8996, pp. 1-14, 2016.

[347] W. C. Skamarock *et al.*, "A description of the advanced research WRF version 4," *NCAR tech. note ncar/tn-556+ str,* vol. 145, 2019.

[348] H. Lu, A. Gaur, E. S. Krayenhoff, Z. Jandaghian, M. Lacasse, and T. Moore, "Thermal effects of cool roofs and urban vegetation during extreme heat events in three Canadian regions," *Sustainable Cities and Society,* vol. 99, p. 104925, 2023.

[349] contributor. *NCEP North American Regional Reanalysis (NARR)*, Research Data Archive at the National Center for Atmospheric Research, Computational and Information Systems Laboratory. [Online]. Available: https://rda.ucar.edu/datasets/ds608.0/

[350] P. Patel *et al.*, "Modeling large-scale heatwave by incorporating enhanced urban representation," *Journal of Geophysical Research: Atmospheres,* vol. 127, no. 2, p. e2021JD035316, 2022.

[351] J. Vogel and A. Afshari, "Comparison of urban heat island intensity estimation methods using urbanized WRF in Berlin, Germany," *Atmosphere,* vol. 11, no. 12, p. 1338, 2020.

[352] I. D. Stewart and T. R. Oke, "Local climate zones for urban temperature studies," *Bulletin of the American Meteorological Society,* vol. 93, no. 12, pp. 1879-1900, 2012.

[353] F. Salamanca, A. Krpo, A. Martilli, and A. Clappier, "A new building energy model coupled with an urban canopy parameterization for urban climate simulations—part I. formulation, verification, and sensitivity analysis of the model," *Theoretical and applied climatology,* vol. 99, pp. 331-344, 2010.

[354] P. D. Broxton, X. Zeng, D. Sulla-Menashe, and P. A. Troch, "A global land cover climatology using MODIS data," *Journal of Applied Meteorology and Climatology,* vol. 53, no. 6, pp. 1593-1605, 2014.

[355] S. Yang, L. L. Wang, T. Stathopoulos, and A. M. Marey, "Urban microclimate and its impact on built environment–a review," *Building and Environment,* p. 110334, 2023.